

ผลกระทบของวิถีความคุ้นต่อกำลังกดของหินภายใต้สภาวะสามแกนจริง



วิทยานิพนธ์นี้เป็นส่วนหนึ่งของการศึกษาตามหลักสูตรปริญญาวิศวกรรมศาสตรดุษฎีบัณฑิต

สาขาวิชาเทคโนโลยีธรณี

มหาวิทยาลัยเทคโนโลยีสุรนารี

ปีการศึกษา 2557

**EFFECTS OF STRESS PATH ON ROCK STRENGTH
UNDER TRUE TRIAXIAL CONDITION**

Surachai Komenthammasopon



**A Thesis Submitted in Partial Fulfillment of the Requirements for the
Doctor of Philosophy of Engineering in Geotechnology**

Suranaree University of Technology

Academic Year 2014

EFFECTS OF STRESS PATH ON ROCK STRENGTH UNDER TRUE TRIAXIAL CONDITION

Suranaree University of Technology has approved this thesis submitted in partial fulfillment of the requirements for the Degree of Doctor of Philosophy.

Thesis Examining Committee

(Dr. Decho Phueakphum)

Chairperson

(Prof. Dr. Kittitep Fuenkajorn)

Member (Thesis Advisor)

(Prof. Dr. Suksun Horpibulsuk)

Member

(Assoc. Prof. Ladda Wannakao)

Member

(Dr. Prachya Tepnarong)

Member

(Prof. Dr. Sukit Limpijumnong)

Vice Rector for Academic Affairs
and Innovation

(Assoc. Prof. Flt. Lt. Dr. Kontorn Chamniprasart)

Dean of Institute of Engineering

สุรัชย์ โภเมนธรรมโสภณ : ผลกระทบของวิถีความเค้นต่อกำลังกดของหินภายใต้สภาวะ
สามแกนจริง (EFFECTS OF STRESS PATH ON ROCK STRENGTH UNDER TRUE
TRIAXIAL CONDITION) อาจารย์ที่ปรึกษา : ศาสตราจารย์ ดร.กิตติเทพ เฟื่องขจร,
129 หน้า.

วัตถุประสงค์ของการศึกษาค้นคว้าครั้งนี้ประกอบด้วย การประดิษฐ์อุปกรณ์สำหรับทดสอบหาค่า
กำลังรับแรงกดในหลายแกนต่อหินที่มีความแข็งอยู่ในช่วงอ่อนถึงปานกลาง ศึกษาผลกระทบของ
ความเค้นหลักปานกลางต่อการแตกของหิน และสร้างเกณฑ์การแตกในสามแกนเพื่อนำไป
ประยุกต์ใช้ในการออกแบบและวิเคราะห์เสถียรภาพของโครงสร้างต่างๆทางธรณีวิทยา อุปกรณ์
สำหรับทดสอบหาค่ากำลังรับแรงกดในหลายแกนถูกนำมาใช้ทดสอบหาค่ากำลังกดในสองแกน
และในหลายแกน เพื่อศึกษาผลกระทบของวิถีความเค้นต่อค่ากำลังรับแรงกดของหิน วิถีความเค้นที่
ใช้ในการทดสอบมี 3 แบบ คือ (1) ความเค้นหลักสูงสุดเพิ่มขึ้นขณะที่ความเค้นหลักปานกลางคงที่
(2) ความเค้นหลักสูงสุด และความเค้นหลักปานกลางเพิ่มขึ้นพร้อมกัน และ (3) ความเค้นหลัก
สูงสุดเพิ่มขึ้น ขณะที่ความเค้นหลักปานกลางลดลง (ความเค้นเฉลี่ยคงที่) ผลการทดสอบระบุว่า วิถี
ความเค้นแบบที่ (1) ที่กำหนดความเค้นหลักปานกลางคงที่มีค่ากำลังรับแรงกดสูงกว่าวิถีความเค้น
แบบที่ (3) ซึ่งจากผลดังกล่าวแสดงให้เห็นว่าความเค้นหลักปานกลางส่งผลกระทบต่อ
ค่ากำลังรับแรงกดของหิน เกณฑ์การแตกแบบโมดิฟาย วาย โบล แอนด์ คูก สามารถคาดคะเนค่า
กำลังรับแรงกดของหินในสองแกนได้เป็นอย่างดี สำหรับการทดสอบหาค่ากำลังรับแรงกดในหลาย
แกน วิถีความเค้นที่ใช้ในการทดสอบมี 5 แบบ คือ (1) ความเค้นหลักสูงสุดเพิ่มขึ้นขณะที่ความเค้น
หลักปานกลางเท่ากับความเค้นหลักต่ำสุด (2) ความเค้นหลักสูงสุดเพิ่มขึ้นขณะที่ความเค้นหลักปาน
กลาง และความเค้นหลักต่ำสุดลดลง (ความเค้นเฉลี่ยคงที่) (3) ความเค้นหลักสูงสุด และความเค้น
หลักปานกลางเพิ่มขึ้นเท่าๆ กัน (4) ความเค้นหลักสูงสุด และความเค้นหลักปานกลางเพิ่มขึ้นเท่ากัน
ขณะที่ความเค้นหลักต่ำสุดลดลง (ความเค้นเฉลี่ยคงที่) และ (5) ความเค้นหลักสูงสุดเพิ่มขึ้นขณะที่
ความเค้นหลักปานกลาง และความเค้นหลักต่ำสุดมีการผันแปร (ความเค้นหลักทั้ง 3 แกน ไม่เท่ากัน)
วิถีความเค้นสองแบบแรกเป็นการทดสอบกำลังรับแรงกดในสามแกน ส่วนวิถีความเค้นสองแบบ
ถัดมาเป็นการทดสอบกำลังรับแรงดึงในสามแกน และวิถีความเค้นแบบสุดท้ายเป็นการทดสอบ
กำลังรับแรงกดในสามแกนจริง ซึ่งกรณีการทดสอบกำลังรับแรงกดในสามแกน วิถีความเค้นแบบที่
(1) จะให้ค่ากำลังรับแรงกดของหินสูงกว่าวิถีความเค้นแบบที่ (2) กรณีการทดสอบกำลังรับแรงดึง
ในสามแกน วิถีความเค้นแบบที่ (3) จะให้ค่ากำลังรับแรงกดของตัวอย่างหินสูงกว่าวิถีความเค้น
แบบที่ (4) การทดสอบกำลังรับแรงดึงจะให้ค่ากำลังรับแรงกดของหินสูงกว่าการทดสอบกำลังรับ

แรงกด สามารถสรุปได้ว่าความเค้นหลักปานกลางอาจส่งผลกระทบต่อค่ากำลังรับแรงกดของตัวอย่างหินภายใต้วิธีความเค้นแต่ละแบบ โดยผลสรุปนี้อาจเป็นเหตุผลที่ทำให้ค่ากำลังรับแรงดึงของหินในสามแกนมีค่าสูงกว่ากรณีกำลังรับแรงกดในสามแกนเสมอ นอกจากนี้ความเค้นหลักปานกลางดูเหมือนจะส่งผลกระทบต่อผลกระทบบากยิ่งขึ้นเมื่อความเค้นหลักต่ำสุดมีค่าสูง ด้วยเหตุนี้การทดสอบในสามแกนกรณีที่มีความเค้นเฉลี่ยคงที่ (ความเค้นหลักต่ำสุดลดลง) จึงให้ค่ากำลังรับแรงกดของตัวอย่างหินต่ำกว่าในกรณีที่มีความเค้นเฉลี่ยไม่คงที่ ซึ่งการทดสอบหาค่ากำลังกดในสามแกนนี้เกณฑ์การแตกแบบ โมดิฟาย วายโบล แอนด์ คูก และแบบเอ็มไพริคัล โมจิ สามารถให้ผลการประเมินค่ากำลังรับแรงกดได้เป็นอย่างดีในทุกสภาวะ



สาขาวิชา เทคโนโลยีธรณี _____
ปีการศึกษา 2557

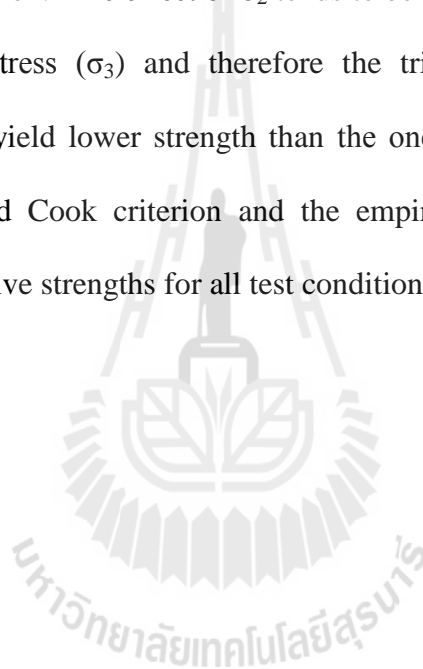
ลายมือชื่อนักศึกษา _____
ลายมือชื่ออาจารย์ที่ปรึกษา _____

SURACHAI KOMENTHAMMASOPON : EFFECTS OF STRESS PATH
ON ROCK STRENGTH UNDER TRUE TRIAXIAL CONDITION. THESIS
ADVISOR : PROF. KITTITEP FUENKAJORN, Ph.D., P.E., 129 PP.

BIAXIAL/INTERMEDIATE PRINCIPAL STRESS/ROCK STRENGTH/FAILURE

The research objectives are to invent a true triaxial testing device to determine the compressive strength of soft to medium strong rocks subjected to polyaxial stress states, to investigate the influence of the intermediate principal stress on rock failure, and to develop a three dimensional failure criterion for the rocks that can be applied in the design and the stability analysis of geologic structures. The true triaxial testing device is used to perform biaxial and polyaxial compression tests to investigate the effects of stress path on rock strengths. Three different stress paths have been implemented : (1) σ_1 increases while σ_2 is maintained constant; (2) σ_1 and σ_2 equally increase; and (3) σ_1 increases while σ_2 decreases (σ_m constant). The results indicate that the stress path (1) with σ_2 constant provides higher strengths than the stress path (3). The intermediate principal stress (σ_2) notably affects the rock strengths. The modified Wiebols and Cook criterion can well predict the biaxial compressive strengths. For the polyaxial compression tests, five different stress paths have been implemented: (1) σ_1 increases while σ_2 equals σ_3 ; (2) σ_1 increases while σ_2 and σ_3 decrease (σ_m constant); (3) σ_1 and σ_2 equally increase while σ_3 is constant; (4) σ_1 and σ_2 equally increase while σ_3 decreases (σ_m constant); (5) σ_1 increases with varied σ_2 and σ_3 ($\sigma_1 \neq \sigma_2 \neq \sigma_3$). The first two stress paths are triaxial compression and another two are triaxial extension while the last one is true triaxial stress condition. Under

triaxial compression tests, the stress path (1) normally provides higher rock strengths than does stress path (2). Under triaxial extension tests, the stress path (3) yields higher strengths than does the stress path (4). The triaxial extension tests give higher strengths than the triaxial compression tests. The intermediate principal stresses (σ_2) have strong influence on different strengths of specimens under each stress path. As a result the rock strengths from triaxial extension tests are always higher than the ones from triaxial compression. The effect of σ_2 tends to be more pronounced under higher minimum principal stress (σ_3) and therefore the triaxial tests with σ_m constant (reduced σ_3) usually yield lower strength than the ones with σ_m not constant. The modified Wiebols and Cook criterion and the empirical Mogi criterion can well describe the compressive strengths for all test conditions.



School of Geotechnology

Academic Year 2014

Student's Signature_____

Advisor's Signature_____

ACKNOWLEDGMENTS

I wish to acknowledge the funding supported by Suranaree University of Technology (SUT). I also would like to express my gratitude to Akara Ltd. for the major fund / financial support for the fabrication of the rock testing device.

I would like to express my sincere thanks to Prof. Dr. Kittitep Fuenkajorn for his valuable guidance and efficient supervision. I appreciate his strong support, encouragement, suggestions and comments during the research period. Many thanks are also extended to Dr. Decho Phueakphum, Prof. Dr. Suksun Horpibulsuk, Assoc. Prof. Ladda Wannakao, and Dr. Prachya Tepnarong, who served on the thesis committee and commented on the manuscript. Grateful thanks are given to all staffs of Geomechanics Research Unit, Institute of Engineering who supported my work.

Finally, I would like to thank beloved parents for their love, support and encouragement.

Surachai Komenthammasopon

TABLE OF CONTENTS

	Page
ABSTRACT (THAI)	I
ABSTRACT (ENGLISH).....	III
ACKNOWLEDGEMENTS	V
TABLE OF CONTENTS.....	VI
LIST OF TABLES	X
LIST OF FIGURES	XV
SYMBOLS AND ABBREVIATIONS.....	XXIII
CHAPTER	
I INTRODUCTION.....	1
1.1 Background and rationale	1
1.2 Research objectives.....	2
1.3 Research methodology	3
1.3.1 Literature review.....	4
1.3.2 Sample collection and preparation.....	4
1.3.3 Design and development of true triaxial testing device	4
1.3.4 Laboratory experiments	4
1.3.5 Data analysis	5
1.3.6 Development of mathematical relations	5

TABLE OF CONTENTS (Continued)

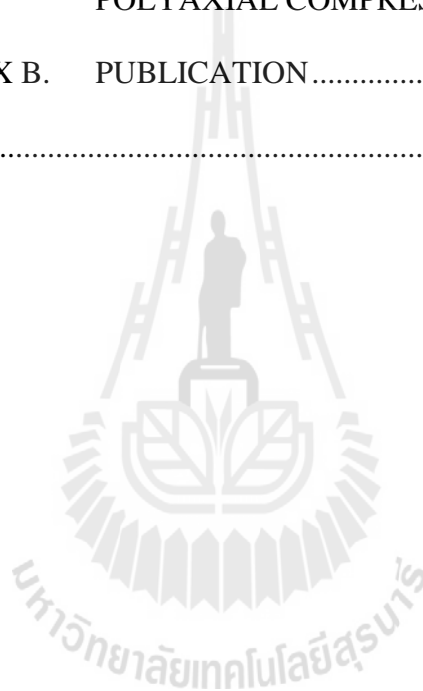
	Page
1.3.7 Thesis writing and presentation	5
1.4 Scope and limitations	5
1.5 Thesis contents	6
II LITERATURE REVIEW	7
2.1 Introduction.....	7
2.2 Biaxial compressive strength tests	7
2.3 Polyaxial compressive strength tests	16
III SAMPLE PREPARATION	34
3.1 Introduction.....	34
3.2 Sample preparation	35
IV TRUE TRIAXIAL LOADING DEVICE	41
4.1 Introduction.....	41
4.2 Design requirements and components	41
4.2.1 Biaxial load frame.....	42
4.2.2 Polyaxial loading device.....	45
4.3 Calculation of factor of safety.....	45
4.3.1 Calculation of factor of safety of supporting steel plates.....	47
4.3.2 Calculation of factor of safety of connecting steel rod.....	49

TABLE OF CONTENTS (Continued)

	Page
V BIAXIAL COMPRESSION TESTS	51
5.1 Introduction.....	51
5.2 Biaxial compression tests.....	51
VI POLYAXIAL COMPRESSION TESTS	63
6.1 Introduction.....	63
6.2 Test equipment.....	63
6.3 Polyaxial compression tests.....	64
6.4 Test results.....	67
6.4.1 Strength results.....	67
6.4.2 Elastic parameters.....	87
VII STRENGTH CRITERIA	100
7.1 Introduction.....	100
7.2 Modified Wiebols and Cook criteria.....	100
7.3 Mogi criterion.....	110
7.4 Coulomb criterion.....	115
7.5 Discussions of the test results.....	118
VIII DISCUSSIONS AND CONCLUSIONS	119
8.1 Discussions.....	119
8.2 Conclusions.....	122
REFERENCES	130

TABLE OF CONTENTS (Continued)

	Page
APPENDICES	
APPENDIX A. STRESS-STRAIN CURVES FROM THE POLYAXIAL COMPRESSION TESTS	135
APPENDIX B. PUBLICATION	148
BIOGRAPHY	168



LIST OF TABLES

Table	Page
3.1 Mineral compositions of three sandstones (Walsri, 2009).....	35
3.2 Phu Phan specimens prepared for biaxial tests.....	36
3.3 Phra Wihan specimens prepared for biaxial tests.....	36
3.4 Phu Kradung specimens prepared for biaxial tests.....	37
3.5 Phu Phan specimens prepared for polyaxial compression tests.....	38
3.6 Phu Kradung specimens prepared for polyaxial compression tests.....	39
3.7 Travertine specimens prepared for polyaxial compression tests.....	40
4.1 Mechanical properties of structural steel based on ASTM-A36 (R.C. Hibbeler, 2013).....	47
5.1 Compressive strengths and elastic parameters of PP sandstone specimens.....	61
5.2 Compressive strengths and elastic parameters of PK sandstone specimens.....	61
5.3 Compressive strengths and elastic parameters of PW sandstone specimens.....	62
6.1 Summary of strengths on Travertine.....	68
6.2 Results of strengths on PK Sandstone.....	68

LIST OF TABLES (Continued)

Table	Page
6.3 Results of strengths on PP Sandstone.....	69
6.4 Compared strength results of triaxial compression tests for travertine.....	74
6.5 Compared strength results of triaxial extension tests for travertine.....	74
6.6 Compared strength results of travertine between triaxial extensions and triaxial compression under similar condition ($\sigma_m \neq \text{constant}$).....	74
6.7 Compared strength results of travertine between triaxial extension and triaxial compression under similar condition ($\sigma_m \text{ constant}$).....	75
6.8 Compared strength results of triaxial compression for PK sandstone.....	75
6.9 Compared strength results of triaxial compression for PK sandstone.....	75
6.10 Compared strength results of PK sandstone between triaxial extension and triaxial compression under similar condition ($\sigma_m \neq \text{constant}$).....	76
6.11 Compared strength results of PK sandstone between triaxial extension and triaxial compression under similar condition ($\sigma_m \text{ constant}$).....	76
6.12 Compared strength results of triaxial compression for PP sandstone.....	76
6.13 Compared strength results of triaxial extension tests for PP sandstone.....	77
6.14 Compared strength results of PP sandstone between triaxial extension and triaxial compression under similar condition ($\sigma_m \neq \text{constant}$).....	77
6.15 Compared strength results of PP sandstone between triaxial extension and triaxial compression under similar condition ($\sigma_m \text{ constant}$).....	77

LIST OF TABLES (Continued)

Table	Page
6.16 Parameters from triaxial compression tests, based on Mohr and Coulomb criterion.....	81
6.17 Summary of the strength results on travertine (TT) specimens from true triaxial compression test.....	83
6.18 Summary of the strength results on PP sandstone specimens from true triaxial compression test.....	84
6.19 Summary result of elastic parameters on Travertine.....	88
6.20 Summary result of elastic parameters on PK Sandstone.....	89
6.21 Summary result of elastic parameters on PP Sandstone.....	90
6.22 Elastic modulus of travertine from the tests under stress path (1) ($\sigma_m \neq \text{constant}$).....	93
6.23 Elastic modulus of travertine from the tests under stress path (2) ($\sigma_m = \text{constant}$).....	93
6.24 Elastic modulus of travertine from the tests under stress path (3) ($\sigma_m \neq \text{constant}$).....	93
6.25 Elastic modulus of travertine from the tests under stress path (4) ($\sigma_m = \text{constant}$).....	94
6.26 Elastic modulus of PK sandstone from the tests under stress path (1) ($\sigma_m \neq \text{constant}$).....	94

LIST OF TABLES (Continued)

Table	Page
6.27	Elastic modulus of PK sandstone from the tests under stress path (2) ($\sigma_m = \text{constant}$).....
	94
6.28	Elastic modulus of PK sandstone from the tests under stress path (3) ($\sigma_m \neq \text{constant}$).....
	95
6.29	Elastic modulus of PK sandstone from the tests under stress path (4) ($\sigma_m = \text{constant}$).....
	95
6.30	Elastic modulus of PP sandstone from the tests under stress path (1) ($\sigma_m \neq \text{constant}$).....
	95
6.31	Elastic modulus of PP sandstone from the tests under stress path (2) ($\sigma_m = \text{constant}$).....
	96
6.32	Elastic modulus of PP sandstone from the tests under stress path (3) ($\sigma_m \neq \text{constant}$).....
	96
6.33	Elastic modulus of PP sandstone from the tests under stress path (4) ($\sigma_m = \text{constant}$).....
	97
6.34	Summarized elastic modulus and Poisson's ratio of travertine.....
	98
6.35	Summarized elastic modulus and Poisson's ratio of PK sandstone.....
	98
6.36	Summarized elastic modulus and Poisson's ratio of PP sandstone.....
	99
7.1	Strength calculation in terms of σ_m and $J_2^{1/2}$ for PP sandstone specimens.....
	102

LIST OF TABLES (Continued)

Table	Page
7.2	Strength calculation in terms of σ_m and $J_2^{1/2}$ for PK sandstone specimens..... 102
7.3	Strength calculation in terms of σ_m and $J_2^{1/2}$ for PW sandstone specimens..... 103
7.4	Calibrated parameters of each sandstone type by the Modified Wiebols & Cook criterion under different stress paths..... 103
7.5	Strength calculation in terms of σ_m and $J_2^{1/2}$ for Travertine specimens..... 105
7.6	Strength calculation in terms of σ_m and $J_2^{1/2}$ for PK sandstone specimens..... 106
7.7	Strength calculation in terms of σ_m and $J_2^{1/2}$ for PP sandstone specimens..... 107
7.8	Calibrated parameters for the Modified Wiebols and Cook criteria..... 108
7.9	Calibrated parameters of each sandstone type by the Mogi (1971) empirical criterion under different stress paths..... 111
7.10	Calibrated parameters for the Mogi criterion..... 113
7.11	Calibrated parameters for the Coulomb criterion..... 116

LIST OF FIGURES

Figure	Page
1.1 Research methodology.....	3
2.1 Biaxial testing equipment, front view general set-up (Bobet et al., 1998).....	8
2.2 Test cell with a specimen inside ready to be transferred to the loading machine (Alsayed, 2002).....	10
2.3 Specimen geometry and loading configuration (Fakhimi et al., 2002).....	10
2.4 Splitting of concrete sample under biaxial compression (Sahouryeh et al., 2002).....	11
2.5 A detailed view around the sample under biaxial compression (Kulatilake et al., 2006).....	13
2.6 Equipment and the data acquisition system used in performing uniaxial and biaxial compression experiments (Kulatilake et al., 2006).....	13
2.7 Typical frame used in making the jointed specimens of the model material (Kulatilake et al., 2006).....	14
2.8 Typical spalling failure mechanisms of granite samples: (a) uniaxial; (b) biaxial-loading path 1; (c) biaxial-loading path 2 – more.....	15

LIST OF FIGURES (Continued)

Figure	Page
2.9	Strength differences between Carrara marble specimens tested under conventional triaxial compression and those under conventional triaxial extension (Wiebols and Cook, 1968).....
	17
2.10	Strength differences between Solenhofen limestone specimens tested under conventional triaxial compression and those under conventional extension (Wiebols and Cook, 1968).....
	17
2.11	Normalized compressive strength of σ_1/c_0 plotted as a function of σ_2/c_0 , for various values of σ_3/c_0 , where c_0 is the uniaxial compressive strength and μ is the frictional coefficient (Wiebols and Cook, 1968).....
	18
2.12	Sandia true-triaxial testing system with “floating” pressure vessel shell (Wawersik et al., 1997).....
	19
2.13	True triaxial system used for study (Tiwari and Rao, 2004).....
	25
2.14	Schematic diagram of true triaxial testing system (Haimson and Chang, 2000).....
	27
2.15	Stress state factor dependence of strength for sandstones: a) highly porous sandstone from A.A. Skotchinsky mine. b) Less porous sandstone of A.F. Zasyadko mine (solid lines) and Yunkom mine (dash line). Figures near curves show values σ_3 . Filled area in Figure 2.2 (a) indicates condition of embrittlement (Alexeev et al., 2008).....
	28

LIST OF FIGURES (Continued)

Figure	Page
2.16	Stress and rock fracturing condition near the tunnel boundary σ_{x0} , σ_{y0} and σ_{z0} are the far field stress components (Cai, 2008).....
	29
2.17	A granite slab show the layered fracturing that occurred at the Mine-by tunnel (depth 420 m) at URL. The stress-induced fractures are parallel to the tunnel surface. The orientation of local in situ σ_1 , σ_2 (45 MPa), and σ_3 ($\sigma_3 \approx 0$) are illustrated in the figure (Cai, 2008).....
	30
2.18	Polyaxial load frame developed for rock testing under true triaxial stresses (Walsri et al., 2009).....
	32
3.1	Sandstones and travertine specimens with nominal size of $55 \times 55 \times 55 \text{ mm}^3$, collected from Saraburi province
	35
4.1	Two steel cross load frames (frame A and B), the main parts of the biaxial rock.....
	42
4.2	Two steel cross load frames (frame A and B) with dimensions.....
	42
4.3	Steel cross load frames with detailed sections.....
	43
4.4	Biaxial rock testing device made from two crossed steel frames, main components.....
	44
4.5	Components of biaxial rock testing devices: main components and accessories.....
	44

LIST OF FIGURES (Continued)

Figure	Page
4.6	General isometric drawing of the true triaxial loading device.....46
4.7	Typical picture of polyaxial loading device during the true triaxial test 46
4.8	Detailed drawing of supporting steel plates for frame A.....48
4.9	Detailed drawing of supporting steel plates for frame B.....48
4.10	Detailed drawing of the connecting steel rod.....50
5.1	The operation during biaxial compression test of PK sandstone specimen 52
5.2	Sandstone specimens with multiple extension fractures from induced stresses of σ_1 and σ_252
5.3	Stress-strain curves from biaxial testing of PP sandstone: Stress path (1) σ_1 increases while σ_2 maintained constant54
5.4	Stress-strain curves from biaxial testing of PK sandstone: Stress path (1) σ_1 increases while σ_2 maintained constant55
5.5	Stress-strain curves from biaxial testing of PW sandstone: Stress path (1) σ_1 increases while σ_2 maintained constant.....56
5.6	Stress-strain curves from biaxial testing of PP, PK and PW sandstones: Stress path (2) σ_2 and σ_1 simultaneously increase.....57
5.7	Stress-strain curves from biaxial testing of PP sandstone:

LIST OF FIGURES (Continued)

Figure	Page
Stress path (3) σ_1 increases and σ_2 decreases.....	58
5.8 Stress-strain curves from biaxial testing of PK sandstone:	
Stress path (3) σ_1 increases and σ_2 decreases.....	59
5.9 Stress-strain curves from biaxial testing of PW sandstone:	
Stress path (3) σ_1 increases and σ_2 decreases.....	60
6.1 Typical picture of polyaxial loading device during the true triaxial test and its general isometric drawing.....	64
6.2 Testing operation and the directions of applied principal stresses.....	65
6.3 Sandstone specimens with multiple extension fractures from induced stresses of σ_1 and σ_2	66
6.4 Post-tested specimens of PP sandstone: (a) Triaxial compression ($\sigma_m \neq \text{constant}$) (b) Triaxial compression ($\sigma_m = \text{constant}$) (c) True triaxial compression ($\sigma_1 \neq \sigma_2 \neq \sigma_3$) (d) Triaxial extension ($\sigma_m \neq \text{constant}$) (e) Triaxial extension ($\sigma_m = \text{constant}$).....	67
6.5 Shear stresses (τ) as a function of normal stress (σ_n).....	70
6.6 Octahedral shear stresses (τ_{oct}) as a function mean stress (σ_m).....	71
6.7 Strength results in terms of second order stress invariant as a function of mean stress.....	72
6.8 Results of triaxial compressive strength tests with the stress path (1)	

LIST OF FIGURES (Continued)

Figure	Page
<p>($\sigma_1 \neq \sigma_2 = \sigma_3$, $\sigma_m \neq \text{constant}$) on travertine in terms of Mohr's circles and Coulomb criterion.....</p>	78
<p>6.9 Results of triaxial compressive strength tests with stress path (2) ($\sigma_1 \neq \sigma_2 = \sigma_3$, $\sigma_m = \text{constant}$) on travertine in terms of Mohr's circles and Coulomb criterion.....</p>	78
<p>6.10 Results of triaxial compressive strength tests with the stress path (1) ($\sigma_1 \neq \sigma_2 = \sigma_3$, $\sigma_m \neq \text{constant}$) on Phu Kradung sandstone in terms of Mohr's circles and Coulomb criterion.....</p>	79
<p>6.11 Results of triaxial compressive strength tests with the stress path (2) ($\sigma_1 \neq \sigma_2 = \sigma_3$, $\sigma_m = \text{constant}$) on Phu Kradung sandstone in terms of Mohr's circles and Coulomb criterion.....</p>	79
<p>6.12 Results of triaxial compressive strength tests with the stress path (1) ($\sigma_1 \neq \sigma_2 = \sigma_3$, $\sigma_m \neq \text{constant}$) on Phu Phan sandstone in terms of Mohr's circles and Coulomb criterion.....</p>	80
<p>6.13 Results of triaxial compressive strength tests with the stress path (2) ($\sigma_1 \neq \sigma_2 = \sigma_3$, $\sigma_m = \text{constant}$) on Phu Phan sandstone in terms of Mohr's circles and Coulomb criterion.....</p>	80
<p>6.14 Compared results of triaxial compressive strength tests between stress path (1) ($\sigma_m \neq \text{constant}$) and the stress path (2) ($\sigma_m = \text{constant}$)</p>	

LIST OF FIGURES (Continued)

Figure	Page
on travertine in terms of Mohr's circles and Coulomb criterion.....	81
6.15 Compared results of triaxial compressive strength tests between stress path (1) ($\sigma_m \neq \text{constant}$) and the stress path (2) ($\sigma_m = \text{constant}$) on Phu Kradung sandstone in terms of Mohr's circles and Coulomb criterion.....	82
6.16 Compared results of triaxial compressive strength tests between the stress path (1) ($\sigma_m \neq \text{constant}$) and the stress path (2) ($\sigma_m = \text{constant}$) on Phu Phan sandstone in terms of Mohr's circles and Coulomb criterion.....	82
6.17 Major principal stress (σ_1) at failure as a function of σ_2 for various σ_3 values.....	85
6.18 Major principal stress (σ_1) at failure as a function of σ_2 for various σ_3 values.....	85
6.19 Elastic modulus calculated along the major principal axis as a function of intermediate and minor principal axes of travertine.....	91
6.20 Elastic modulus calculated along the major principal axis as a function of intermediate and minor principal axes of PK sandstone.....	91
6.21 Elastic modulus calculated along the major principal axis as a function of intermediate and minor principal axes of PP sandstone.....	92

LIST OF FIGURES (Continued)

Figure	Page
7.1 Test results fitted by the modified Wiebols & Cook criterion.....	104
7.2 Strength results in terms of second order stress invariant as a function of mean stress (Modified Wiebols and Cook criterion).....	109
7.3 Test results fitted by the Mogi criterion.....	112
7.4 Strength results in terms of octahedral shear stresses as a function of mean stress (Mogi criterion).....	114
7.5 Strength results in terms of second order stress invariant as a function of mean stress (Coulomb criterion).....	117

SYMBOLS AND ABBREVIATIONS

σ_1	=	Compressive strength at failure
σ_2	=	Intermediate stress
σ_3	=	Minor principal stress
c_0	=	Uniaxial compressive strength
μ	=	Frictional coefficient
m	=	Dimensionless strength parameters
s	=	Dimensionless strength parameters
τ	=	Shear stress
S_0	=	Shear strength or cohesion
σ_n	=	Normal stress
I_1	=	First order invariant of stress
I_3	=	Third order invariant of stress
c	=	Cohesion
ϕ	=	Friction angle
η	=	Material constants
J_1	=	First order stress invariant or the mean stress
$J_2^{1/2}$	=	Second order of the stress deviation
σ_{oct}	=	Octahedral normal stresses
τ_{oct}	=	Octahedral shear stresses
S_Y	=	Yield strength of supporting steel plate

SYMBOLS AND ABBREVIATIONS (Continued)

σ_w	=	Maximum working stress
σ_{cr}	=	Critical loading stress of connecting steel rod
E	=	Young modulus
ν	=	Poisson's ratio
L_e	=	Effective length of steel rod
r	=	Radius of gyration
σ_m	=	Mean stress
E_1	=	Elastic moduli along the major directions
E_2	=	Elastic moduli along directions
E_3	=	Elastic moduli along minor directions
ϵ_1	=	Major principal strains
ϵ_2	=	Intermediate principal strains
ϵ_3	=	Minor principal strains
f_1	=	Monotonically increasing function
$\sigma_{m,2}$	=	Effective mean stress
σ_c	=	Uniaxial compressive strength
A	=	Empirical constant for equation (7.2)
B	=	Empirical constant for equation (7.2)
A'	=	Empirical constant for equation (7.9)
B'	=	Empirical constant for equation (7.9)
C	=	Empirical constant for equation (7.3)

CHAPTER I

INTRODUCTION

1.1 Background and rationale

Rock strength and deformation are important parameters for the design and the stability analysis of geological structures in civil and mining engineering works e.g., foundations of dams, buildings and bridges, and host rocks for tunnels and underground mines. The effects of confining pressures at great depth on these structures are therefore simulated in the laboratory by performing either uniaxial or triaxial compression testing of cylindrical rock specimens. A significant limitation of the conventional triaxial test method is that the intermediate and the minimum principal stresses have to be equal during the test while the rock in actual in-situ condition is normally subjected to an anisotropic stress state where the maximum, the intermediate and the minimum principal stresses are different ($\sigma_1 \neq \sigma_2 \neq \sigma_3$).

In addition, it has been experimentally found that the intermediate principal stresses (σ_2) can notably reduce the maximum principal stress (σ_1) at failure for intact rock specimens (Haimson, 2006). The σ_2 – dependence on failure varies for different rock types. The intermediate stress hardly affects the failure of Shirahama sandstone and Yuubari shale at some values of σ_3 . However, Dunham dolomite and Solenhofen limestone are the rocks with highly σ_2 – dependent failure behavior (Colmenares and Zoback, 2002).

The compressive strength test of rock specimens proposed in this study uses invented loading device exerting forces in true triaxial manner, providing varied σ_1 , σ_2 and σ_3 as required. The effect of stress path is investigated. Polyaxial testing ($\sigma_1 \neq \sigma_2 \neq \sigma_3$) is also performed to examine the effect of stress path. This testing device should provide useful experimental results for the application in the design of tunnel, open channel and rock slope.

1.2 Research objectives

1. To invent a biaxial rock testing device.
2. To determine the compressive strength of the rock having soft to medium strength subjected to biaxial stress states.
3. To investigate the influence of the stress path on rock failure.
4. To develop two failure criterions of the rocks that can be readily applied in the design and the stability analysis of geologic structures.

The efforts involve the determination of maximum principal stresses at failure of the rock specimens under various intermediate principal stresses and the development of mathematical relationship between the two stresses at failure. The invented biaxial rock testing device is used to apply varied σ_2 onto the specimens while the σ_1 is increased until failure. The applied σ_2 at different magnitudes are varied from 0-100 MPa. The failure stresses is measured, and mode of failure is examined. The results are compared with those obtained from the conventional compressive strength tests. The strength criterion is derived. Such criterion is useful for determining or predicting the rock strengths under anisotropic stress conditions.

1.3 Research methodology

The research methodology shown in Figure 1.1 comprises 7 steps: literature review, sample collection and preparation, design and develop true triaxial testing device, laboratory experiments, data analysis, development of mathematical relations, and thesis writing and presentation.

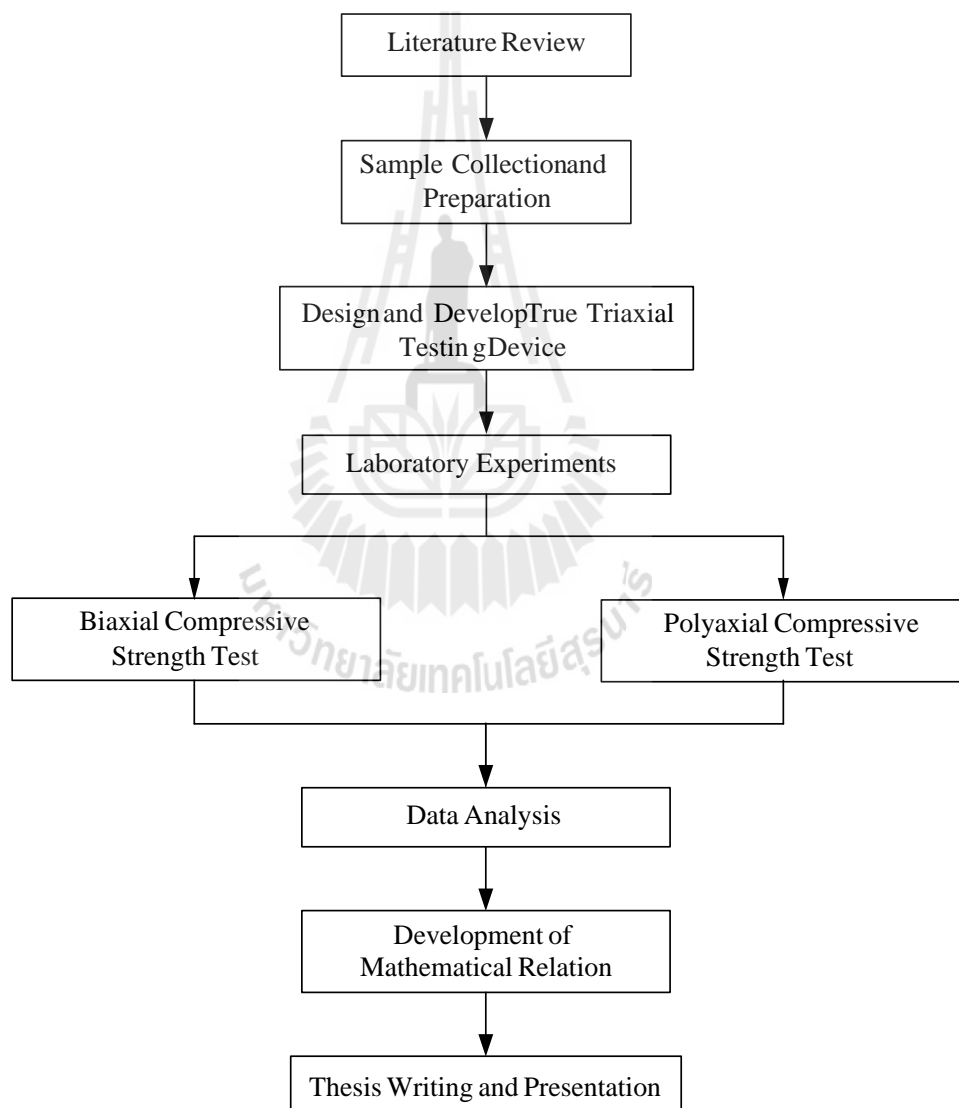


Figure 1.1 Research methodology.

1.3.1 Literature review

Literature review are carried out to study the previous research on compressive strength in biaxial and polyaxial states, the effect of intermediate principal stress on rock failure, rock deformation and strength in biaxial stress state, conventional stress state and true triaxial stress state. The sources of information are from text books, journals, technical reports and conference papers. A summary of the literature review are given in the thesis.

1.3.2 Sample collection and preparation

Rock samples of soft to medium strength are collected from the site. A sample preparation is carried out in the laboratory at the Suranaree University of Technology. Samples for the true triaxial compressive strength test are $5.5 \times 5.5 \times 5.5$ cm³ rectangular blocks. Sample for the biaxial compressive strength test are $5.5 \times 5.5 \times 5.5$ cm³ rectangular blocks. A minimum of 40 samples is prepared for each test and each rock type.

1.3.3 Design and development of true triaxial testing device

A true triaxial testing device, comprising of steel frame work and a system of the load cells of at least 50 tons and hydraulic pumps, is proposed. Detailed design and designed components are further developed.

1.3.4 Laboratory experiments

The laboratory experiments include biaxial, conventional triaxial and polyaxial compressive strength tests. Three types of sandstone are used as rock specimens for the biaxial and the conventional triaxial compressive strength tests. The polyaxial compressive strength tests are performed on two types of sandstone and travertine. All test results are used to develop failure criterion of the rocks.

1.3.5 Data analysis

The experimental results are used to calculate compressive strengths, elastic modulus and Poisson's ratio of rock specimens. These three parameters from conventional compressive strength tests and biaxial compressive strength tests are investigated. The discrepancy of the results are identified and discussed.

1.3.6 Development of mathematical relations

Results from laboratory measurements in terms of the intermediate principal stresses and strength of rock are used to formulate mathematical relations. All principal stresses can be incorporated to the equation. A new failure criterion for rocks under three dimension stress states is derived.

1.3.7 Thesis writing and presentation

All research activities, methods, and results are documented and compiled in the thesis. The research or findings is published in the conference proceedings or journals.

1.4 Scope and limitations

The scope and limitations of the research include as follows.

1. Laboratory experiments are conducted on rock specimens having soft to medium strengths.
2. Testing is performed under intermediate principal stresses ranging from 0 to 100 MPa.
3. The test specimens of about three different rock types in Thailand, that have homogeneous quality, are tested.
4. The specimen nominal size is about $2.5 \times 2.5 \times 2.5 \text{ cm}^3$.

5. All tests are conducted under ambient temperature.
6. Testing is performed under dry condition.
7. No field testing is conducted.

1.5 Thesis contents

This research thesis is divided into six chapters. The first chapter includes background and rationale, research objectives, research methodology, and scope and limitations. **Chapter II** presents results of the literature review to improve an understanding of rock compressive strength as affected by the intermediate principal stress. **Chapter III** describes sample collection and preparation. **Chapter IV** describes the laboratory testing; both conventional and true triaxial compressive strength tests. **Chapter V** presents strength criterion. **Chapter VI** is discussions, conclusions and future studies. **Appendix A** provides detailed of technical publications.

CHAPTER II

LITERATURE REVIEW

2.1 Introduction

Relevant topics and previous research results are reviewed to improve an understanding of rock compressive strength in biaxial and polyaxial compression tests. This review also includes the investigation of the effects of stress path and intermediate principal stress on rock strengths, some biaxial rock testing devices and some polyaxial compression apparatuses. The summary of the results of this literature review is described below.

2.2 Biaxial compressive strength tests

Song and Haimson (1997) conducted laboratory simulation tests of borehole breakouts and investigated their potential use as an indicator of in situ stress magnitudes in Westerly granite and Berea sandstone. They also carried out simple triaxial tests and used the results to derive several strength criteria for these rocks. Truly triaxial strength criteria, which incorporate the effect of the intermediate principal stress on failure, are much more in agreement with the stress at the breakout boundary. One such criterion due to Nadai and another due to Mogi, appear suitable for determining breakout failure in the sandstone and the granite. Thin-section analysis suggests that breakout failure mechanism may play an important role in determining the appropriate strength criterion for a given rock type.

Bobet et al. (1998) described fracture coalescence, which plays an important role in the behavior of brittle materials, is investigated by loading pre-fractured specimens of gypsum, used as a rock model material, in uniaxial and biaxial compression. The biaxial testing machine consists of an existing 200 kip Baldwin machine for the major (vertical) load application and a specifically developed, horizontal loading frame for the confining (horizontal) load. The frame has a 100 kN Instron actuator and a 50 kN load cell, as shown in Figure 2.1. The horizontal actuator and the Baldwin machine are powered by the Baldwin oil pump, and are feedback controlled by a computer and a software program written for this purpose. Several new phenomena and their dependence on geometry and other conditions are observed. The specimens have two pre-existing fractures or flaw that are arranged in different geometries, and that can be either open or closed. Two different test series are performed with these two geometries, one under uniaxial loading and one.

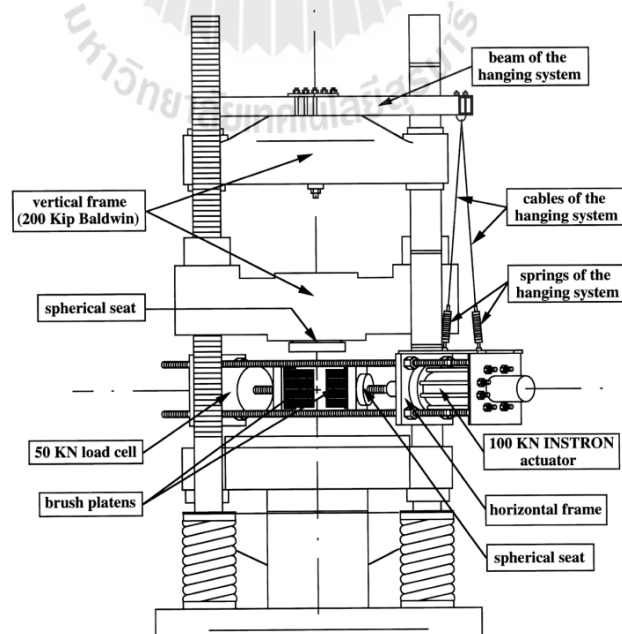


Figure 2.1 Biaxial testing equipment, front view general set-up (Bobet et al., 1998).

Alsayed (2002) used hollow cylinder specimens for simulating stress condition around the opening to study the behavior of rock under a much wider variety of stress paths. The hollow cylinder specimens are used in conventional triaxial test cell, shown in Figure 2.2. It was developed by Hoek and Franklin (1970) and specially designed of internal of pressure loading configuration. Springwell sandstone specimens were subjected to under uniaxial, biaxial, triaxial and polyaxial compression, as well as indirect tension. The results obtained confirm the effect of the intermediate principal stress on rock failure and show that the apparent strength of rock is markedly influenced by the stress condition imposed. Multiaxial testing system can provide realistic prediction of the actual behavior of rock and guide the formulation of more adequate numerical models.

Fakhimi et al. (2002) present the simulation of failure around a circular opening in rock. A biaxial compression test was performed on a sandstone specimen with a circular opening to simulate a loading-type failure around an underground excavation in brittle rock, as shown in Figure 2.3. The axial force and displacements were monitored throughout the failure process, and micro cracking was detected by the acoustic emission technique. To model the observed damage zone around the opening, the distinct element computer program, particle flow code (PFC^{2D}), was used. The numerical model consisted of several circular elements that can interact through contact stiffness, exhibit strength through contact bonds and particle friction, and develop damage through fracture of bonds. For the determination of micro-mechanical parameters needed in the calibration process of the computer program, only the macroscopic parameters of Young's modulus, Poisson's ratio and uniaxial compressive strength were used.

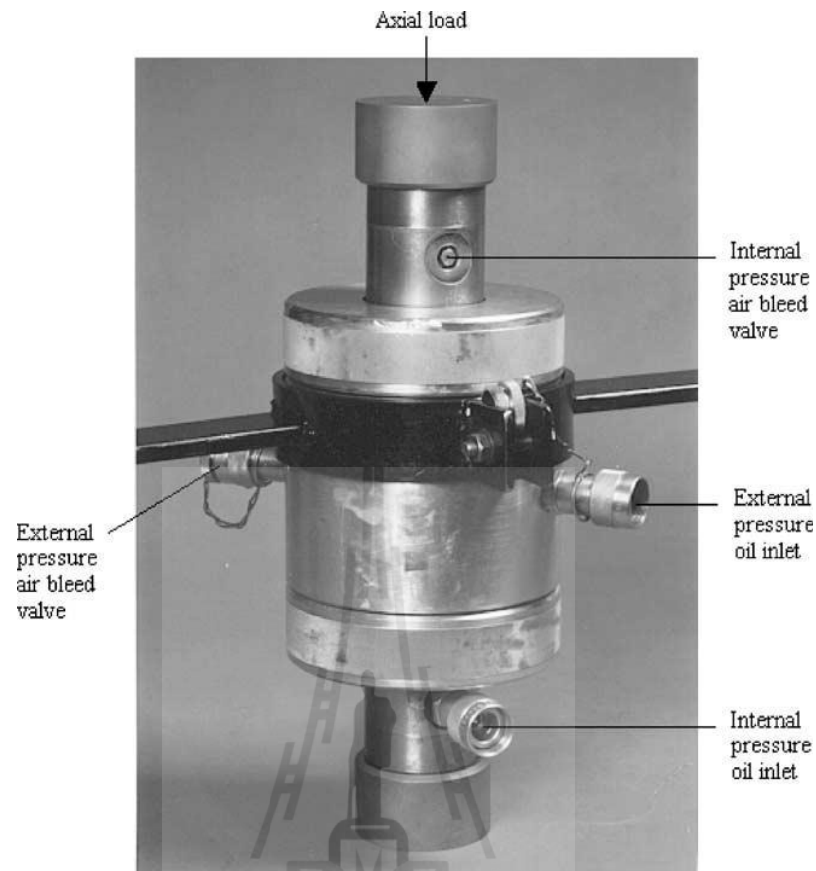


Figure 2.2 Test cell with a specimen inside ready to be transferred to the loading machine (Alsayed, 2002).

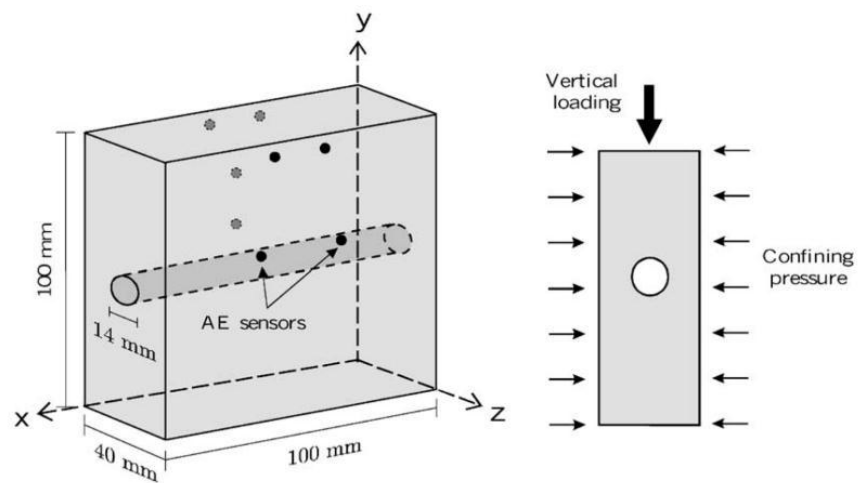


Figure 2.3 Specimen geometry and loading configuration (Fakhimi et al., 2002).

It is shown that PFC^{2D} was capable of simulating the localization behavior of the rock and the numerical model was able to reproduce the damage zone observed in the laboratory test.

Sahouryeh et al. (2002) described an experimental and analytical investigation into three-dimensional crack growth under biaxial compression is presented. Tests were carried out on different materials, including transparent resin samples, each with a single embedded disk-like crack. These cracks grew extensively parallel to the load directions causing splitting, shown in Figure 2.4. This behavior is markedly different from that observed under uniaxial compression where the crack growth is limited in size, and is not capable on its own to induce failure. The presence of the intermediate principal compressive stress radically changes the mechanism of crack growth. A model is proposed where the growing crack is represented as a disk-like crack oriented parallel to the loading direction and opened by a pair of concentrated forces at its center. It is shown that the crack growth is stable until it reaches a size comparable to its distance from the free surface.



Figure 2.4 Splitting of concrete sample under biaxial compression (Sahouryeh et al., 2002).

Zhu et al. (2005) present the simulation of progressive fracturing processes around underground excavations under biaxial compression. Fractures that develop progressively around underground excavations can be simulated using a numerical code called RFPA (rock failure process analysis). The results of the simulations show that the code can be used not only to produce fracturing patterns similar to those reported in previous studies, but also to predict fracturing patterns under a variety of loading conditions. Based on these fracturing patterns, failure mechanisms are identified for various loading conditions.

Kulatilake et al. (2006) conducted experiments for the research: A new rock mass failure criterion for biaxial loading conditions. They investigated the model materials simulating brittle rocks, a mixture of glassstone, sand and water. Thin galvanized sheets of thickness 0.254 mm were used to create joints in blocks made out of model material. To investigate the failure modes and strength, both the intact material blocks as well as jointed model material blocks of size 35.6×17.8×2.5 cm having different joint geometry configurations were subjected to uniaxial and biaxial compressive loadings. A new intact rock failure criterion is proposed at the 3-D level. This criterion is validated for biaxial loading through laboratory experimental results obtained on intact model material blocks. Results obtained from both the intact and jointed model material blocks are used to develop a strongly non-linear new rock mass failure criterion for biaxial loading. The equipment for biaxial loading is shown in the below Figures 2.5 and 2.6, including the typical frame used in making the jointed specimens of the model material, as show in Figure 2.7.

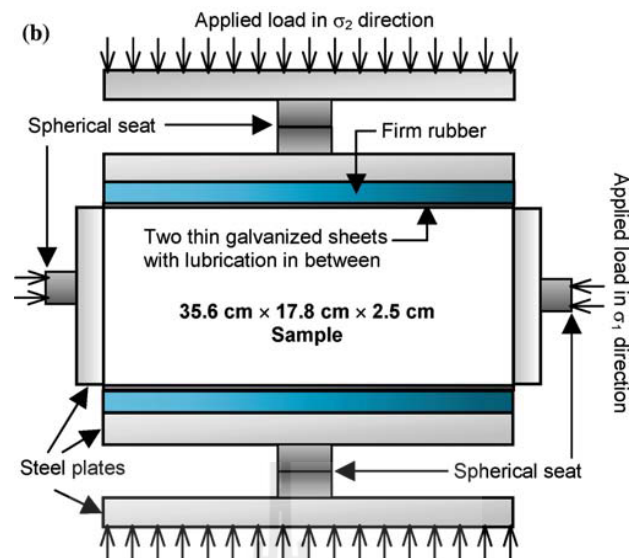


Figure 2.5 A detailed view around the sample under biaxial compression (Kulatilake et al., 2006).

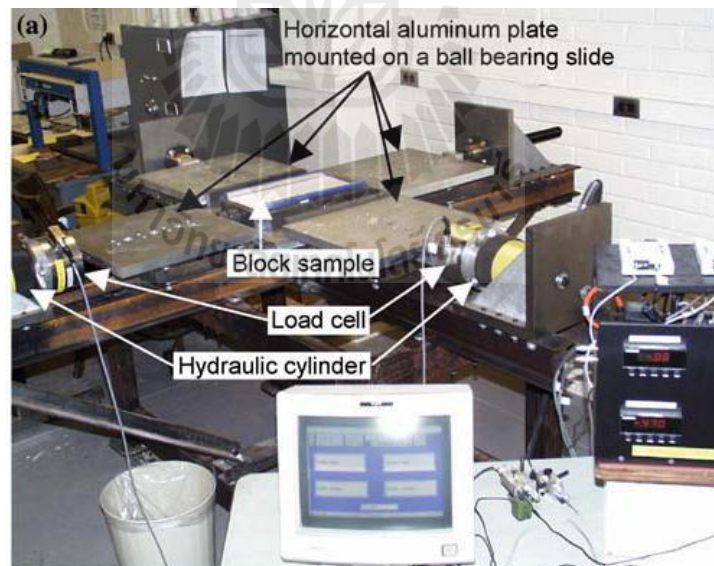


Figure 2.6 Equipment and the data acquisition system used in performing uniaxial and biaxial compression experiments (Kulatilake et al., 2006).

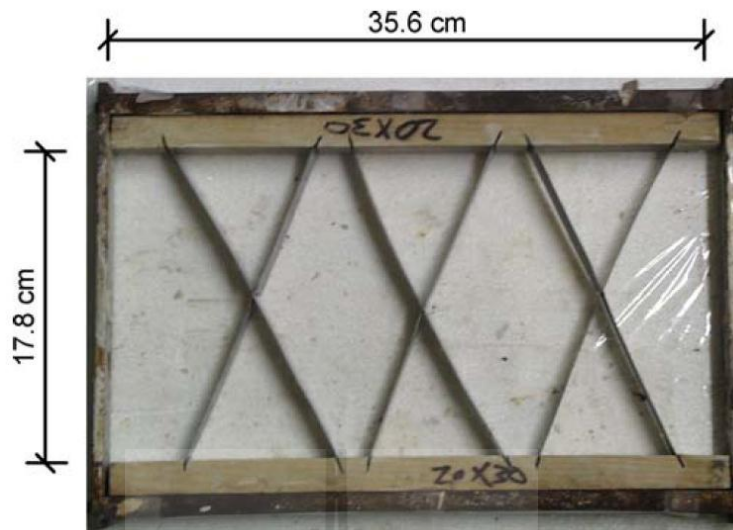


Figure 2.7 Typical frame used in making the jointed specimens of the model material (Kulatilake et al., 2006).

Yun et al. (2010) described the biaxial tests of granite cubes of size of 75, 100 and 125 mm. Testing was done with a newly developed biaxial test apparatus, housed in the structural engineering laboratory of Henan Polytechnic University, China. It has a capacity of 500 metric tons in each direction and is equipped with servo-controlled load and displacement systems. Loading rate can be anywhere between 1.25 and 125 kN/s, and displacement rate can range from 4 to 30 $\mu\text{m/s}$. The availability of high loading rate has permitted the examination of the quasidynamic response of granite to sudden load application, as in the case of drift heading excavated by blasting. The failure mechanisms of granite samples show in Figure 2.8.

Sagong et al. (2011) experimented in rock fracture and joint sliding behaviors of jointed rock masses with an opening under biaxial compression which are investigated through experimental and numerical analyses to study in the tunnel construction in rock mass produces damage around the tunnel by concentration of

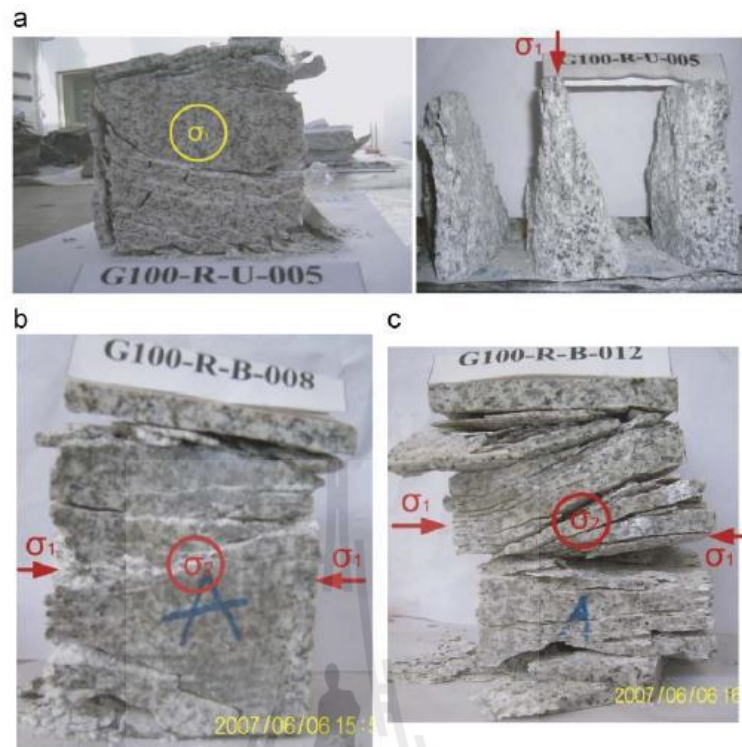


Figure 2.8 Typical spalling failure mechanisms of granite samples: (a) uniaxial; (b) biaxial-loading path 1; (c) biaxial-loading path 2 – more.

in-situ stress and by construction activity such as blasting. The generated damage changes the mechanical and hydraulic properties of the rock mass. The test rock models have a persistent joint set with dip angles of 30° , 45° and 60° to the horizontal. Spalling is observed under higher confinement (Yun et al, 2010). Under the applied biaxial compression, tension crack initiation and propagation are the dominant fracture behaviors around the hole in a low joint dip angle rock model (30° to the horizontal). The propagation direction of the tensile cracks is roughly normal to the joint surface, and with propagation of tensile cracks, removable rock blocks are generated. The experimental results are simulated using discrete element code. The numerical analysis simulates several aspects of rock mass cracking and the joint

sliding processes around an opening: progressive fracture behaviors in a low joint angle rock model, abrupt initiation and propagation of tensile cracks and joint sliding in a high joint angle rock model (60° to the horizontal), propagation of tensile cracks normal to the joint surface, generation of removable blocks in rock segments, an increase of lower hoop stress threshold inducing tensile fractures with a decrease in the joint rock angle, and an increase of the damage zone around the hole with a decrease in the joint angle.

2.3 Polyaxial compressive strength tests

Wiebols and Cook (1968) investigate the effect of σ_2 on rock strength, based on the earlier testing results. Early attempts to examine the influence of σ_2 on rock strength were made in 1960s by Murrell (1963) and Handin et al. (1967). They compared the results from a series of triaxial tests conducted in marble, limestone, dolomite, and glass [triaxial compression tests ($\sigma_1 > \sigma_2 = \sigma_3$) and triaxial extension test ($\sigma_1 = \sigma_2 > \sigma_3$)] and noted that the rock strength for any given σ_3 was larger in triaxial extension than in triaxial compression, thus suggesting that the intermediate principal stress does, in fact, affect mechanical properties (Figure 2.9). Handin and coworkers carried out several triaxial compression and triaxial extension tests in Solenhofen limestone, Blaire dolomite and Pyrex glass. They obtained results similar to those of Murrell's showing that rock strength was higher when the larger intermediate principal stress ($\sigma_2 = \sigma_1$) was applied (Figure 2.10). Based on these earlier experimental results, Wiebols and Cook pursued a theoretical approach to further investigate the effect of σ_2 on rock strength. They derived a strength criterion based on the strain energy stored by the rock in the absence of discontinuities,

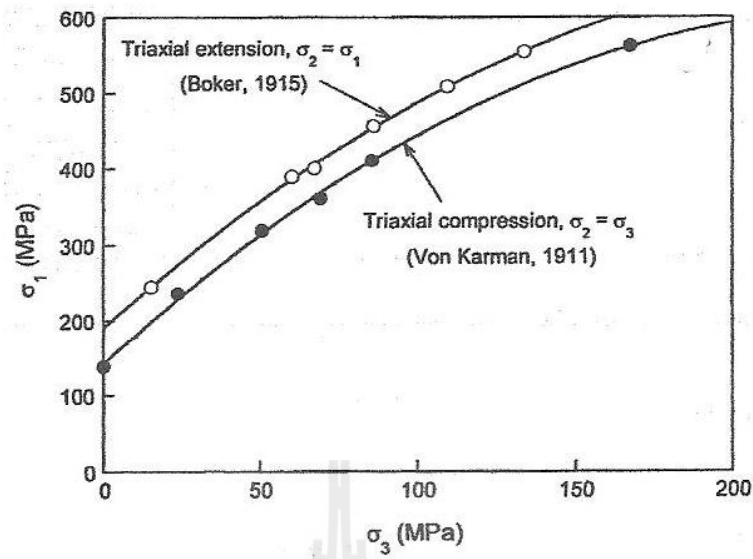


Figure 2.9 Strength differences between Carrara marble specimens tested under conventional triaxial compression and those under conventional triaxial extension (Wiebols and Cook, 1968).

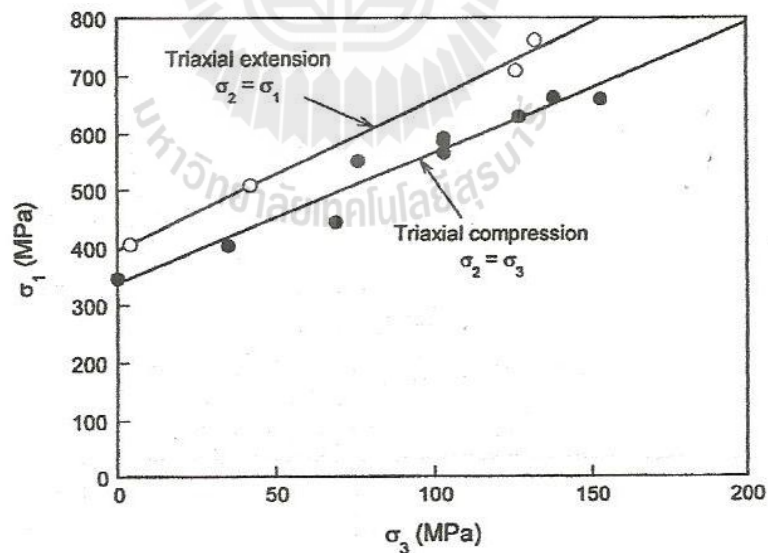


Figure 2.10 Strength differences between Solenhofen limestone specimens tested under conventional triaxial compression and those under conventional extension (Wiebols and Cook, 1968).

and the additional strain energy around Griffith cracks as a result of sliding of crack surfaces over each other. They found that under true triaxial (polyaxial) compressive stress conditions the intermediate principal stress has a pronounced effect, predictable if the coefficient of sliding friction between crack surfaces is known. In particular, Wiebols and Cook determined from their model that if σ_3 is held constant and σ_2 is increased from $\sigma_2 = \sigma_3$ to $\sigma_2 = \sigma_1$ the strength first increases, reaches a maximum at some value of σ_2 and then decreases to a level higher than that obtained in a triaxial test, i.e. when $\sigma_2 = \sigma_3$ (Figure 2.11).

Wawersik et al. (1997) develop the true-triaxial apparatus (Figure 2.12) that makes use of conventional triaxial pressure vessels in combination with specially

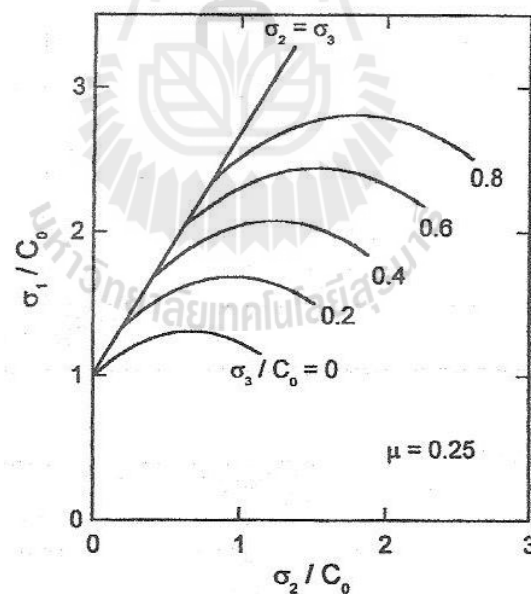


Figure 2.11 Normalized compressive strength of σ_1/c_0 plotted as a function of σ_2/c_0 , for various values of σ_3/c_0 , where c_0 is the uniaxial compressive strength and μ is the frictional coefficient (Wiebols and Cook, 1968).

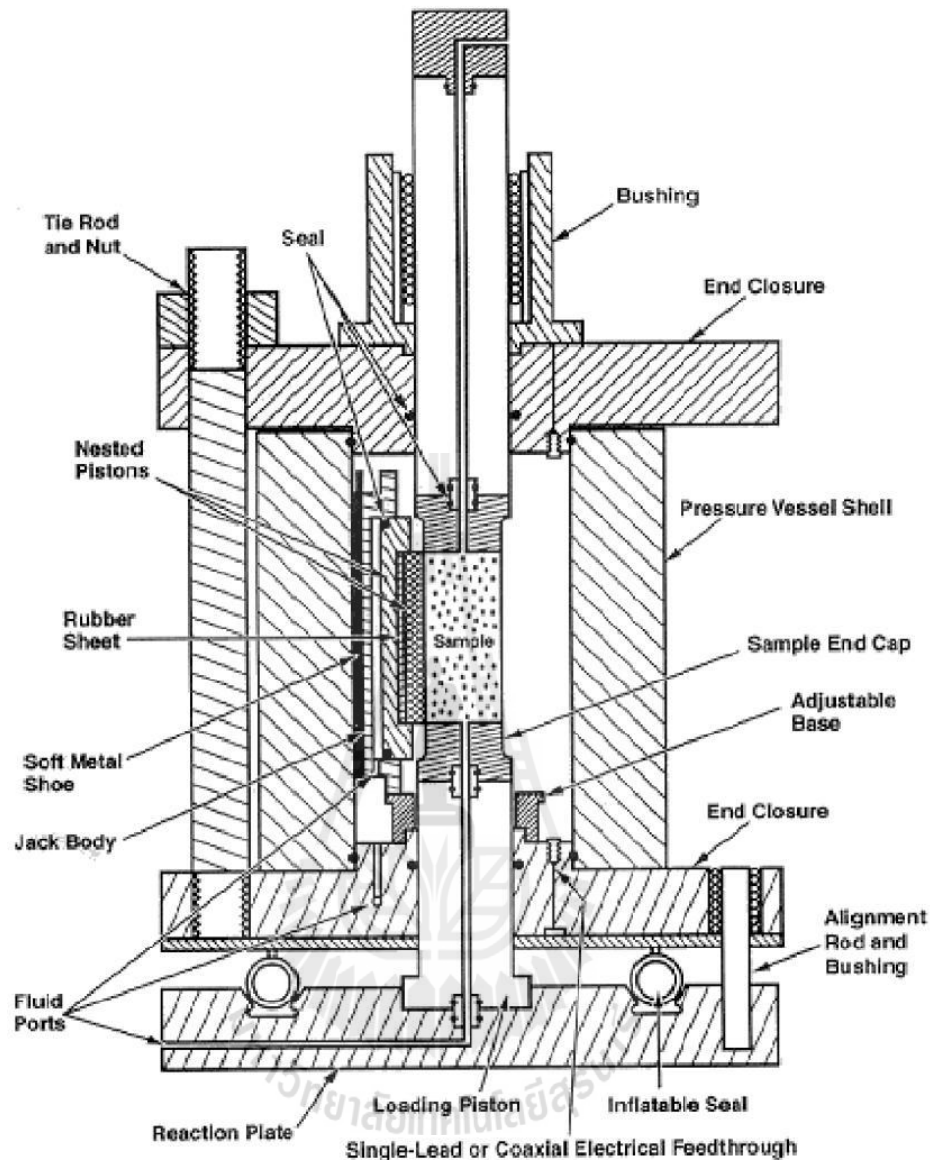


Figure 2.12 Sandia true-triaxial testing system with “floating” pressure vessel shell (Wawersik et al., 1997).

configured, high-pressure hydraulic jacks inside these vessels. The development combines advantages not found in existing facilities, including a compact design, pore-pressure and flow-through capabilities, the ability to attain high principal stresses and principal stress differences, direct access to parts of the sample, and

provisions to relatively large deformations without developing serious stress field in homogeneities.

Colmenares and Zoback (2002) examine seven different failure criteria by comparing them to published polyaxial test data ($\sigma_1 \neq \sigma_2 \neq \sigma_3$) for five different rock types at a variety of stress states. A grid search algorithm was employed to find the best set of parameters that describe failure for each criterion and the associated misfit. Overall, the polyaxial criteria Modified Wiebols and Cook and Modified Lade achieved a good fit to most of the test data. And this is especially true for the rocks with a highly σ_2 – dependent failure behavior (e.g. Dunham dolomite, Solenhofen limestone). However, for some rock types (e.g. Shirahama sandstone, Yuubari shale), the intermediate stress hardly affects failure and the Mohr-Coulomb and Hoek and Brown criteria fit these test data equally well or even better than the more complicated polyaxial criteria. The details of the failure criteria that are referred above to provide a good fit for different rock types are below.

Hoek and Brown criterion

$$\sigma_1 = \sigma_3 + C_0 (m\sigma_3 / c_0 + s)^{1/2} \quad (2.1)$$

where σ_1 = major principal stress at failure

σ_3 = least principal stress at failure

C_0 = uniaxial compressive strength

m and s are dimensionless strength parameters (m depends on rock type and s depends on the characteristics of rock mass).

Ranges of m-values for some characteristic rock types are as follows.

$5 < m < 8$ = Carbonate rocks with well-developed crystal cleavage (dolomite, limestone, marble)

$4 < m < 10$ = Lithified argillaceous rocks (mudstone, siltstone, shale, slate)

$15 < m < 24$ = Arenaceous rocks with strong crystals and poorly developed crystal cleavage (sandstone, quartzite)

$16 < m < 19$ = Fine-grained polyminerallic igneous crystalline rocks (andesite, dolerite, diabase, rhyolite)

$22 < m < 33$ = Coarse-grained polyminerallic igneous and metamorphic rocks (amphibolite, gabbro, gneiss, granite, norite, quartz-diorite)

For the parameter s :

$s = 1$ for intact rock

$s = 0$ for a completely granulated specimen or a rock aggregate

Mohr-Coulomb criterion

$$\tau = S_0 + \mu \sigma_n \quad (2.2)$$

where τ = shear stress

S_0 = shear strength or cohesion

μ = coefficient of internal friction of the material

σ_n = normal stress

Another linearized form of Mohr-Coulomb to be written:

$$\sigma_1 = C_0 + q \sigma_3 \quad (2.3)$$

where σ_1 = major principal stress at failure

σ_3 = least principal stress at failure

C_0 = uniaxial compressive strength

$$q = [(\mu^2 + 1)^{1/2} + \mu]^2 = \tan^2 (\pi/4 + \phi/2)$$

(Assume: σ_2 has no influence on failure)

Modified Lade criterion

$$(I_1)^3 / I_3 = 27 + \eta \quad (2.4)$$

where $I_1 = (\sigma_1 + S) + (\sigma_2 + S) + (\sigma_3 + S)$

$$I_3 = (\sigma_1 + S) (\sigma_2 + S) (\sigma_3 + S)$$

$$S = S_0 / \tan \phi$$

$$\eta = 4(\tan \phi)^2 (9 - 7 \sin \phi) / (1 - \sin \phi)$$

$$\tan \phi = \mu$$

$$S_0 = C_0 / (2q^{1/2}) \text{ and}$$

$$q = [(\mu^2 + 1)^{1/2} + \mu]^2 = \tan^2 (\pi/4 + \phi/2)$$

(S and η are material constants: S related to cohesion of rock; η representing the internal friction)

Modified Wiebols and Cook criterion

$$J_2^{1/2} = A + BJ_1 + C J_1^2 \quad (2.5)$$

where $J_1 = (1/3) \cdot (\sigma_1 + \sigma_2 + \sigma_3)$

$$J_2^{1/2} = [1/6 ((\sigma_1 - \sigma_2)^2 + (\sigma_1 - \sigma_3)^2 + (\sigma_2 - \sigma_3)^2)]^{1/2} = (3/2)^{1/2} \tau_{oct}$$

$$\tau_{oct} = 1/3 [(\sigma_1 - \sigma_2)^2 + (\sigma_2 - \sigma_3)^2 + (\sigma_3 - \sigma_1)^2]^{1/2}$$

$$A = C_0/3^{1/2} - BC_0/3 - CC_0^2/9$$

$$B = 3^{1/2} (q-1)/(q+2) - C/3(2C_0 + (q+2)\sigma_3)$$

$$C = [27^{1/2}/(2C_1 + (q-1)\sigma_3 - C_0) \times [(C_1 + (q-1)\sigma_3 - C_0)/(2C_1 + (2q+1)\sigma_3 - C_0)] - [(q-1)/(q+2)]]$$

$$C_1 = (1 + 0.6\mu) C_0; q = [(\mu^2 + 1)^{1/2} + \mu]^2 = \tan^2 (\pi/4 + \phi/2)$$

The values of C_0 (uniaxial compressive strength) yielded by the Inscribed and the Circumscribed Drucker–Prager criteria bounded the C_0 (uniaxial compressive strength) value obtained using the Mohr–Coulomb criterion as expected. In general, the Drucker–Prager failure criterion did not accurately indicate the value of σ_1 at failure. The value of the misfits achieved with the empirical 1967 and 1971 Mogi criteria were generally in between those obtained using the triaxial and the polyaxial criteria. The disadvantage of these failure criteria is that they cannot be related to strength parameters such as C_0 : They also found that if only data from triaxial tests are available, it is possible to incorporate the influence of σ_2 on failure by using a polyaxial failure criterion. The results for two out of three rocks that could be analyzed in this way were encouraging.

Kwasniewski et al. (2003) use prismatic samples of medium-grained sandstone from Śląsk Colliery for testing under uniaxial compression, conventional triaxial compression and true triaxial compression conditions. Results of the studies show that confining pressure strongly inhibited dilatant behavior of rock samples tested under conventional triaxial compression conditions; the increasing confinement resulted in the growing compaction of the rock material. The effect of dilatancy was also highly suppressed by the intermediate principal stress. While important dilatant, negative volumetric strain corresponded to the peak differential stress at low

intermediate principal stress conditions, at high intermediate stresses the rock material was damaged to much lesser extent. As a result, faulting of rock samples in the post-peak region was much more violent and was accompanied by a strong acoustic effect.

Alexeev et al. (2004) present two generations of true triaxial loading (TTAL) apparatus. First generation was intended primarily for true stress state imitation in rock or mineral specimens. Advanced second-generation is designed to provide precise measurements in any stress and simulation of rock outburst at sudden relief of one sample face. Both TTAL apparatuses can apply pressure up to 250 MPa, corresponding to earth depth about 10,000 m, independently along each of three axes. Experimental results are given on effect of absorbed water on ultimate state in coal as well as adsorbed methane influence on simulated coal outbursts.

Tiwari and Rao (2004) described physical modeling of a rock mass under a true triaxial stress state by using block mass models having three smooth joint sets. The testing used true-triaxial system (TTS) developed by Rao and Tiwari (2002), shown in Figure 2.13. The test results show the strength of rock mass (σ_1) and deformation modulus (E_j) increase significantly which is confirmed by fracture shear planes developed on σ_2 face of specimen. Most of the specimens failed in shearing with sliding in some cases. The effect of interlocking and rotation of principal stresses σ_2 and σ_3 on strength and deformation response was also investigated.

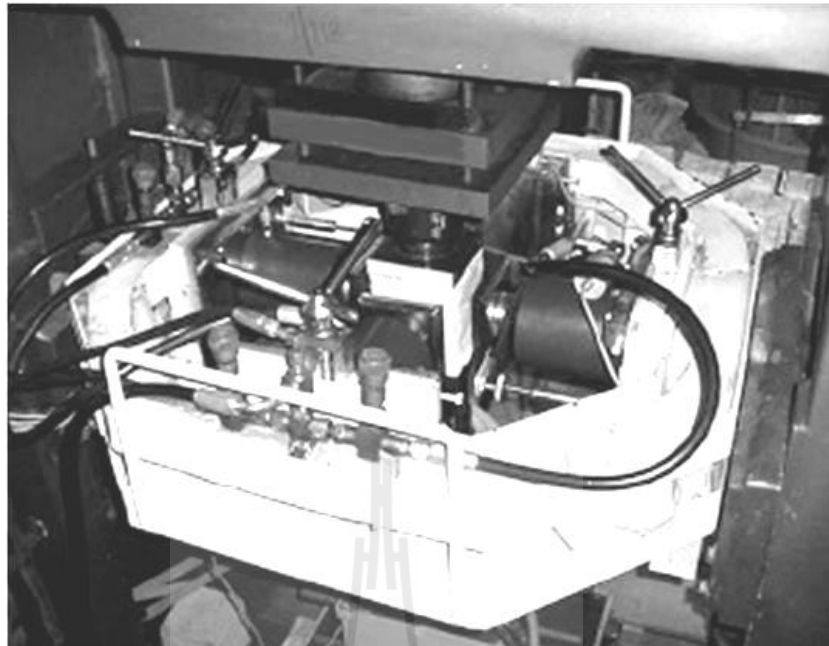


Figure 2.13 True triaxial system used for study (Tiwari and Rao, 2004).

Chang and Haimson (2005) discuss the non-dilatant deformation and failure mechanism under true triaxial compression. They conducted laboratory rock strength experiments on two brittle rocks, hornfels and metapelite, which together are the major constituent of the long valley Caldera (California, USA) basement in the 2025 – 2996 m depth range. Both rocks are banded, very high porosity. Uniaxial compression test at different orientations with respect to banding planes reveal that the hornfels compressive strength is nearly isotropic, the metapelite possesses distinct anisotropy. Conventional triaxial tests in these rocks reveal that their respective strengths in a specific orientation increase approximately linearly with confining pressure. True triaxial compressive experiments in specimens oriented at a consistent angle to banding, in which the magnitude of the least (σ_3) and the intermediate (σ_2) principal stress are different but kept constant during testing while the maximum

principal stress is increased until failure, exhibit a behavior unlike that previously observed in other rocks under similar testing conditions. For a given magnitude of σ_3 , compressive strength σ_1 does not vary significantly in both regardless of the applied σ_2 , suggesting little or no intermediate principal stress effect. Strains measured in all three principal directions during loading were used to obtain plots σ_1 versus volumetric strain. These are consistently linear almost to the point of rock failure, suggesting no dilatants.

Haimson (2006) describes the effect of the intermediate principal stress (σ_2) on brittle fracture of rocks, and on their strength criteria. Testing equipment emulating Mogi's but considerably more compact was developed at the University of Wisconsin and used for true triaxial testing (Figure 2.14) of some very strong crystalline rocks. Test results revealed three distinct compressive failure mechanisms, depending on loading mode and rock type: shear faulting resulting from extensile microcrack localization, multiple splitting along the axis, and nondilatant shear failure. The true triaxial strength criterion for the KTB amphibolite derived from such tests was used in conjunction with logged breakout dimensions to estimate the maximum horizontal in situ stress in the KTB ultra deep scientific hole.

Alexeev et al. (2008) determine the effect of stress state factor on fracture of limestone under true triaxial loading. Experimental results on rock deformation revealed a misfit between strain state and stress state, strain state varying from generalized compression to generalized shear at $\sigma_3 = 0$. This misfit can lead to data misinterpretation during the stress field reconstruction after loading. Fracture of rock specimens under true triaxial compression occurs by a combined longitudinal / transverse shear and produces the highest dilatancy effect.

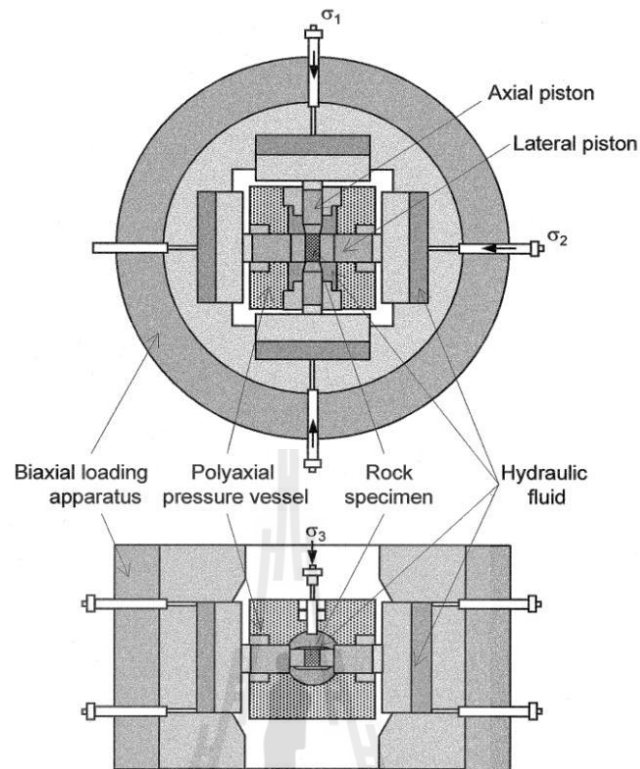


Figure 2.14 Schematic diagram of true triaxial testing system (Haimson, 2006).

An increase in the hydrostatic pressure level diminishes limiting values of shear strains and suppresses the dilatancy effect. A maximum of dilatancy coincides with a maximum of fresh surface area formed during the fracture of rock. The generalized cleavage of rocks becomes energetically disadvantageous in a true triaxial compressive stress field. Some sandstone becomes more brittle under true triaxial compression ($\sigma_2 \neq 0$) at low values of the minimal stress component (σ_3) due to high initial porosity and dilatancy. The embrittlement effect found experimentally is inconsistent with the conclusion of Mogi (1971) and Haimson and Chang (2000) who found an additive effect of minimal compressive stress σ_3 and intermediate compressive stress σ_2 on strength of rocks. This discrepancy is obviously caused by

the high initial porosity and dilatancy of some sandstone, as seen in the data comparison in Figure 2.15.

Cai (2008) study the influence of the intermediate principal stress on rock fracturing and strength near excavation boundaries, using a FEM/DEM combined numerical tool. At the boundary in an underground setting, the intermediate principal stress is often parallel to the tunnel axis, the minimum stress is zero, and the maximum principal stress is the tangential stress. A loading condition of $\sigma_3 = 0$, $\sigma_1 \neq 0$, and $\sigma_2 \neq 0$ thus exists at the boundary (Figure 2.16). It is seen from the simulation

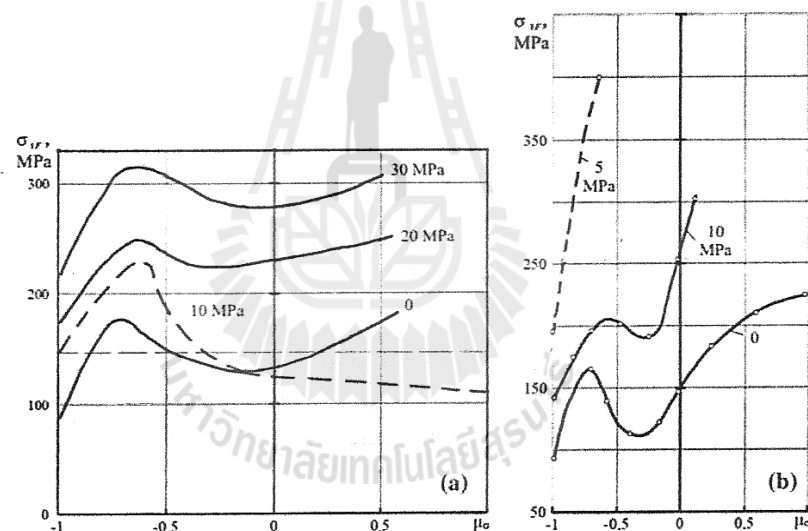


Figure 2.15 Stress state factor dependence of strength for sandstones: a) highly porous sandstone from A.A. Skotchinsky mine. b) Less porous sandstone of A.F. Zasyadko mine (solid lines) and Yunkom mine (dash line). Figures near curves show values σ_3 . Filled area in Figure 2.2 (a) indicates condition of embrittlement (Alexeev et al., 2008).

that the generation of tunnel surface parallel fractures (onion skins, spalling and slabbing) is attribute to the existence of moderate intermediate principal stress and low to zero minimum confinement (Figure 2.17). Material heterogeneity also plays a major role as local tensile stresses need to be generated for crack initiation and propagation. The intermediate principal stress confines the rock in such a way that fractures can only be developed in the direction parallel to σ_1 and σ_2 . This fracturing process changes the rock behavior from the original isotropic state to an anisotropic

You (2008) reviewed some strength criteria which include the role of the intermediate principal stress, and proposed a new criterion. Strength criteria of the form $\sigma_{oct} = f_n(\sigma_{oct})$, such as Drucker–Prager represent a rotation surface in the principal stress space, symmetric to the line $\sigma_1 = \sigma_2 = \sigma_3$ in the meridian plane. Because $\sigma_{oct} = f_n(\sigma_{oct})$ must fit the pseudo-triaxial compressive strength, it will have a non-physical outcome for triaxial extension. Mogi's criteria, $\sigma_{oct} = g_1(\sigma_{m,2})$ and $\sigma_{max} = g_2(\sigma_b)$ are able to fit experimental data reasonably well, but the prediction

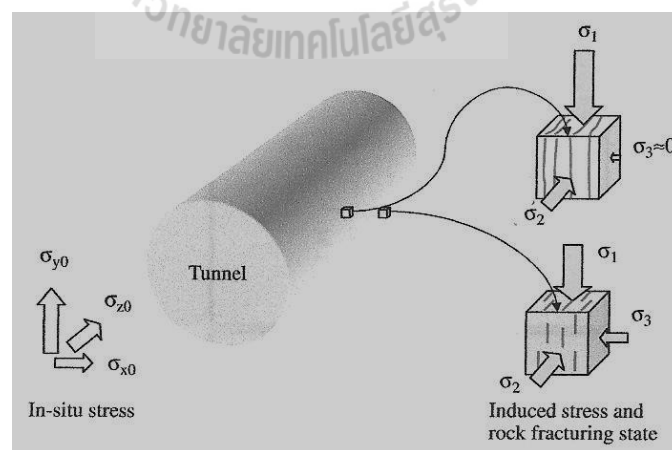


Figure 2.16 Stress and rock fracturing condition near the tunnel boundary σ_{x0} , σ_{y0} and σ_{z0} are the far field stress components (Cai, 2008).

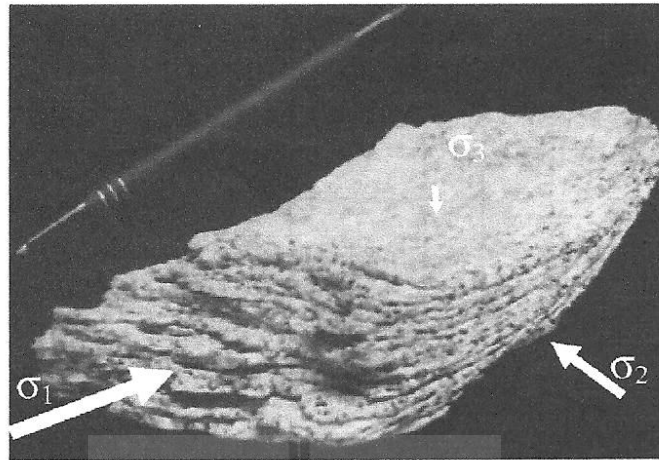


Figure 2.17 A granite slab show the layered fracturing that occurred at the Mine-by tunnel (depth 420 m) at URL. The stress-induced fractures are parallel to the tunnel surface. The orientation of local in situ σ_1 , σ_2 (45 MPa), and σ_3 ($\sigma_3 \approx 0$) are illustrated in the figure (Cai, 2008).

of strength is not good and sometimes problematic. Strength criterion with the form $\lambda(\sigma_1, \sigma_2, \sigma_3) = F[\eta(\sigma_1, \sigma_2, \sigma_3)]$, or a curve of two variables which can be decided by fitting pseudo-triaxial experimental data, is not expected to describe the strength under various stress states, no matter how high the correlation coefficient of λ and η is, or how low the misfit of the equation $\lambda = F(\eta)$ is, as these seemingly good correlations usually result from the dominant influence of the maximum principal stress in the metrics of λ and η . The intermediate principal stress may improve the strength of rock specimen, but its influence will be restricted by σ_3 . Also when σ_2 is high enough to cause failure in the $\sigma_2 - \sigma_3$ direction, the strength will decrease with the increasing σ_2 . The new strength criterion with exponent form has just such a character, and gives much lower misfits than do all seven criteria discussed by

Colmenares and Zoback (2002). A statistical evaluation of intact rock failure criteria constrained by polyaxial test data for five different rocks.

Walsri et al. (2009) developed polyaxial load frame (Figure 2.18) to determine the compressive and tensile strengths of three types of sandstone under true triaxial stresses. Results from the polyaxial compression tests on rectangular specimens of sandstones suggest that the rocks are transversely isotropic. The measured elastic modulus in the direction parallel to the bedding planes is slightly greater than that normal to the bed. Poisson's ratio on the plane normal to the bedding planes is lower than those on the parallel ones. Under the same σ_3 , σ_1 at failure increases with σ_2 . Results from the Brazilian tension tests under axial compression reveal the effects of the intermediate principal stress on the rock tensile strength. The Coulomb and modified Wiebols and Cook failure criteria derived from the characterization test results predict the sandstone strengths in term of $J_2^{1/2}$ as a function of J_1 under true triaxial stresses. The modified Wiebols and Cook criterion describes the failure stresses better than does the Coulomb criterion when all principal stresses are in compressions. When the minimum principal stresses are in tension, the Coulomb criterion over-estimate the second order of the stress invariant at failure by about 20% while the modified Wiebols and Cook criterion fails to describe the rock tensile strengths.

Sriapai et al. (2011) have used polyaxial load frame to determine true triaxial compressive strength of Maha Sarakham (MS) salt. The load frame equipped with two pairs of cantilever beam is used to apply the constant lateral stress (σ_2 and σ_3) to salt specimen while the axial stress (σ_1) is increased at 0.5-1.0 MPa/s until failure occurs.

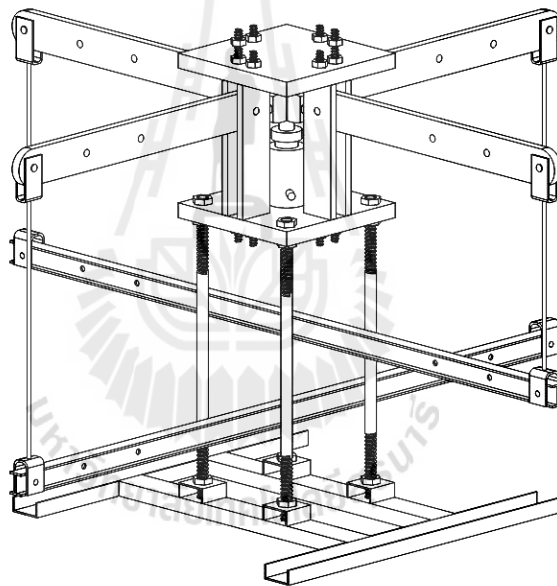
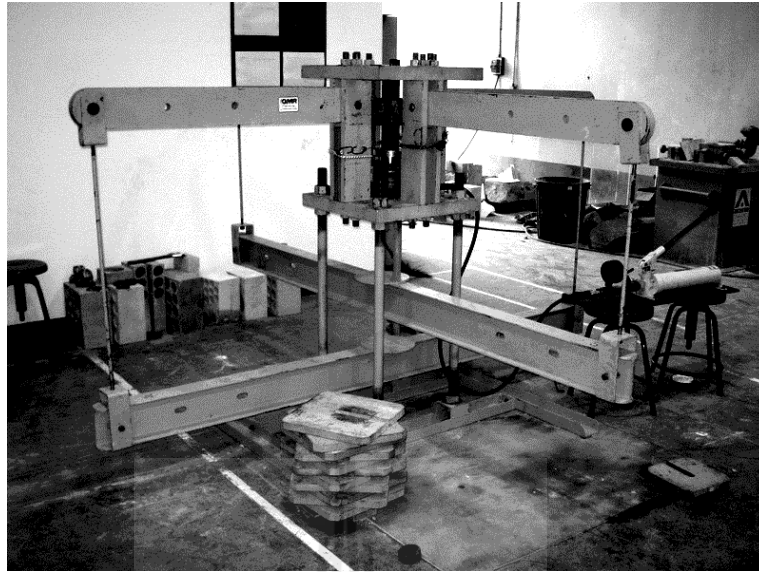


Figure 2.18 Polyaxial load frame developed for rock testing under true triaxial stresses (Walsri et al., 2009).

The deformations induced along the three loading directions are monitored and used to calculate the tangent elastic modulus and Poisson's ratio of the salt. For the Coulomb criterion the internal friction angle determined from the triaxial loading condition ($\sigma_2 = \sigma_3$). The effect σ_2 of on the salt strengths can be best described by the

modified Wiebols and Cook criterion. The empirical (power law) Mogi criterion tends to underestimate the salt strengths particularly under high σ_3 values. The modified Lade criterion overestimates the actual strengths at all levels of σ_3 . The Coulomb and Hoek and Brown criteria can not describe the salt strengths beyond the condition where $\sigma_2 = \sigma_3$, as they can not incorporate the effects of σ_2 . Both circumscribed and inscribed Drucker-Prager criteria severely underestimate σ_1 at failure for all stress conditions.



CHAPTER III

SAMPLE PREPARATION

3.1 Introduction

This chapter describes the rock sample preparation. The rock samples used in this study are sandstones and travertine. The tested sandstones are from three sources: PhuPhan (PP), PhraWihan (PW) and PhuKradung (PK) formations (Boonsener and Sonpirom, 1997). These three types of sandstone are homogeneous with soft to medium strength and their typical colors are yellowish, white and greenish respectively, as shown in Figure 3.1. These fine-grained quartz sandstones are selected primarily because of their highly uniform texture, density and strengths. The main mineral compositions of these three sandstones obtained by x-ray diffraction analyses are given in Table 3.1. Their average grain size is 0.1-1.0 mm. They are commonly found in the north and northeast of Thailand. Their mechanical properties and responses play a significant role in the stability of tunnels, slope embankments and dam foundations in this region.

Another type of rock used as rock specimens is travertine (Bunopas, 1992). This travertine specimen is homogeneous with compact to earthy texture and it is composed almost wholly of calcite. Its testing results will be used to further compare and analyze.

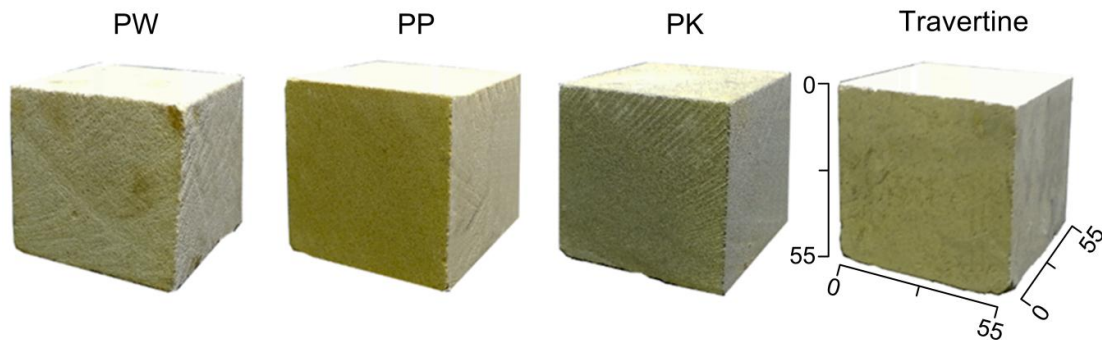


Figure 3.1 Sandstones and travertine specimens with nominal size of $55 \times 55 \times 55$ mm³, collected from Saraburi province.

Table 3.1 Mineral compositions of three sandstones (Walsri, 2009).

Rock Types	Density (g/cc)	Color	Composition				
			Quartz (%)	Albite (%)	Kaolinite (%)	Feldspar (%)	Mica (%)
PW sandstone	2.35	white	99.47	-	0.53	-	-
PP sandstone	2.45	yellow	98.40	-	-	-	1.60
PK sandstone	2.63	green	48.80	46.10	5.10	-	-

3.2 Sample preparation

Sandstone and travertine samples are collected from Saraburi province. These sandstone and travertine samples are prepared to obtain cubical specimens of the nominal sizes of $55 \times 55 \times 55$ mm³ for the biaxial and polyaxial compression tests (Figure 3.1). A minimum of 40 specimens are prepared for each rock type. Tables 3.2 through 3.7 shows the dimensions and weights of the specimens.

Table 3.2 Phu Phan specimens prepared for biaxial tests.

Specimen No.	Weigh (g)	Dimension (mm ³)	Dry density (g/cc)
PP-Bai-01	443.50	55.00×55.00×54.98	2.67
PP-Bai-02	444.36	54.98×54.98×54.89	2.68
PP-Bai-03	445.76	54.89×54.89×55.03	2.68
PP-Bai-04	444.64	55.02×54.96×54.87	2.68
PP-Bai-05	443.26	55.04×55.03×54.93	2.66
PP-path-06	444.28	54.96×54.93×54.92	2.68
PP-path-07	445.68	55.03×54.92×54.67	2.70
PP-path-08	446.87	54.87×54.67×54.92	2.71
PP-path-09	446.52	54.93×50.05×54.67	2.69
PP-path-10	442.40	54.92×55.00×55.30	2.65

Table 3.3 Phra Wihan specimens prepared for biaxial tests.

Specimen No.	Weigh (g)	Dimension (mm ³)	Dry density (g/cc)
PW-Bai-01	429.89	55.00×54.92×50.05	2.62
PW-Bai-02	429.00	54.98×54.67×54.89	2.60
PW-Bai-03	430.00	54.89×55.04×55.03	2.59
PW-Bai-04	431.93	54.96×55.00×54.87	2.60
PW-Bai-05	431.00	55.03×54.98×54.93	2.59
PW-Bai-06	430.80	54.93×54.89×54.92	2.60
PW-path-07	430.59	54.92×55.02×54.67	2.61
PW-path-08	328.90	54.67×54.67×54.92	2.58
PW-path-09	429.78	55.04×50.05×54.67	2.62
PW-path-10	428.97	55.00×54.89×54.87	2.59
PW-path-11	431.50	54.98×55.03×54.93	2.60
PW-path-12	430.43	54.89×54.87×54.92	2.60

Table 3.4 Phu Kradung specimens prepared for biaxial tests.

Specimen No.	Weigh (g)	Dimension (mm³)	Dry density (g/cc)
PK-Bai-01	441.30	55.03×54.87×55.21	2.65
PK-Bai-02	441.00	54.87×54.93×54.89	2.67
PK-Bai-03	441.90	54.93×54.92×55.03	2.66
PK-Bai-04	442.00	54.92×54.67×54.78	2.69
PK-Bai-05	442.80	54.67×54.92×54.86	2.69
PK-Bai-06	443.40	54.92×54.67×54.96	2.69
PK-path-07	440.80	54.67×54.87×54.93	2.68
PK-path-08	441.00	54.87×54.93×55.05	2.66
PK-path-09	441.90	54.93×54.92×55.08	2.66
PK-path-10	442.87	54.92×54.67×54.87	2.69
PK-path-11	442.65	54.67×54.92×54.93	2.68
PK-path-12	442.89	55.04×54.92×54.92	2.67
PK-path-13	442.78	54.92×54.67×54.67	2.70

Table 3.5 Phu Phan specimens prepared for polyaxial compression tests.

Specimen No.	Weigh (g)	Dimension (mm³)	Dry density (g/cc)
PP-Poly-01	444.10	54.67×54.98×54.67	2.70
PP-Poly-02	443.47	55.05×54.89×54.98	2.67
PP-Poly-03	445.41	54.34×55.02×55.00	2.71
PP-Poly-04	442.54	55.08×54.67×55.02	2.67
PP-Poly-05	443.73	55.03×54.39×55.04	2.69
PP-Poly-06	446.80	55.00×54.89×54.96	2.69
PP-Poly-07	445.21	54.98×55.03×55.03	2.67
PP-Poly-08	444.87	54.89×54.87×54.87	2.69
PP-Poly-09	443.94	54.96×54.93×54.93	2.68
PP-Poly-10	444.27	55.03×54.92×54.92	2.68
PP-Poly-11	443.73	54.93×54.67×54.67	2.70
PP-Poly-12	443.52	54.92×54.92×50.05	2.67
PP-Poly-13	445.01	54.67×54.67×54.34	2.74
PP-Poly-14	444.87	55.20×55.05×55.08	2.92
PP-Poly-15	444.91	55.00×54.93×55.03	2.68
PP-Poly-16	443.60	54.98×54.92×55.00	2.67
PP-Poly-17	443.28	54.89×54.92×54.98	2.67
PP-Poly-18	442.83	55.02×54.67×54.89	2.68
PP-Poly-19	442.78	54.67×55.09×54.96	2.67
PP-Poly-20	443.72	54.79×54.34×55.03	2.71
PP-Poly-21	443.67	54.39×54.93×54.98	2.70
PP-Poly-22	443.55	54.89×54.92×54.89	2.68
PP-Poly-23	443.24	55.03×54.92×54.93	2.67
PP-Poly-24	443.32	54.87×54.67×54.92	2.69
PP-Poly-25	444.03	54.93×55.09×54.92	2.67

Table 3.6 Phu Kradung specimens prepared for polyaxial compression tests.

Specimen No.	Weigh (g)	Dimension (mm³)	Dry density (g/cc)
PK-Poly-01	441.87	55.02×54.93×54.67	2.67
PK-Poly-02	441.00	54.67×54.92×55.04	2.67
PK-Poly-03	441.02	55.05×54.67×55.00	2.66
PK-Poly-04	441.34	54.89×54.92×54.98	2.66
PK-Poly-05	440.98	55.03×54.67×54.89	2.67
PK-Poly-06	440.89	54.87×54.87×55.02	2.66
PK-Poly-07	441.87	54.93×54.93×54.67	2.68
PK-Poly-08	441.59	54.92×54.92×55.05	2.66
PK-Poly-09	442.02	54.67×54.67×54.89	2.69
PK-Poly-10	442.65	54.92×54.92×55.03	2.67
PK-Poly-11	441.48	54.67×54.67×54.92	2.69
PK-Poly-12	440.57	54.98×54.98×54.92	2.65
PK-Poly-13	441.32	54.93×54.92×55.02	2.66
PK-Poly-14	441.93	54.92×54.67×54.67	2.69
PK-Poly-15	442.37	54.92×55.04×55.05	2.66
PK-Poly-16	442.16	54.67×55.00×54.89	2.68
PK-Poly-17	440.98	54.98×54.98×55.03	2.65
PK-Poly-18	440.91	54.34×54.89×54.87	2.69
PK-Poly-19	441.43	54.93×54.98×54.92	2.66
PK-Poly-20	441.98	54.92×54.89×54.89	2.67
PK-Poly-21	442.98	54.67×55.02×55.03	2.68
PK-Poly-22	423.02	55.04×54.67×54.92	2.56
PK-Poly-23	442.54	55.00×55.05×54.92	2.66
PK-Poly-24	443.23	54.98×54.89×55.02	2.67
PK-Poly-25	441.98	54.89×55.03×54.67	2.68

Table 3.7 Travertine specimens prepared for polyaxial compression tests.

Specimen No.	Weigh (g)	Dimension (mm³)	Dry density (g/cc)
TT-Poly-01	400.00	55.00×54.87×50.05	2.41
TT-Poly-02	401.50	54.98×54.93×54.89	2.42
TT-Poly-03	401.32	54.89×54.92×55.03	2.42
TT-Poly-04	399.89	55.02×54.67×54.87	2.42
TT-Poly-05	398.90	55.04×54.92×54.93	2.40
TT-Poly-06	402.13	54.96×54.67×54.92	2.44
TT-Poly-07	401.97	55.03×54.87×54.67	2.44
TT-Poly-08	400.75	54.87×54.93×54.92	2.42
TT-Poly-09	399.54	54.93×54.92×54.67	2.42
TT-Poly-10	400.23	54.92×54.67×54.87	2.43
TT-Poly-11	399.82	54.67×54.92×54.93	2.42
TT-Poly-12	398.96	55.05×54.92×54.92	2.40
TT-Poly-13	401.34	54.34×54.67×54.67	2.47
TT-Poly-14	402.39	55.08×54.87×55.04	2.42
TT-Poly-15	402.23	55.03×54.93×55.00	2.42
TT-Poly-16	401.45	55.00×54.92×54.98	2.42
TT-Poly-17	400.75	54.98×54.67×54.89	2.43
TT-Poly-18	401.58	54.89×55.04×55.02	2.42
TT-Poly-19	399.92	54.96×54.87×54.67	2.43
TT-Poly-20	402.31	55.03×54.93×55.05	2.42
TT-Poly-21	401.43	54.93×54.92×54.89	2.42
TT-Poly-22	400.82	54.92×54.67×55.03	2.43
TT-Poly-23	399.93	54.67×54.92×54.92	2.43
TT-Poly-24	399.87	55.20×54.67×54.92	2.41
TT-Poly-25	400.89	55.00×54.87×55.02	2.41

CHAPTER IV

TRUE TRIAXIAL LOADING DEVICE

4.1 Introduction

The true triaxial loading device is developed to test rock specimens under biaxial and polyaxial stress states. This device is designed for a true triaxial load frame. Its performance is assessed by conducting both biaxial and true triaxial compression tests to determine the compressive strengths and elastics of rock specimens with soft to medium strengths. The influence of the intermediate principal stress on rock failure is investigated. At the beginning, the loading device is developed to be a biaxial load frame for the biaxial compression tests. This load frame is then further modified by adding another set of loading frame in a vertical position, making it becomes a true triaxial loading device. This chapter describes the design requirements, the components of the true triaxial load frame and the calculation of factor of safety of the main components.

4.2 Design requirements and components

The functional requirements for the true triaxial loading device which is modified from the biaxial load frame are: (1) capable of exerting load up to 50 tons to the rock specimens, (2) capable of providing the intermediate principal stress ranging 0 to 100 MPa for $5.5 \times 5.5 \times 5.5 \text{ cm}^3$ specimens and (3) allowing the measurements of specimen deformations along the principal axes.

4.2.1 Biaxial load frame

Figures 4.1 through 4.3 show two steel cross load frames (frame A and B), the main parts of the biaxial rock testing device.

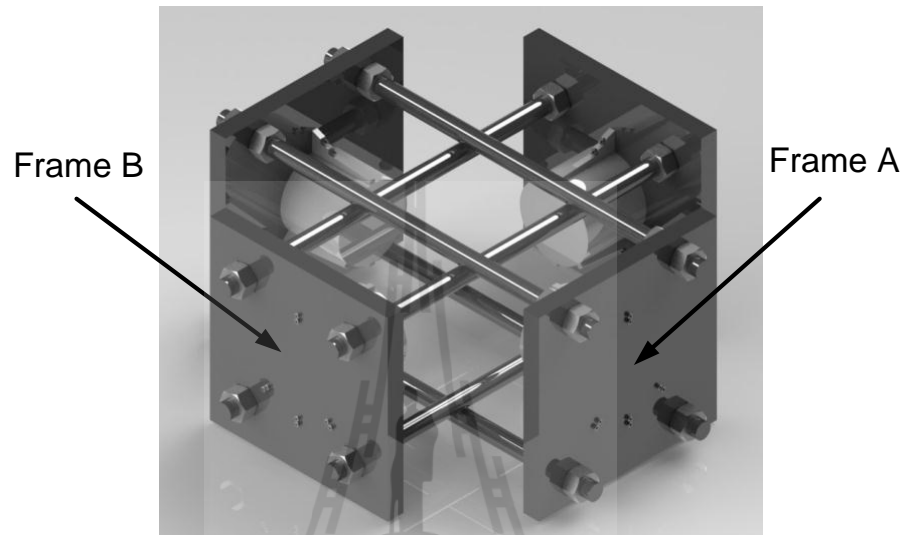


Figure 4.1 Two steel cross load frames (frame A and B), the main parts of the biaxial rock.

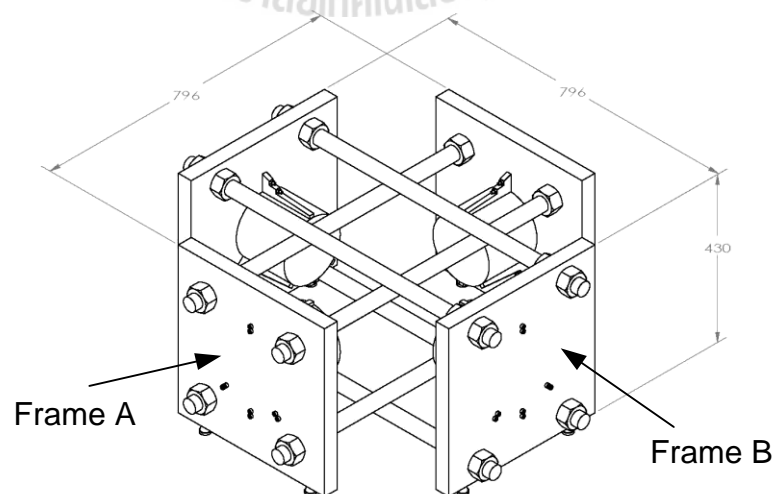


Figure 4.2 Two steel cross load frames (frame A and B) with dimensions.

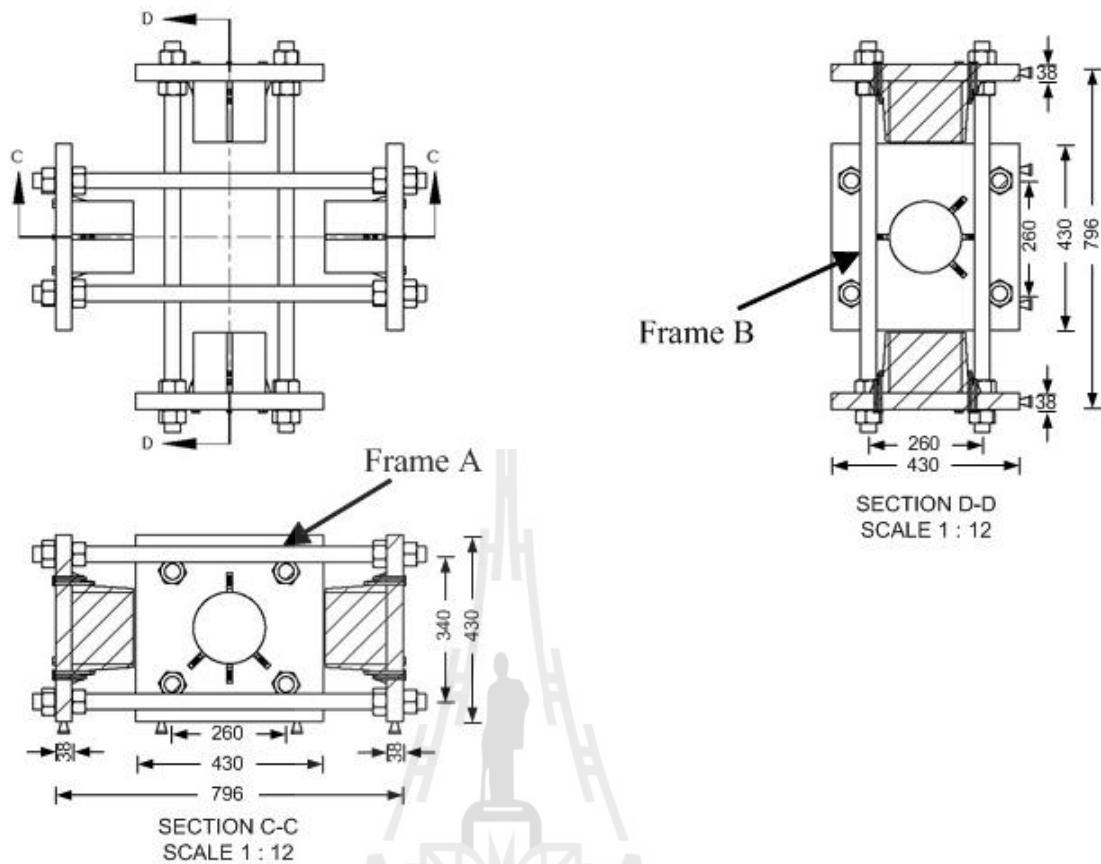


Figure 4.3 Steel cross load frames with detailed sections.

This device comprises three main components: two steel cross load frames, four hydraulic load cells and two hand pumps (Figures 4.4 and 4.5). Each load frame has two thick supporting steel plates, connected by four steel rods. They support the structures of the two load cells (Figure 4.4). The four load cells, installed at the supporting plates, are connected to two hand pumps with the capacity of 1000 kN. Besides the three main parts, other accessories designed to measure and monitor the rock stresses and deformations during testing include two 4-inch pressure gauges and three dial gauges (Figure 4.5). The two pressure gauges are installed at two

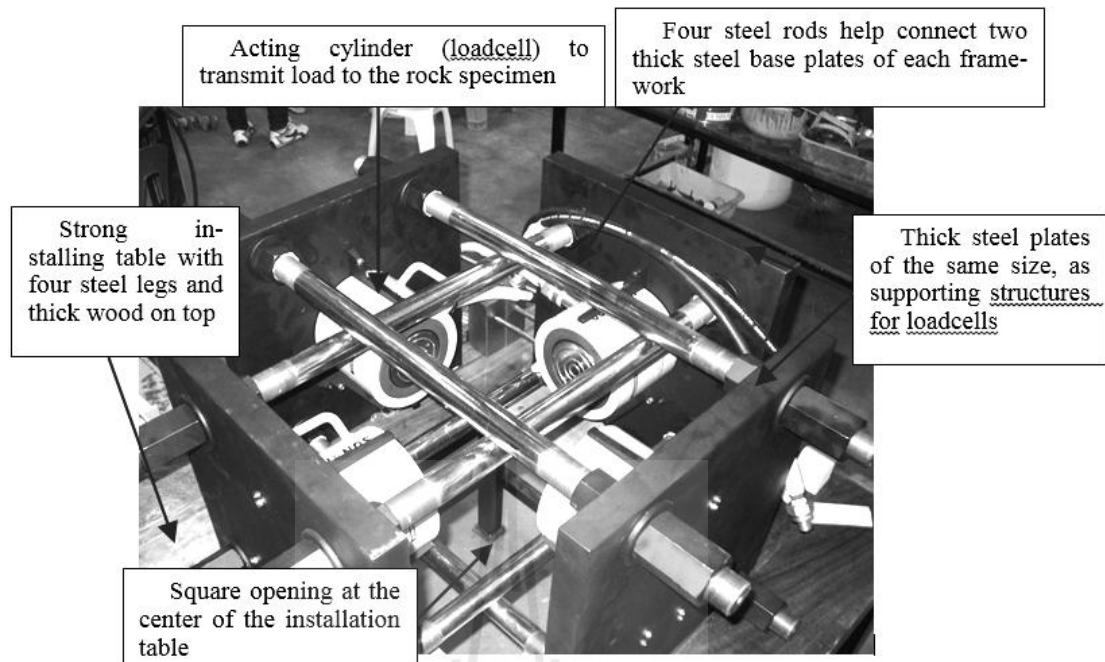


Figure 4.4 Biaxial rock testing device made from two crossed steel frames, main components.

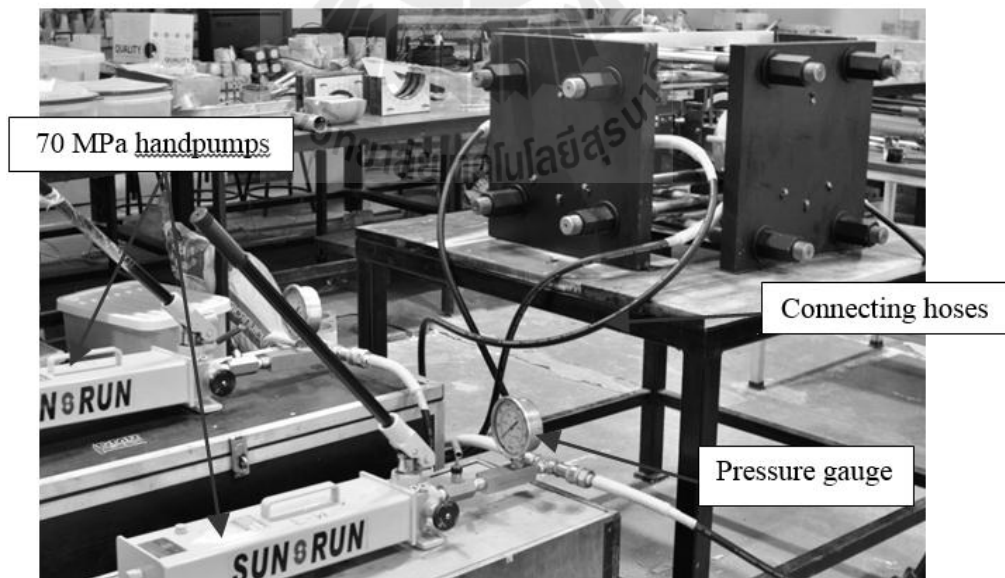


Figure 4.5 Components of biaxial rock testing devices: main components and accessories.

hand pumps to measure the applied load, while the three dial gauges measure the deformations along the principal axes for further strain calculation.

4.2.2 Polyaxial loading device

Figure 4.6 shows the general isometric drawing of the true triaxial loading device. The above biaxial load frame is further modified to become the true triaxial loading device by inserting vertically the third set of load frame into this crossed load frame. This inserted set is installed on the steel support and the hand pump with other accessories (e.g. pressure gauges, hoses) is equipped similarly to the installation of the biaxial load frame. During the test each set of the frame will apply the independent loads to provide different principal stresses ($\sigma_1 \neq \sigma_2 \neq \sigma_3$) onto the rock specimens (Figure 4.7). This loading device can accommodate the cubic or rectangular specimens of different sizes by adjusting the distances between the opposite steel loading platens. For this research, the rock specimens have the nominal size of $5.5 \times 5.5 \times 5.5 \text{ cm.}^3$, placed around the center of this device.

4.3 Calculation of factor of safety

The true triaxial loading device is mainly the load frames that are made of structural steel. The properties of this material are based on ASTM-A36 as shown in Table 4.1. Two major components of the frames that need the calculation of factor of safety are the supporting steel plates and the connecting steel rods. The following detailed calculation of factor of safety is based on the load frames A and B, the main components of the biaxial load frame.

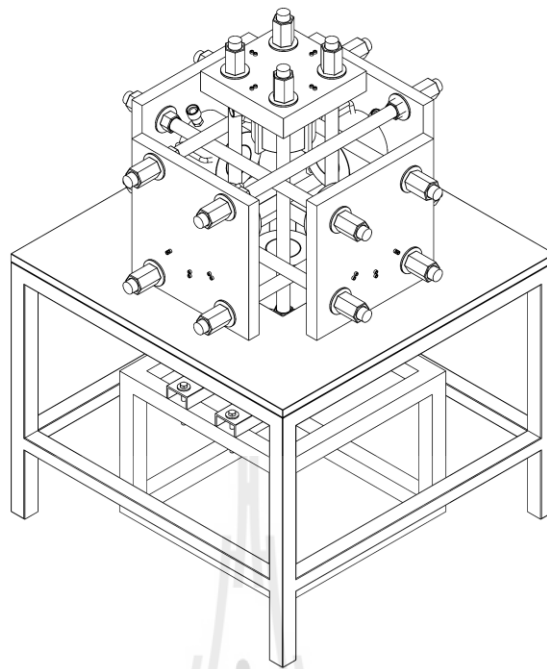


Figure 4.6 General isometric drawing of the true triaxial loading device.

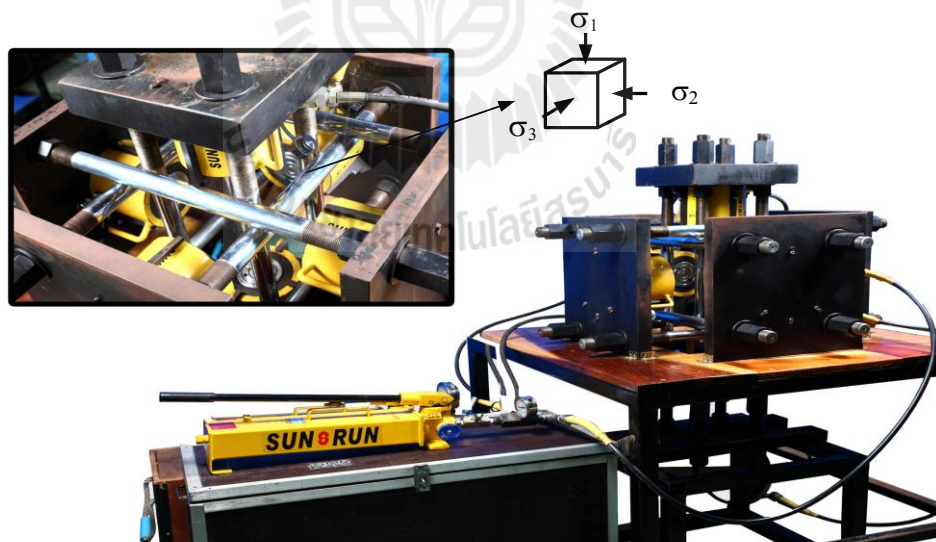


Figure 4.7 Typical picture of polyaxial loading device during the true triaxial test.

Table 4.1 Mechanical properties of structural steel based on ASTM-A36 (Hibbeler, 2008).

Density (Mg/m ³)	Poisson's Ratio (ν)	Modulus of Elasticity (GPa)	Modulus of Rigidity (GPa)	Yield Strength (MPa)		Ultimate Strength (MPa)	
				Tens	Com	Tens	Com
7.85	0.32	200	75	250	250	400	400

4.3.1 Calculation of factor of safety of supporting steel plates

The factor of safety of supporting steel plates under stress is calculated in details below.

$$\text{Factor of safety} = \frac{\text{The yield strength of supporting steel plate } (S_Y)}{\text{The maximum working stress } (\sigma_w)} \quad (4.1)$$

The value S_Y based on ASTM-A36 as shown in Table 4.1 is 250 MPa and the maximum working stress is calculated by:

$$\sigma_w = \frac{\text{Maximum working force}}{\text{Area of supporting steel plate}} \quad (4.2)$$

The maximum force for each supporting steel plate is 1000 kN. The dimensions of each steel plate are 430×430×38 mm, which provides the area of 184,900 mm² (Figures 4.8 and 4.9). Therefore, σ_w is 5.41 MPa. Thus, the factor of safety of supporting steel plate is 46.21.

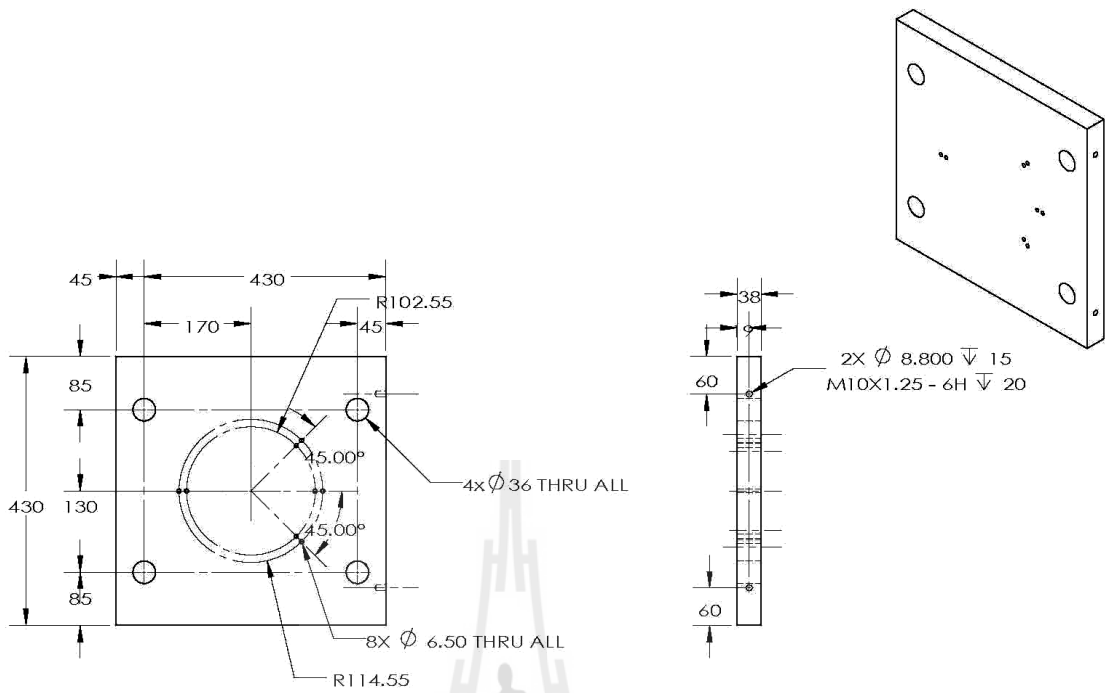


Figure 4.8 Detailed drawing of supporting steel plates for frame A.

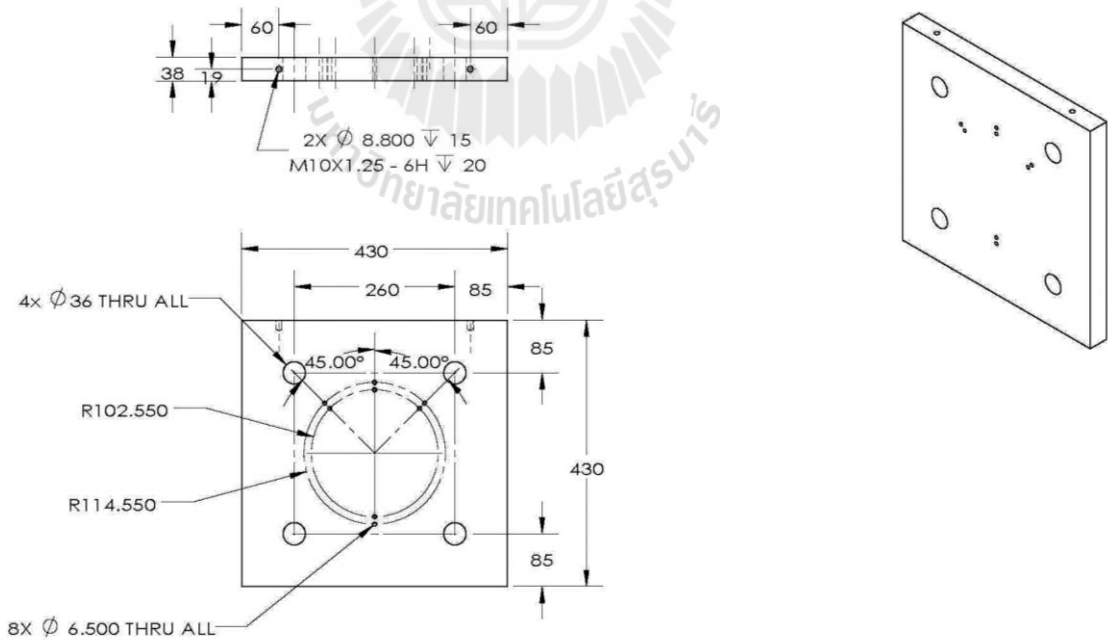


Figure 4.9 Detailed drawing of supporting steel plates for frame B.

4.3.2 Calculation of factor of safety of connecting steel rod

The factor of safety of connecting steel rod under stress condition is calculated in details below.

$$\text{Factor of safety} = \frac{\text{Critical loading stress of connecting steel rod } (\sigma_{cr})}{\text{Maximum working stress } (\sigma_w)} \quad (4.3)$$

The critical loading stress is calculated by using below formula (Hibbeler, 2008).

$$\sigma_{cr} = \frac{\pi^2 E}{(L_e/r)^2} \quad (4.4)$$

Young modulus (E) is 200 GPa (Table 4.1). The effective length of steel rod (L_e) is 440 mm. and the rod diameter is 36 mm. (Figure 4.10). The radius of gyration (r) is calculated as follows (Hibbeler, 2008).

$$r = (I / A)^{1/2} \quad (4.5)$$

$$I = \frac{\pi d^2}{64} \quad (4.6)$$

$$A = \frac{\pi d^4}{4} \quad (4.7)$$

The radius r is 9.0 mm. and the critical loading stress of connecting steel rod σ_{cr} is 825.87 MPa.

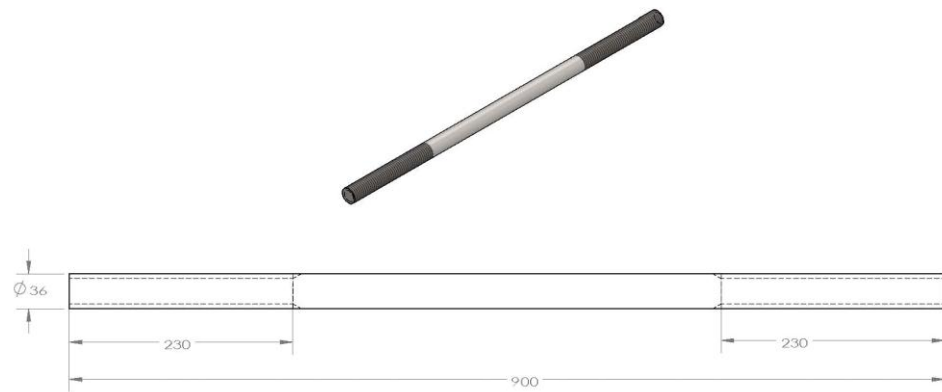


Figure 4.10 Detailed drawing of the connecting steel rod.

$$\sigma_w = \frac{\text{Maximum working load (F)}}{\text{Area of connecting steel rod (A)}} \quad (4.8)$$

The maximum working load of each connecting steel rod is 250 kN and the rod area is 1017.88 mm². The maximum working stress is 245.61 MPa. The factor of safety of each connecting steel rod is 3.36.

CHAPTER V

BIAXIAL COMPRESSION TESTS

5.1 Introduction

The objective of this research is to determine the compressive strengths of rock having soft to medium strengths subjected to biaxial stress states. Three different stress paths have been applied on this laboratory tests. Their influence on rock failure is investigated. The failure stresses are recorded. The modes of failure are examined and the elastic parameters calculated. This chapter describes the method and results, which include characterization tests and biaxial compression strength tests.

5.2 Biaxial compression tests

The biaxial compression tests are performed to investigate the effects of stress path on the compressive strengths of sandstones and their deformation. The specimens prepared from PP, PK and PW sandstone have the nominal sizes of $5.5 \times 5.5 \times 5.5 \text{ cm}^3$. Three different stress paths have been implemented: (1) σ_1 increases while σ_2 is maintained constant; (2) σ_1 and σ_2 simultaneously increase; and (3) σ_1 increases while σ_2 decreases. For all tests, neoprene sheets are used to minimize the friction at all interfaces between the loading platen and the specimen surfaces (Figure 5.1). The measured deformations of sandstone specimens are used to determine the strains along the principal axes during loading. The failure stresses are recorded and modes of failure are examined (Figure 5.2).

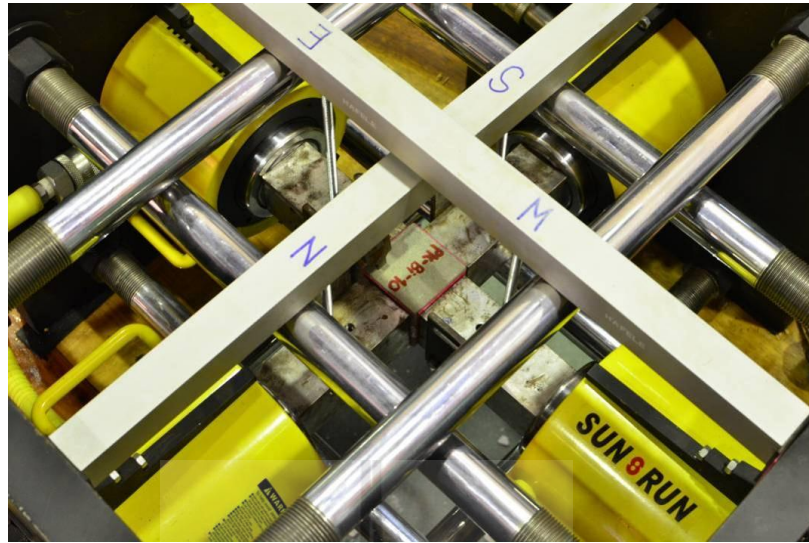


Figure 5.1 The operation during biaxial compression test of PK sandstone specimen.

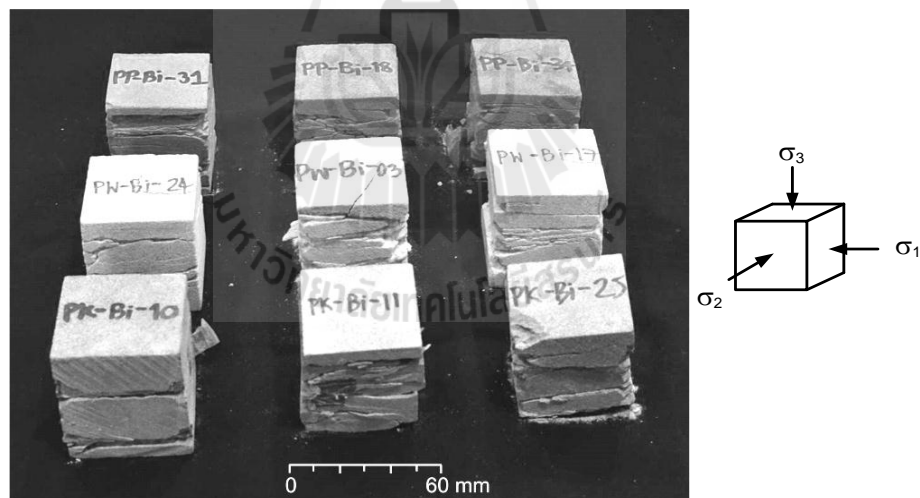


Figure 5.2 Sandstone specimens with multiple extension fractures from induced stresses of σ_1 and σ_2 .

For the first stress path, the intermediate stress (σ_2) is varied from 0 to 70 MPa. For the other two stress paths, the mean stress (σ_m) used in the tests ranges from 10 to 45

MPa. The stress-strain curves obtained from biaxial strength tests are shown in Figures 5.3 through 5.9 for the above stress paths (1), (2) and (3). Assessment of the loading path effect on the rock elasticity is attempted. The calculations of the Poisson's ratios and tangent elastic moduli are made at 50% of the maximum principal stress. The results of the calculations are shown in Tables 5.1 through 5.3. The tables also provide the octahedral shear strength (τ_{oct}), mean stress (σ_m), and the second order of the stress deviation ($J_2^{1/2}$) at failure. These parameters can be calculated from the principal stresses at failure. Multiple extension fractures from induced stressed σ_1 and σ_2 are observed on sandstone specimens (Figure 5.2). The minimum principal stress (σ_3) is zero, therefore the intermediate principal stress (σ_2) and the maximum principal stress (σ_1) confine the sandstone specimens in such a way that fractures can only be developed in the direction parallel to σ_1 and σ_2 . This observed mode of failure agrees with what Cai (2008) studied about the influence of the intermediate principal stress on rock fracturing and strength near excavation boundary, using a FEM/DEM combined numerical tool. At the boundary in an underground setting, the intermediate principal stress is often parallel to the tunnel axis, the minimum principal stress is zero, and the maximum principal stress is the tangential stress. A loading condition of $\sigma_3 = 0$, $\sigma_1 \neq 0$ and $\sigma_2 \neq 0$ thus exists at the boundary. It is seen from the simulation that the generation of tunnel surface parallel fractures (onion skins, spalling and slabbing) attribute to the existence of moderate intermediate principal stress and low to zero minimum confinement.

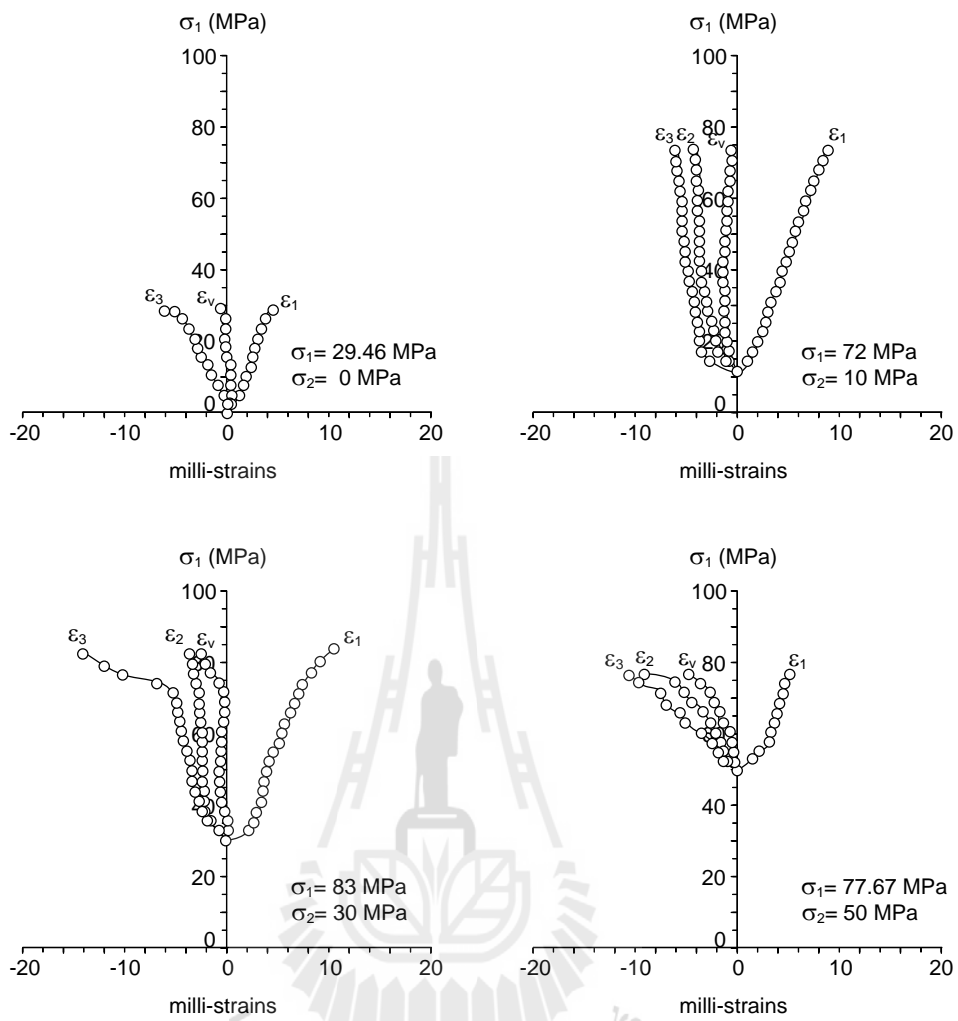


Figure 5.3 Stress-strain curves from biaxial testing of PP sandstone: Stress path (1)

σ_1 increases while σ_2 maintained constant.

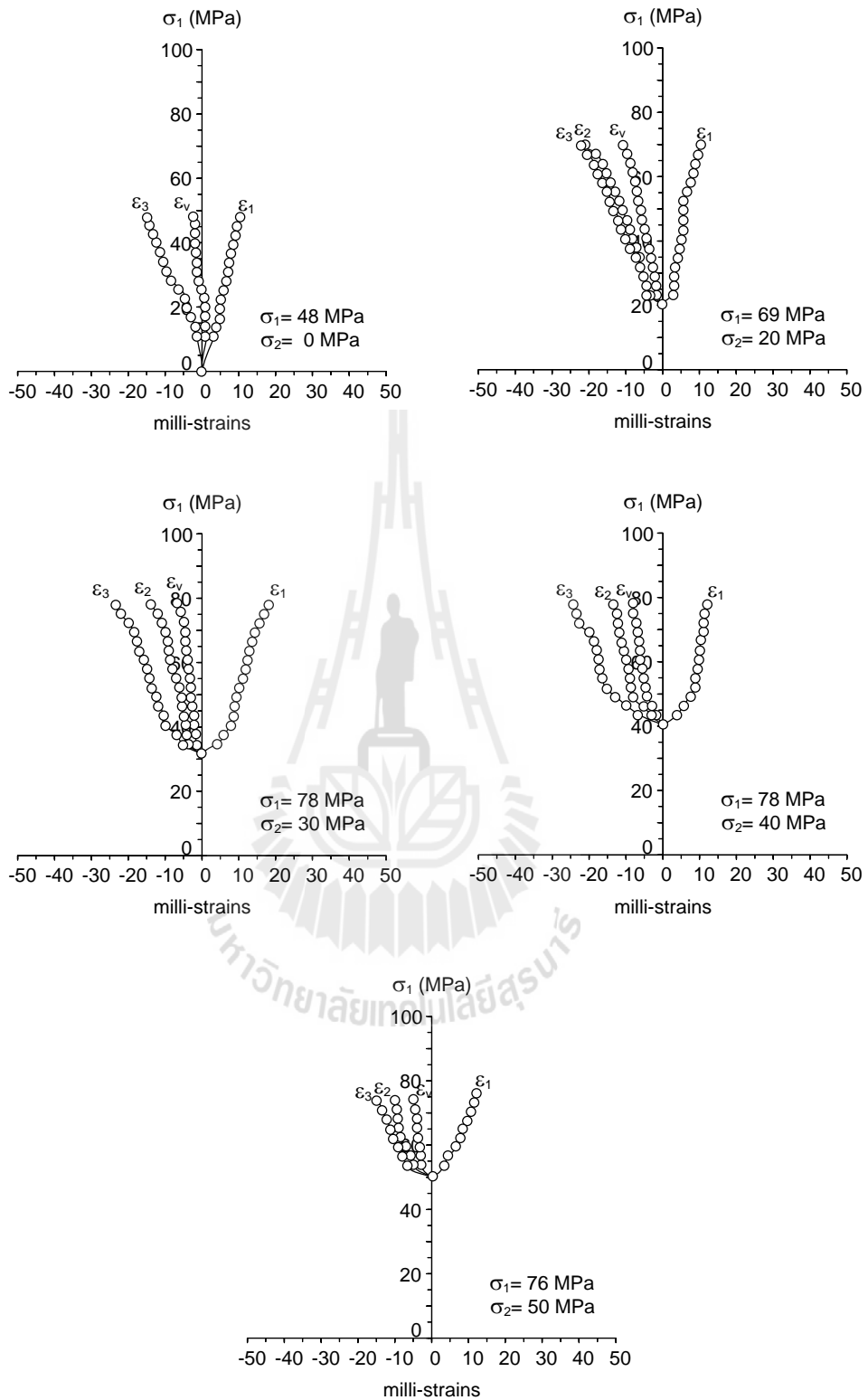


Figure 5.4 Stress-strain curves from biaxial testing of PK sandstone: Stress path (1)

σ_1 increases while σ_2 maintained constant.

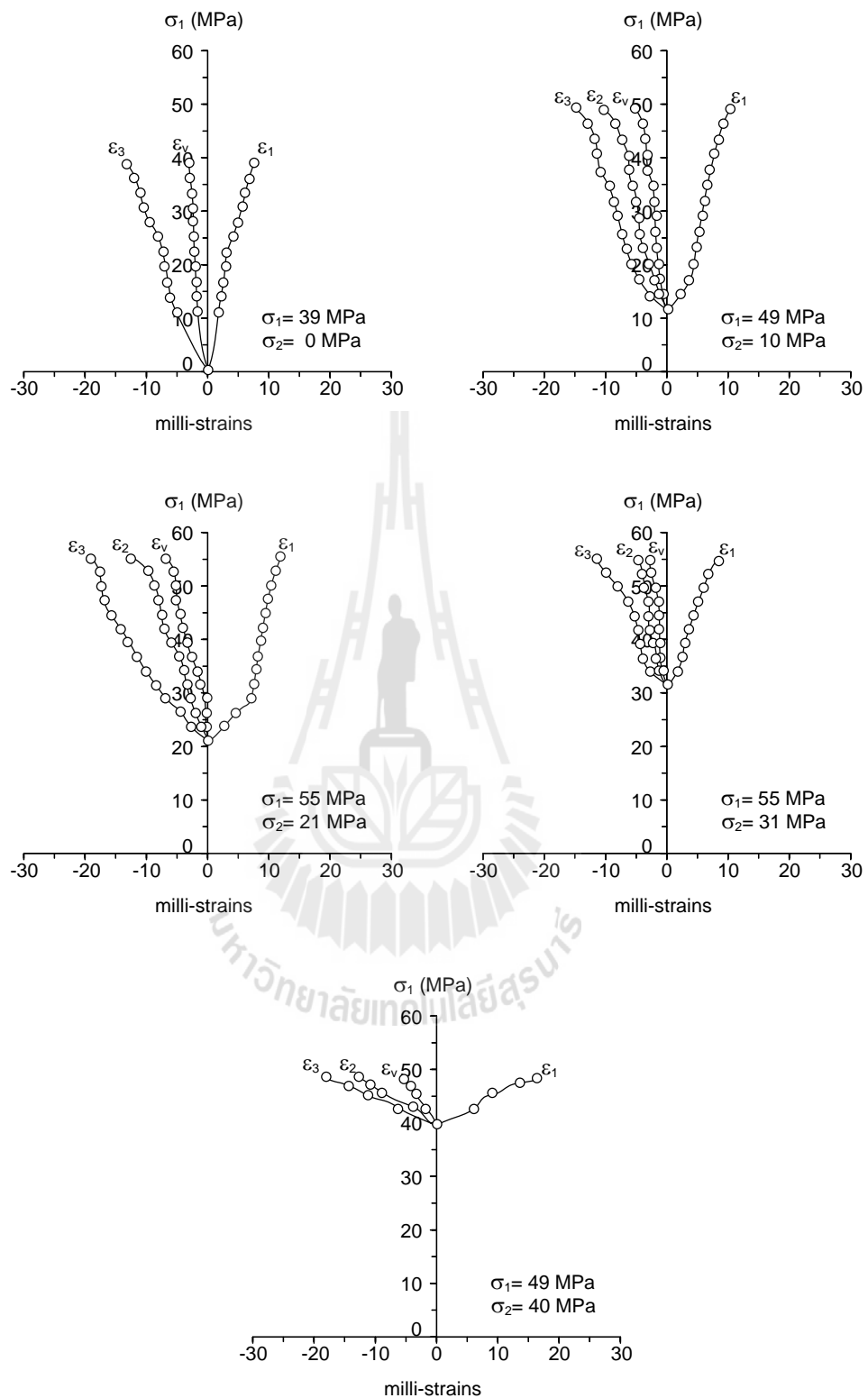


Figure 5.5 Stress-strain curves from biaxial testing of PW sandstone: Stress path (1)

σ_1 increases while σ_2 maintained constant.

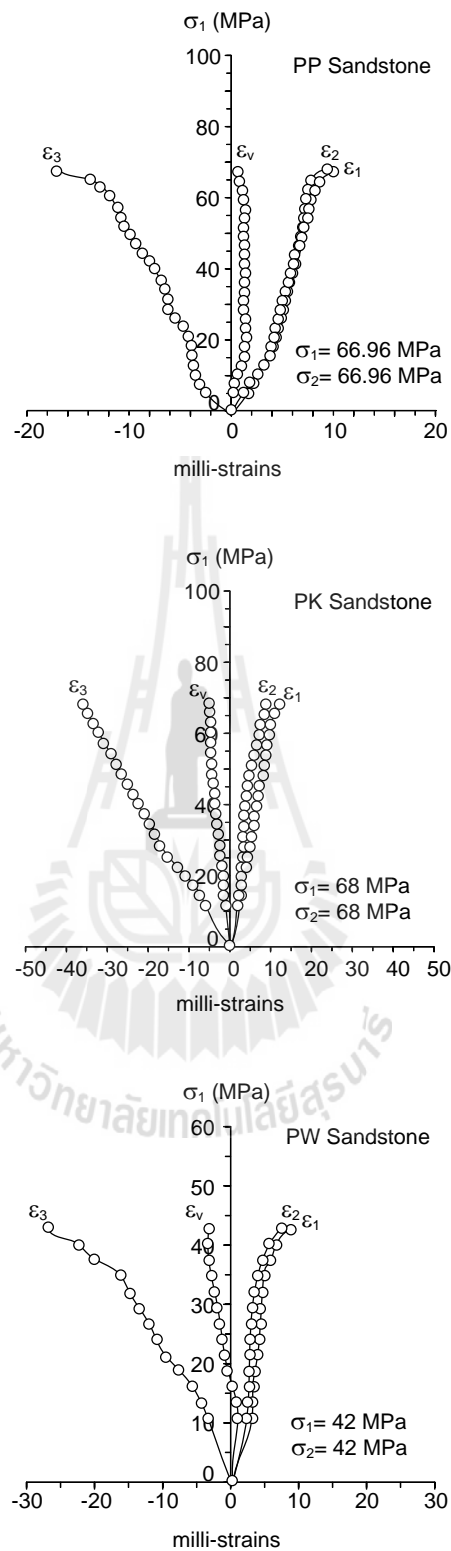


Figure 5.6 Stress-strain curves from biaxial testing of PP, PK and PW sandstones:

Stress path (2) σ_2 and σ_1 simultaneously increase.

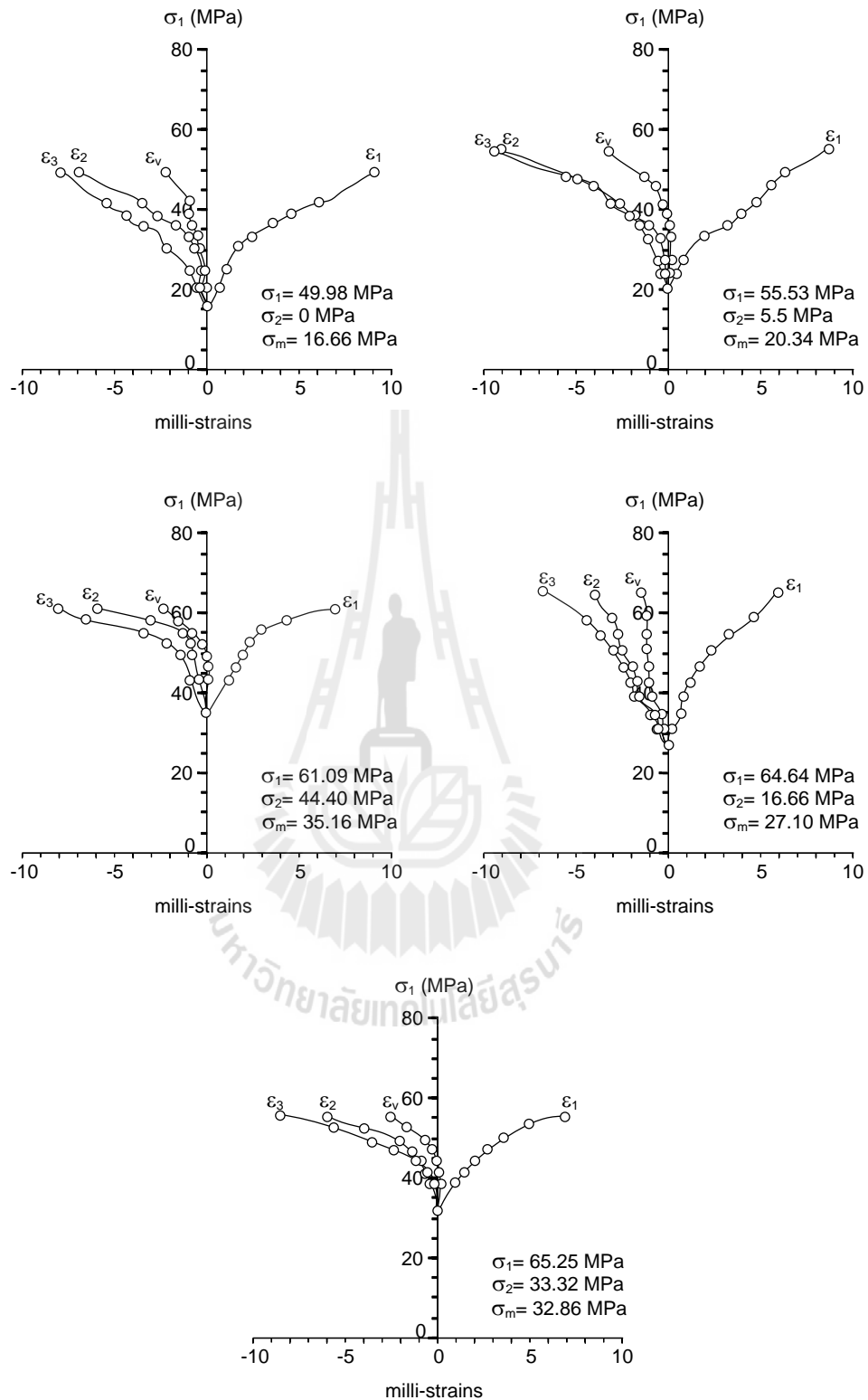


Figure 5.7 Stress-strain curves from biaxial testing of PP sandstone: Stress path (3)

σ_1 increases and σ_2 decreases.

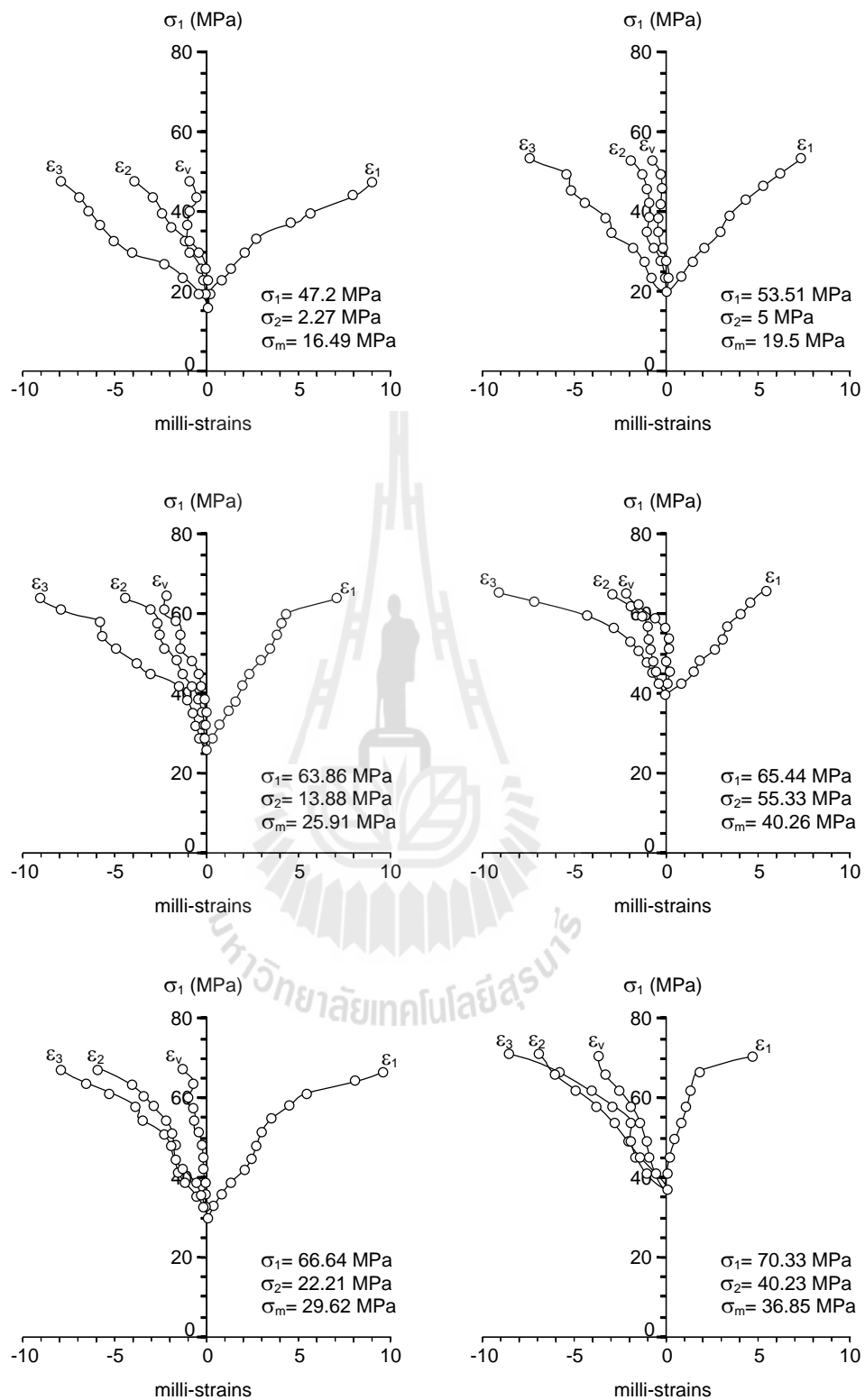


Figure 5.8 Stress-strain curves from biaxial testing of PK sandstone: Stress path (3)

σ_1 increases and σ_2 decreases.

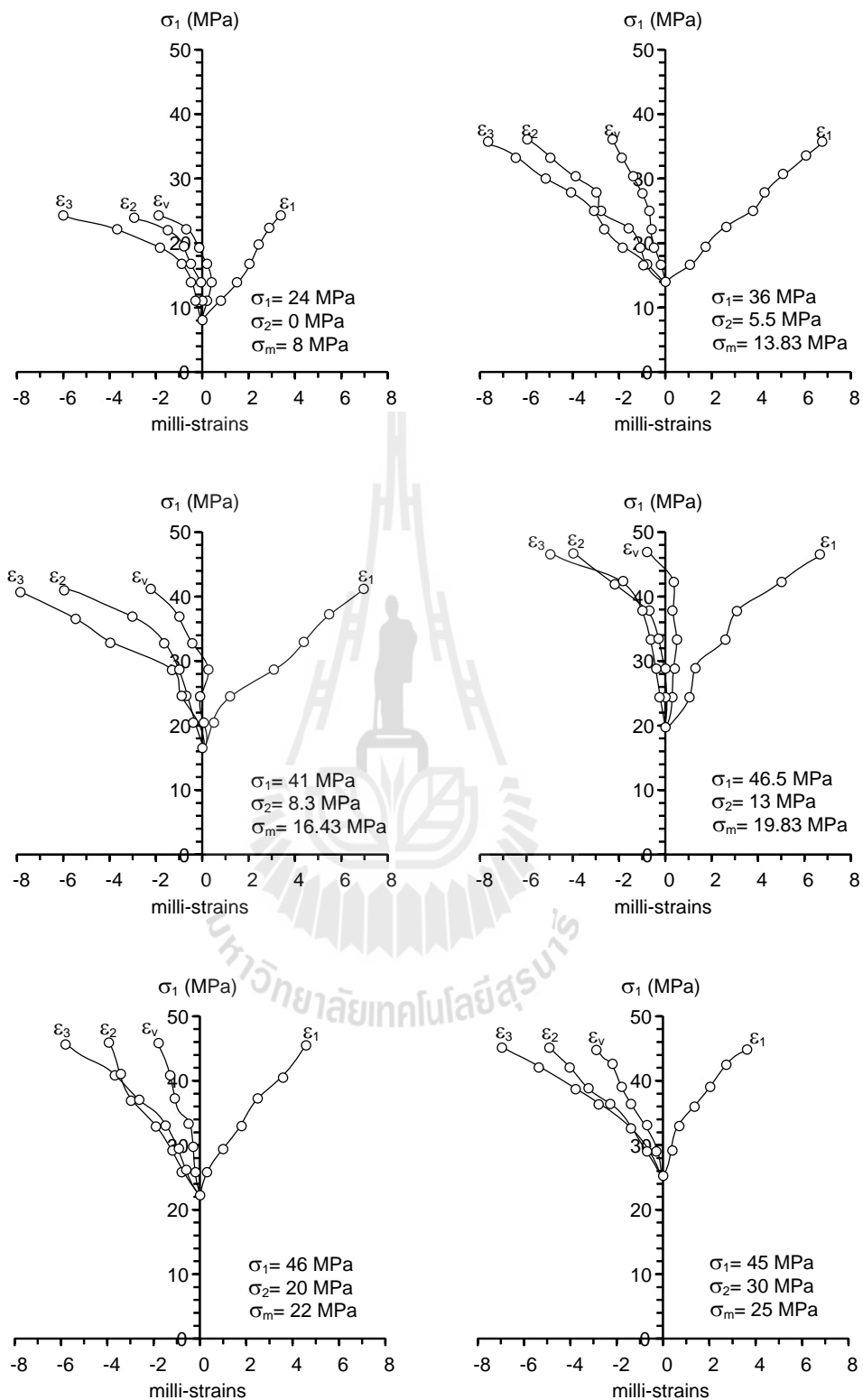


Figure 5.9 Stress-strain curves from biaxial testing of PW sandstone: Stress path (3)

σ_1 increases and σ_2 decreases.

Table 5.1 Compressive strengths and elastic parameters of PP sandstone specimens.

Specimen Number	Failure Stresses			σ_m (MPa)	τ_{oct} (MPa)	$J_2^{1/2}$ (MPa)	Elastic Modulus, E (GPa)	Poisson's Ratio (ν)
	σ_3 (MPa)	σ_2 (MPa)	σ_1 (MPa)					
PP-Bai-01	0.00	0.00	29.46	9.82	13.89	17.01	8.5	0.21
PP-Bai-02	0.00	10.00	72.00	27.33	31.85	39.00	9.1	0.22
PP-Bai-03	0.00	30.00	83.03	37.68	34.33	42.04	9.33	0.25
PP-Bai-04	0.00	50.00	77.67	42.56	32.14	39.37	9.6	0.18
PP-Bai-05	0.00	66.96	66.96	44.64	31.57	38.66	9.8	0.19
PP-path-06	0.00	0.00	49.98	16.66	23.56	28.86	8.7	0.25
PP-path-07	0.00	5.50	55.53	20.34	24.98	30.60	9.7	0.21
PP-path-08	0.00	44.40	61.09	35.16	25.78	31.58	8.3	0.22
PP-path-09	0.00	16.66	64.64	27.10	27.40	33.56	10.2	0.23
PP-path-10	0.00	33.32	65.25	32.86	26.64	32.63	9.20	0.20
Mean \pm Standard Deviation							9.2 \pm 0.6	0.22 \pm 0.02

Table 5.2 Compressive strengths and elastic parameters of PK sandstone specimens.

Specimen Number	Failure Stresses			σ_m (MPa)	τ_{oct} (MPa)	$J_2^{1/2}$ (MPa)	Elastic Modulus, E (GPa)	Poisson's Ratio (ν)
	σ_3 (MPa)	σ_2 (MPa)	σ_1 (MPa)					
PK-Bai-01	0.00	0.00	48.00	16.00	22.63	27.71	7.82	0.21
PK-Bai-02	0.00	20.00	69.00	29.67	28.99	35.50	8.12	0.22
PK-Bai-03	0.00	30.00	78.00	36.00	32.12	39.34	7.98	0.20
PK-Bai-04	0.00	40.00	78.00	39.33	31.85	39.00	8.54	0.23
PK-Bai-05	0.00	50.00	76.00	42.00	31.54	38.63	8.11	0.22
PK-Bai-06	0.00	68.00	68.00	45.33	32.06	39.26	8.23	0.21
PK-path-07	0.00	0.00	38.80	12.93	18.29	22.40	8.18	0.23
PK-path-08	0.00	2.27	47.20	16.49	21.74	26.62	8.32	0.24
PK-path-09	0.00	5.00	53.51	19.50	24.13	29.56	7.22	0.22
PK-path-10	0.00	13.88	63.86	25.91	27.42	33.59	7.44	0.21
PK-path-11	0.00	55.33	65.44	40.26	28.76	35.23	7.86	0.23
PK-path-12	0.00	22.21	66.64	29.62	27.71	33.93	8.23	0.22
PK-path-13	0.00	40.23	70.33	36.85	28.81	35.29	7.55	0.21
Mean \pm Standard Deviation							8.0 \pm 0.4	0.22 \pm 0.01

Table 5.3 Compressive strengths and elastic parameters of PW sandstone specimens.

Specimen Number	Failure Stresses			σ_m (MPa)	τ_{oct} (MPa)	$J_2^{1/2}$ (MPa)	Elastic Modulus, E (GPa)	Poisson's Ratio (ν)
	σ_3 (MPa)	σ_2 (MPa)	σ_1 (MPa)					
PW-Bai-01	0.00	0.00	39.00	13.00	18.38	22.52	8.30	0.23
PW-Bai-02	0.00	10.00	49.00	19.67	21.14	25.89	7.90	0.22
PW-Bai-03	0.00	21.00	55.00	25.33	22.66	27.75	8.43	0.20
PW-Bai-04	0.00	31.00	55.00	28.67	22.51	27.57	7.32	0.21
PW-Bai-05	0.00	40.00	48.97	29.66	21.29	26.07	9.43	0.25
PW-Bai-06	0.00	42.00	42.00	28.00	19.80	24.25	8.77	0.19
PW-path-07	0.00	0.00	24.00	8.00	11.31	13.86	8.45	0.21
PW-path-08	0.00	5.50	36.00	13.83	15.83	19.39	8.67	0.23
PW-path-09	0.00	8.30	41.00	16.43	17.70	21.68	8.37	0.22
PW-path-10	0.00	13.00	46.50	19.83	19.59	23.99	7.98	0.23
PW-path-11	0.00	20.00	46.00	22.00	18.83	23.07	7.93	0.22
PW-path-12	0.00	30.00	45.00	25.00	18.71	22.91	8.11	0.24
Mean \pm Standard Deviation							8.3 \pm 0.5	0.22 \pm 0.02

CHAPTER VI

POLYAXIAL COMPRESSION TESTS

6.1 Introduction

The objective of this study is to examine the influence of stress paths on rock deformation and failure. Polyaxial compression tests are performed on two types of sandstone and travertine to examine the effects of stress paths. Five different stress paths are conducted on this laboratory test. The failure stresses are recorded, the modes of failure examined and the elastic parameters calculated. This chapter describes the methods, results and analysis of the polyaxial compressive strength tests of the rocks.

6.2 Test equipment

The test equipment for the polyaxial compression tests is the true triaxial loading device. Figure 6.1 shows the isometric drawing of the true triaxial loading device (on the right side) and the picture of this device during the tests. This device is developed to test the rock specimens with soft to medium strengths under biaxial and polyaxial stress states. During the test each set of the three load frames will apply independent loads to provide different principal stresses ($\sigma_1 \neq \sigma_2 \neq \sigma_3$) on to the rock specimens. This loading device can accommodate the cubic or rectangular specimens of different sizes by adjusting the distances between the opposite steel loading platens. For this study, the rock specimens have the nominal sizes of $5.5 \times 5.5 \times 5.5 \text{ cm}^3$, placed around the center of the device.

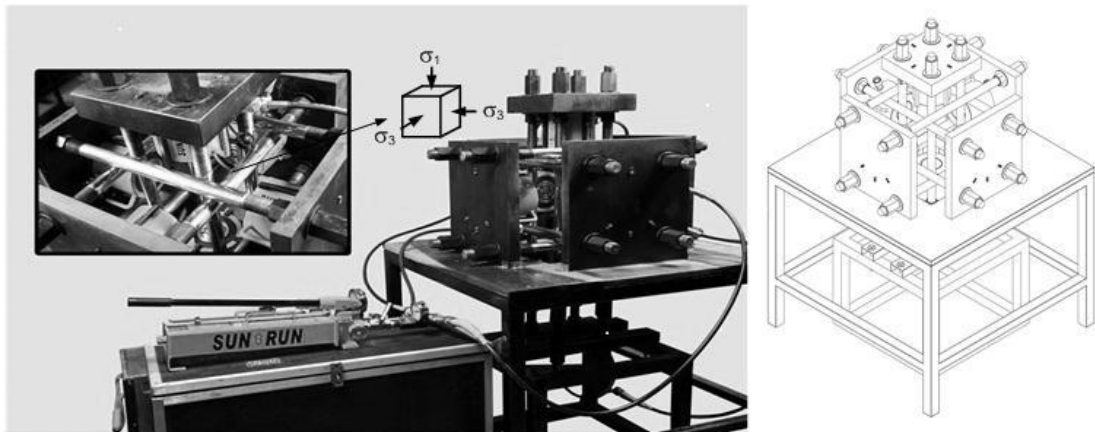


Figure 6.1 Typical picture of polyaxial loading device during the true triaxial test and its general isometric drawing.

The specimens for the polyaxial compression tests are Phu Phan (PP) sandstone, Phu Kradung (PK) sandstone and travertine (TT). Five different stress paths have been implemented to investigate their effects of stress path on the compressive strengths and the deformation of the rocks.

6.3 Polyaxial compression tests

The polyaxial compression tests are performed to investigate the effects of stress paths on the compressive strengths and the deformations of PP, PK and TT. The specimens of the three rock types have the nominal sizes of $5.5 \times 5.5 \times 5.5 \text{ cm}^3$. Five different stress paths have been implemented: (1) σ_1 increases while σ_2 equals σ_3 ; (2) σ_1 increases while σ_2 and σ_3 decrease (σ_m constant); (3) σ_1 and σ_2 equally increase while σ_3 is constant; (4) σ_1 and σ_2 equally increase while σ_3 decreases (σ_m constant); (5) σ_1 increases with varied σ_2 and σ_3 ($\sigma_1 \neq \sigma_2 \neq \sigma_3$). The first two stress paths are

triaxial compression and another two are triaxial extension while the last one is true triaxial stress condition.

For all tests, neoprene sheets are used to minimize the friction at all interfaces between the loading platens and the specimen surfaces (Figure 6.2). The measured deformations are used to determine the strains along the principal axes during loading. The failure stresses are recorded and modes of failure are examined (Figures 6.3 and 6.4). Appendix A shows the stress-strain curves from the start of loading to failure for all specimens.

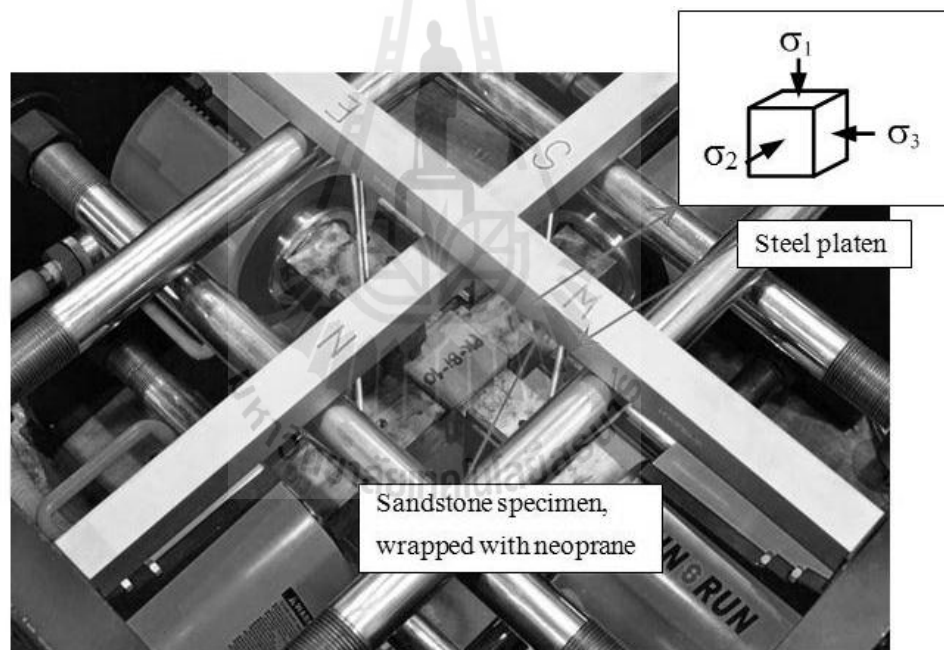


Figure 6.2 Testing operation and the directions of applied principal stresses.

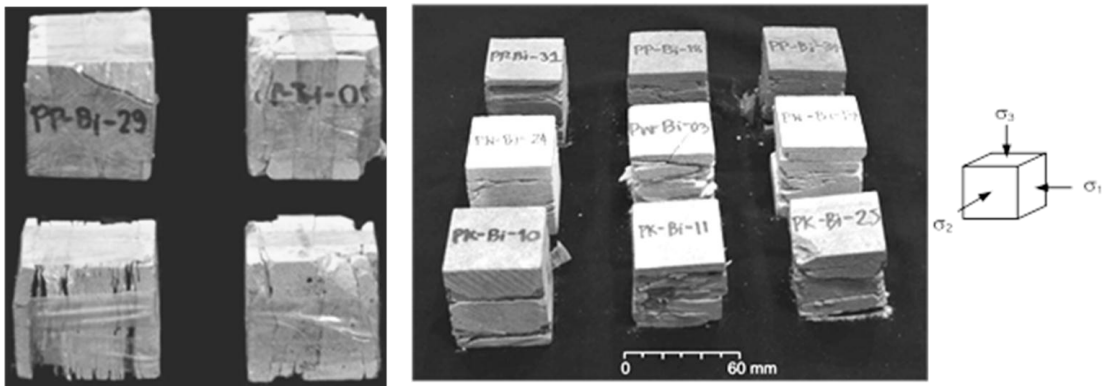


Figure 6.3 Sandstone specimens with multiple extension fractures from induced stresses of σ_1 and σ_2 .

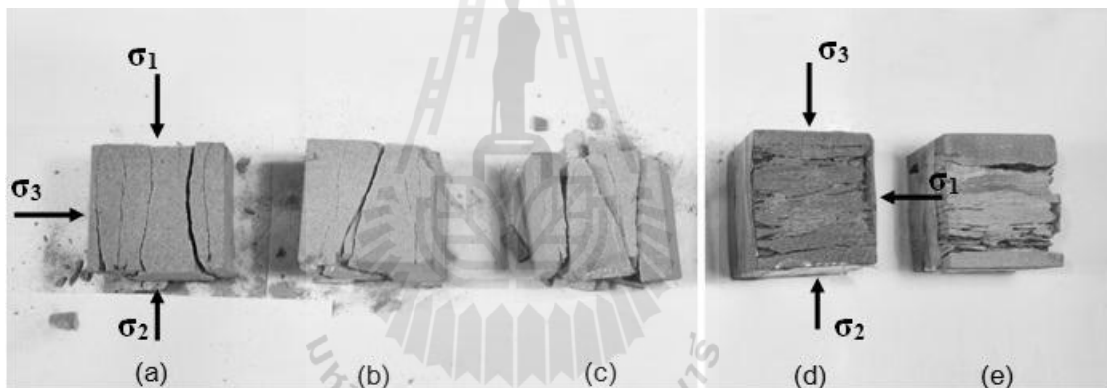


Figure 6.4 Post-tested specimens of PP sandstone: (a) Triaxial compression ($\sigma_m \neq$ constant) (b) Triaxial compression ($\sigma_m =$ constant) (c) True triaxial compression ($\sigma_1 \neq \sigma_2 \neq \sigma_3$) (d) Triaxial extension ($\sigma_m \neq$ constant) (e) Triaxial extension ($\sigma_m =$ constant).

Post-failure observations in Figures 6.3 and 6.4 suggest that compressive shear failures are predominant in the specimens tested under low σ_2 while splitting tensile fractures parallel to σ_1 and σ_2 directions dominate under higher σ_2 . Figure 6.4 (b) and

(c) clearly show compressive shear failure. The stress path (2) with reduced σ_3 which make the effect of σ_2 less pronounced should cause the mode of failure in Figure 6.4 (b). Figures 6.4 (a), (d) and (e) suggest the splitting tensile fractures. The stress path (1) with σ_3 constant that enhance greater effect of σ_2 should be the cause of the failure mode in Figure 6.4 (a). The stress paths (3) and (4) which are both triaxial extension apply higher σ_2 that influence the posted failure in Figures 6.4 (d) and (e). Moreover, compared to Figure 6.4 (e), Figure 6.4 (d) shows more severe splitting failure, suggesting more pronounced effect of σ_2 under greater σ_3 .

The observed splitting tensile fractures under relatively high σ_2 suggest that the fracture initiation has no influence from the friction at the loading interface in the σ_2 direction. As a result the increase of σ_1 with σ_2 should not be due to the interface friction. This does not agree with a conclusion drawn by Cai (2008) that friction at the interface in the σ_2 direction contributes to the increase of σ_1 at failure.

6.4 Test results

This section describes test results in terms of strengths and elasticity. The details of the strength results and the calculated elastic parameters are described below.

6.4.1 Strength results

Tables 6.1 through 6.3 summarize the strength results from polyaxial compression tests of different stress paths for each rock type. Figures 6.5 through 6.7 show graphs with different relationships: shear stresses (τ) as a function of normal stress (σ_n), octahedral shear stresses (τ_{oct}) as a function mean stress (σ_m) and strength

Table 6.1 Summary of strengths on Travertine.

Stress Path No.	σ_3 (MPa)	σ_2 (MPa)	σ_1 (MPa)	σ_m (MPa)	τ_{oct} (MPa)	$J_2^{1/2}$ (MPa)
1	0	0	30.20	10.07	14.24	17.44
3		43.24	43.24	28.83	20.38	24.96
1	1.00	1.00	38.58	13.53	17.72	21.70
3		51.35	51.35	34.57	23.74	29.07
1	3.00	3.00	50.44	18.81	22.36	27.39
3		59.46	59.46	40.64	26.62	32.60
4	5.00	52.00	52.00	36.33	22.16	27.14
1	7.00	7.00	67.57	27.19	28.55	34.97
3		75.00	75.00	52.33	32.06	39.26
2	8.11	8.11	56.25	24.16	22.69	27.79
2	10.81	10.81	69.64	30.42	27.73	33.97
4		75.00	75.00	53.60	30.26	37.06
1	12.00	12.00	90.00	38.00	36.77	45.03
3		95.00	95.00	67.33	39.13	47.92
2	16.22	16.22	86.00	39.48	32.89	40.29
4		93.00	93.00	67.41	36.19	44.33
2	27.03	27.03	109.08	54.38	38.68	47.37
4		115.18	115.18	85.80	41.55	50.89

Table 6.2 Results of strengths on PK Sandstone.

Stress Path No.	σ_3 (MPa)	σ_2 (MPa)	σ_1 (MPa)	σ_m (MPa)	τ_{oct} (MPa)	$J_2^{1/2}$ (MPa)
1	0	0	38.88	12.96	18.33	38.88
3		43.00	43.00	28.67	14.33	43.00
2	2.50	2.50	47.44	17.48	21.19	47.44
1	3.00	3.00	58.00	21.33	25.93	58.00
3		65.00	65.00	44.33	20.67	65.00
4	4.50	58.00	58.00	40.17	17.83	58.00
1	7.00	7.00	77.75	30.58	33.35	77.75
3		80.00	80.00	55.67	24.33	80.00
4	8.01	72.06	72.06	50.71	21.35	72.06
2	10.91	10.91	70.90	30.91	28.28	70.90
1	12.00	12.00	97.19	40.40	40.16	97.19
3		103.00	103.00	72.67	30.33	103.00
4	12.50	87.47	87.47	62.48	24.99	87.47
2	16.01	16.01	85.41	39.14	32.71	85.41
4	18.00	108.00	108.00	78.00	30.00	108.00
2	24.77	24.77	107.32	52.29	38.92	107.32

Table 6.3 Results of strengths on PP Sandstone.

Stress Path No.	σ_3 (MPa)	σ_2 (MPa)	σ_1 (MPa)	σ_m (MPa)	τ_{oct} (MPa)	$J_2^{1/2}$ (MPa)
1	0	0.00	55.00	18.33	25.93	31.75
2		0.00	50.00	16.67	23.57	28.87
3		66.90	66.90	44.60	22.30	27.31
4		55.00	55.00	36.67	18.33	22.45
1	1.00	1.00	68.00	23.33	31.58	38.68
3		74.00	74.00	49.67	24.33	29.80
1	3.00	3.00	80.50	28.83	36.53	44.74
2		3.00	62.00	22.67	27.81	34.06
3		88.00	88.00	59.67	28.33	34.70
1	5.00	5.00	92.20	34.07	41.11	50.34
3		98.00	98.00	67.00	31.00	37.97
4		73.00	73.00	50.50	22.50	27.56
2	6.00	6.00	70.00	27.33	30.17	36.95
1	7.00	7.00	100.00	38.00	43.84	53.69
3		110.00	110.00	75.67	34.33	42.05
4	10.50	85.00	85.00	60.17	24.83	30.41
2	13.50	13.50	85.00	37.33	33.71	41.28
4	18.00	107.00	107.00	77.33	29.67	36.33
2	27.00	27.00	112.00	55.33	40.07	49.07
4		125.00	125.00	92.33	32.67	40.01



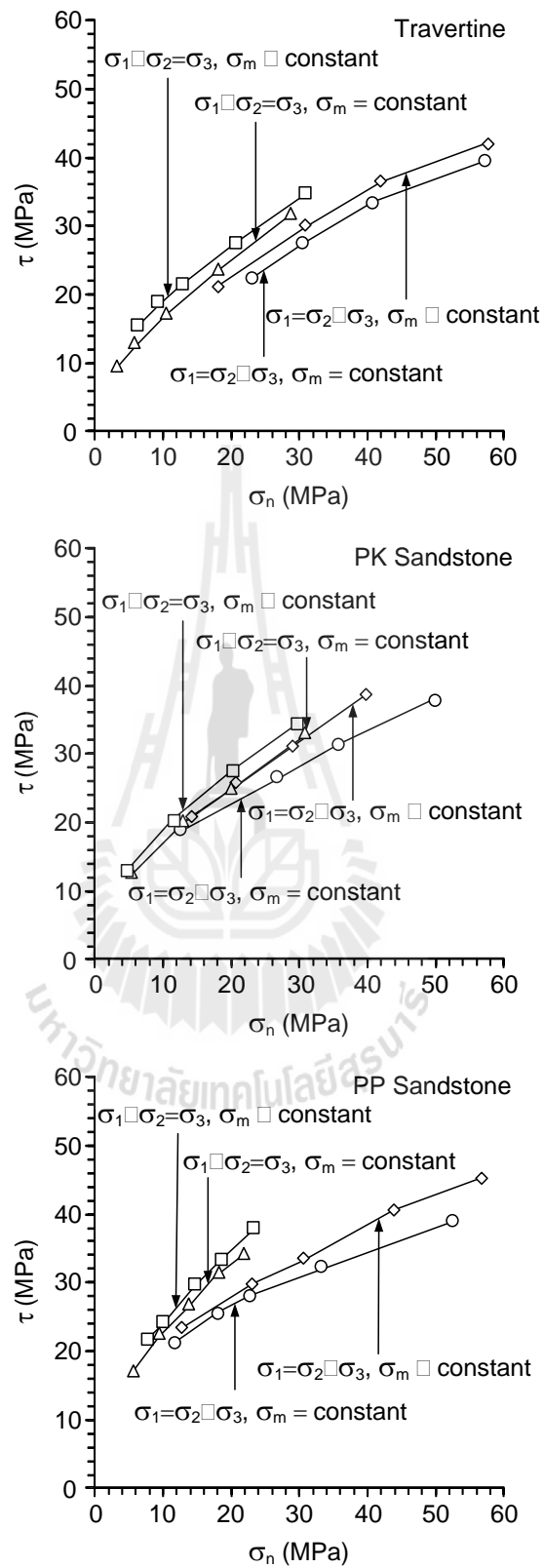


Figure 6.5 Shear stresses (τ) as a function of normal stress (σ_n).

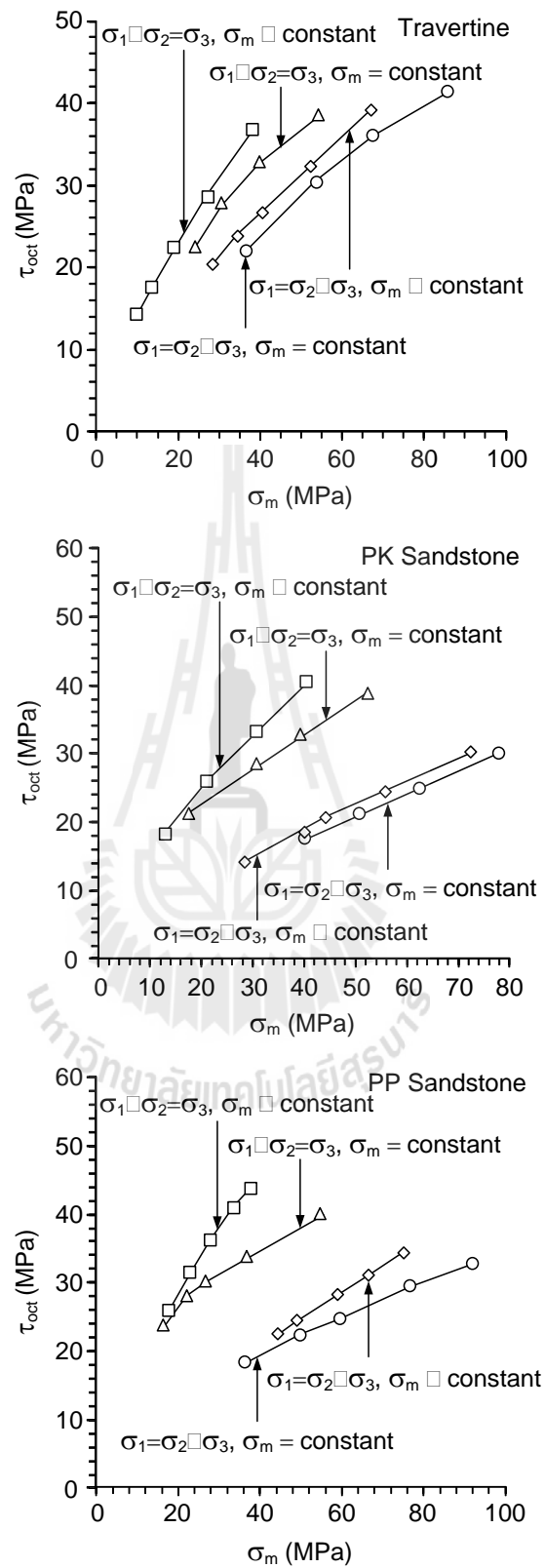


Figure 6.6 Octahedral shear stresses (τ_{oct}) as a function mean stress (σ_m).

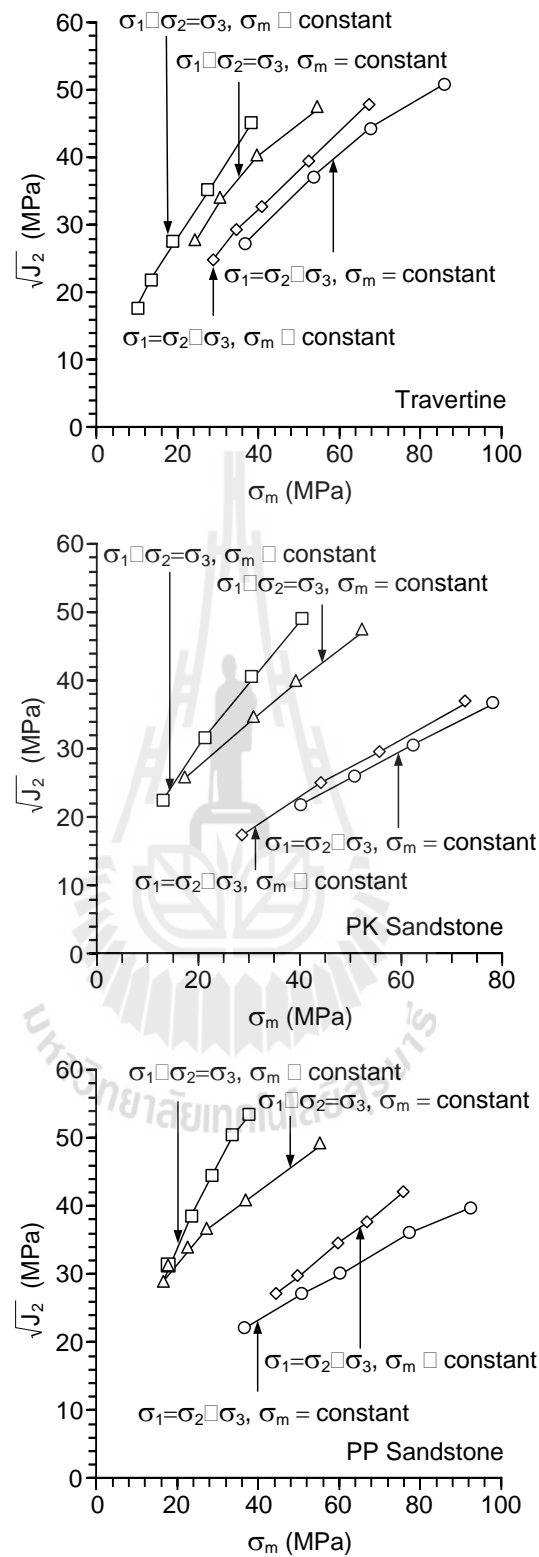


Figure 6.7 Strength results in terms of second order stress invariant as a function of mean stress.

results in terms of second order stress invariant ($J_2^{1/2}$) as a function of mean stress (σ_m).

Based on Tables 6.1 through 6.3 above and Figures 6.5 through 6.7, the strength results of the tests are described as follows. To better clarify the following description, the compared rock strengths from different stress paths are also shown in Tables 6.4 through 6.7 for travertine, Tables 6.8 through 6.11 for PK sandstone and Tables 6.12 through 6.15 for PP sandstone.

The results of triaxial compression tests of the stress path (1) (σ_3 constant) and the stress path (2) (σ_m constant) are shown in Figures 6.8 through 6.13 in the form of Mohr circles of the results with shear stresses as ordinates and normal stresses as abscissas. The relationship can be represented by the Coulomb criterion:

$$\tau = c + \sigma_n \tan \phi \quad (6.1)$$

where τ is the shear stress, c is the cohesion, σ_n is the normal stress and ϕ is the angle of internal friction. Table 6.16 summarizes the parameters based on Mohr and Coulomb criterion and Figures 6.14 through 6.16 show graphs to compare the strength results between the stress path (1) (σ_3 constant) and the stress path (2) (σ_m constant). Tables 6.17 and 6.18 summarize the strength results from the true triaxial compression tests (stress path (5)). Figures 6.17 and 6.18 plot σ_1 at failure as a function of σ_2 tested under various σ_3 for different rock specimens.

For triaxial compression tests, stress path (1) ($\sigma_m \neq$ constant) provides higher rock strengths than stress path (2) (σ_m constant). Based on the Table 6.12 ($\sigma_2 = \sigma_3 = 3$ MPa), PP sandstone has failure stress at 80.5 under stress path (1) and 62.0 MPa

Table 6.4 Compared strength results of triaxial compression tests for travertine.

Stress path (1) ($\sigma_m \neq \text{constant}$)		Stress path (2) ($\sigma_m \text{ constant}$)	
$\sigma_2 = \sigma_3$ (MPa)	σ_1 (MPa)	$\sigma_2 = \sigma_3$ (MPa)	σ_1 (MPa)
0	30.2	8.1	56.2
1	38.5	10.8	69.6
3	50.4	16.2	91.6
7	67.6	27.0	109.1
12	91.8	-	-

Table 6.5 Compared strength results of triaxial extension tests for travertine.

Stress path (3) ($\sigma_m \neq \text{constant}$)		Stress path (4) ($\sigma_m \text{ constant}$)	
σ_3 (MPa)	$\sigma_1 = \sigma_2$ (MPa)	σ_3 (MPa)	$\sigma_1 = \sigma_2$ (MPa)
0	43.2	5.0	52.0
1	51.3	10.8	75.0
3	59.5	16.2	93.0
7	75.0	27.0	115.2
12	95.0	-	-

Table 6.6 Compared strength results of travertine between triaxial extensions and triaxial compression under similar condition ($\sigma_m \neq \text{constant}$).

Stress path (3): triaxial extension		Stress path (1): triaxial compression	
σ_3 (MPa)	$\sigma_1 = \sigma_2$ (MPa)	$\sigma_2 = \sigma_3$ (MPa)	σ_1 (MPa)
0	43.2	0	30.2
1	51.3	1	38.5
3	59.5	3	50.4
7	75.0	7	67.6
12	95.0	12	91.8

Table 6.7 Compared strength results of travertine between triaxial extension and triaxial compression under similar condition (σ_m constant).

Stress path (4): triaxial extension		Stress path (2): triaxial compression	
σ_3 (MPa)	$\sigma_1 = \sigma_2$ (MPa)	$\sigma_2 = \sigma_3$ (MPa)	σ_1 (MPa)
5	52.0	8.1	56.2
10.8	75.0	10.8	69.6
16.2	93.0	16.2	91.9
27	115.2	27.0	109.1

Table 6.8 Compared strength results of triaxial compression for PK sandstone.

Stress path (1) ($\sigma_m \neq$ constant)		Stress path (2) (σ_m constant)	
$\sigma_2 = \sigma_3$ (MPa)	σ_1 (MPa)	$\sigma_2 = \sigma_3$ (MPa)	σ_1 (MPa)
0	38.9	2.5	47.4
3	58.0	10.9	70.9
7	77.7	16.0	85.4
12	97.2	24.8	107.3

Table 6.9 Compared strength results of triaxial compression for PK sandstone.

Stress path (3) ($\sigma_m \neq$ constant)		Stress path (4) (σ_m constant)	
σ_3 (MPa)	$\sigma_1 = \sigma_2$ (MPa)	σ_3 (MPa)	$\sigma_1 = \sigma_2$ (MPa)
0	43.0	4.5	58.0
3	65.0	8.0	72.1
7	80.0	12.5	87.5
12	103.0	18.0	108.0

Table 6.10 Compared strength results of PK sandstone between triaxial extension and triaxial compression under similar condition ($\sigma_m \neq \text{constant}$).

Stress path (3): triaxial extension		Stress path (1): triaxial compression	
σ_3 (MPa)	$\sigma_1 = \sigma_2$ (MPa)	$\sigma_2 = \sigma_3$ (MPa)	σ_1 (MPa)
0	43.0	0	38.9
3	65.0	3	58.0
7	80.0	7	77.7
12	103.0	12	97.2

Table 6.11 Compared strength results of PK sandstone between triaxial extension and triaxial compression under similar condition (σ_m constant).

Stress path (4): triaxial extension		Stress path (2): triaxial compression	
σ_3 (MPa)	$\sigma_1 = \sigma_2$ (MPa)	$\sigma_2 = \sigma_3$ (MPa)	σ_1 (MPa)
4.5	58.0	2.5	47.4
8.0	72.1	10.9	70.9
12.5	87.5	16.0	85.4
18.0	108.0	24.8	107.3

Table 6.12 Compared strength results of triaxial compression for PP sandstone.

Stress path (1) ($\sigma_m \neq \text{constant}$)		Stress path (2) (σ_m constant)	
$\sigma_2 = \sigma_3$ (MPa)	σ_1 (MPa)	$\sigma_2 = \sigma_3$ (MPa)	σ_1 (MPa)
0	55.0	0	50.0
1	68.0	3	62.0
3	80.5	6	70.0
5	92.2	13.5	85.0
7	100.0	27	112.0

Table 6.13 Compared strength results of triaxial extension tests for PP sandstone.

Stress path (3) ($\sigma_m \neq \text{constant}$)		Stress path (4) ($\sigma_m \text{ constant}$)	
σ_3 (MPa)	$\sigma_1 = \sigma_2$ (MPa)	σ_3 (MPa)	$\sigma_1 = \sigma_2$ (MPa)
0	66.9	0	55.0
1	74.0	5.5	73.0
3	88.0	10.5	85.0
5	98.0	18	107.0
7	110.0	27	125.0

Table 6.14 Compared strength results of PP sandstone between triaxial extension and triaxial compression under similar condition ($\sigma_m \neq \text{constant}$).

Stress path (3): triaxial extension		Stress path (1): triaxial compression	
σ_3 (MPa)	$\sigma_1 = \sigma_2$ (MPa)	$\sigma_2 = \sigma_3$ (MPa)	σ_1 (MPa)
0	66.9	0	55.0
1	74.0	1	68.0
3	88.0	3	80.5
5	98.0	5	92.2
7	110.0	7	100.0

Table 6.15 Compared strength results of PP sandstone between triaxial extension and triaxial compression under similar condition ($\sigma_m \text{ constant}$).

Stress path (4): triaxial extension		Stress path (2): triaxial compression	
σ_3 (MPa)	$\sigma_1 = \sigma_2$ (MPa)	$\sigma_2 = \sigma_3$ (MPa)	σ_1 (MPa)
0	55.0	0	50.0
5.5	73.0	3	62.0
10.5	85.0	6	70.0
18	107.0	13.5	85.0
27	125.0	27	112.0

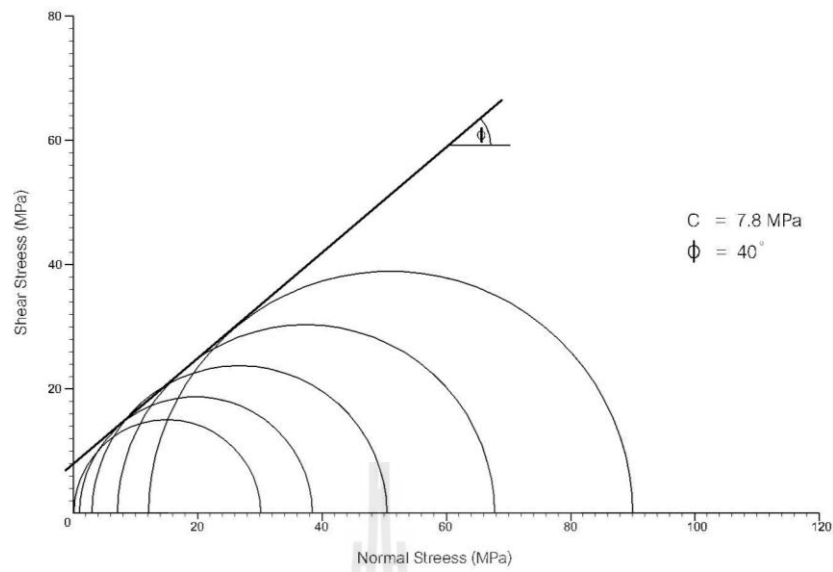


Figure 6.8 Results of triaxial compressive strength tests with the stress path (1) ($\sigma_1 \neq \sigma_2 = \sigma_3$, $\sigma_m \neq \text{constant}$) on travertine in terms of Mohr's circles and Coulomb criterion.

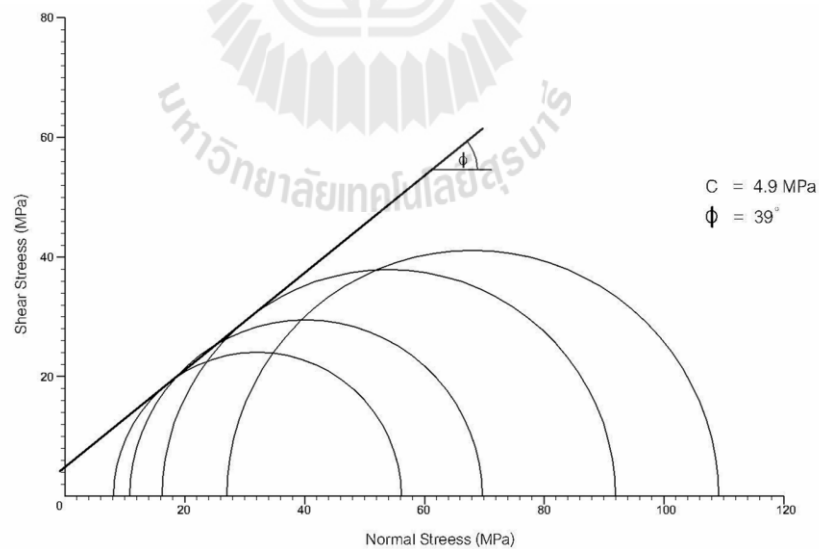


Figure 6.9 Results of triaxial compressive strength tests with stress path (2) ($\sigma_1 \neq \sigma_2 = \sigma_3$, $\sigma_m = \text{constant}$) on travertine in terms of Mohr's circles and Coulomb criterion.

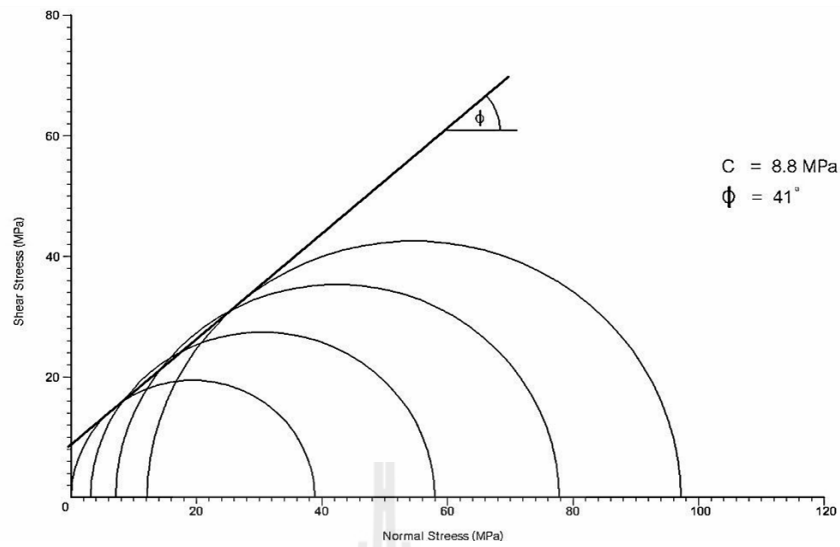


Figure 6.10 Results of triaxial compressive strength tests with the stress path (1) ($\sigma_1 \neq \sigma = \sigma_3$, $\sigma_m \neq \text{constant}$) on Phu Kradung sandstone in terms of Mohr's circles and Coulomb criterion.

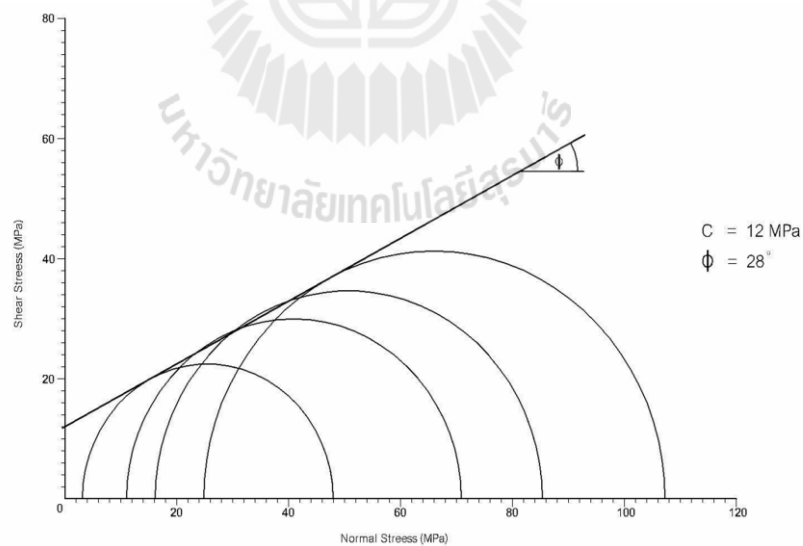


Figure 6.11 Results of triaxial compressive strength tests with the stress path (2) ($\sigma_1 \neq \sigma = \sigma_3$, $\sigma_m = \text{constant}$) on Phu Kradung sandstone in terms of Mohr's circles and Coulomb criterion.

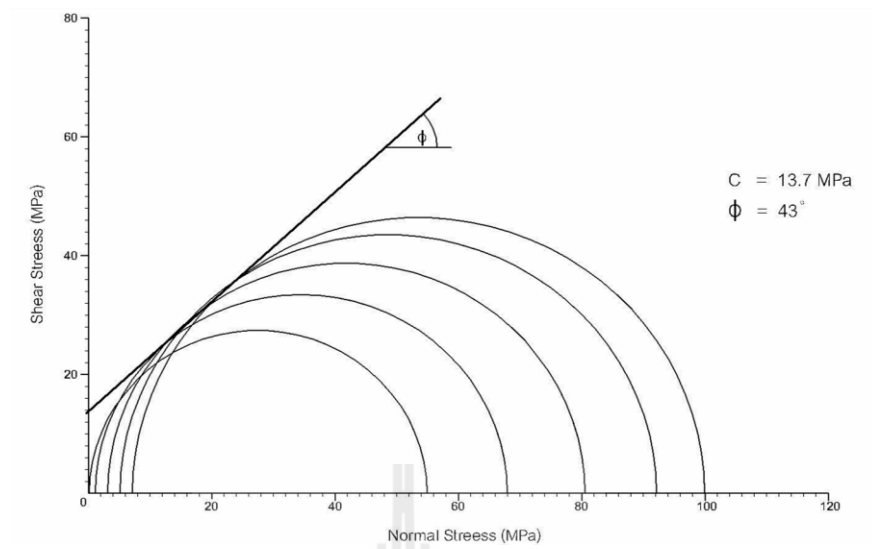


Figure 6.12 Results of triaxial compressive strength tests with the stress path (1) ($\sigma_1 \neq \sigma = \sigma_3$, $\sigma_m \neq \text{constant}$) on Phu Phan sandstone in terms of Mohr's circles and Coulomb criterion.

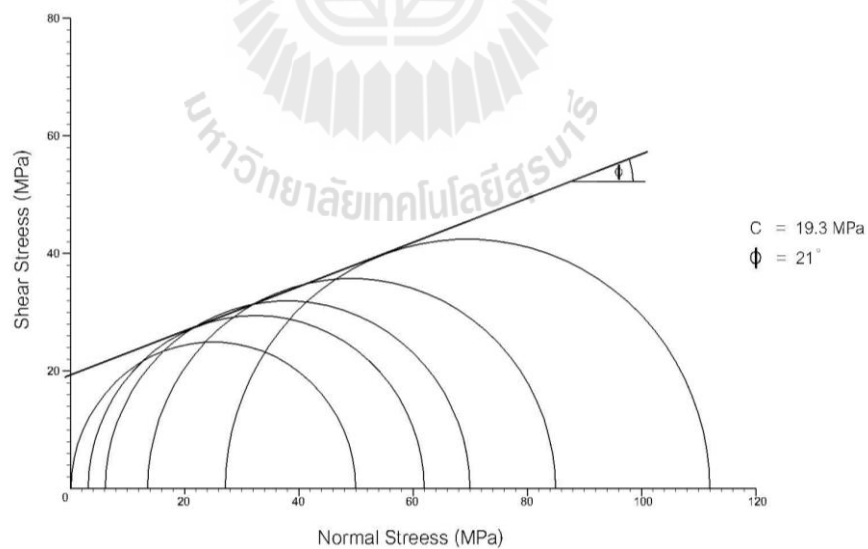


Figure 6.13 Results of triaxial compressive strength tests with the stress path (2) ($\sigma_1 \neq \sigma = \sigma_3$, $\sigma_m = \text{constant}$) on Phu Phan sandstone in terms of Mohr's circles and Coulomb criterion.

Table 6.16 Parameters from triaxial compression tests, based on Mohr and Coulomb criterion.

Rock Types	$\sigma_m \neq \text{constant}$		$\sigma_m = \text{constant}$	
	c (MPa)	ϕ (Degree)	c (MPa)	ϕ (Degree)
Travertine	7.8	40	4.9	39
PKSS	8.8	41	12	28
PPSS	13.7	43	19.3	21

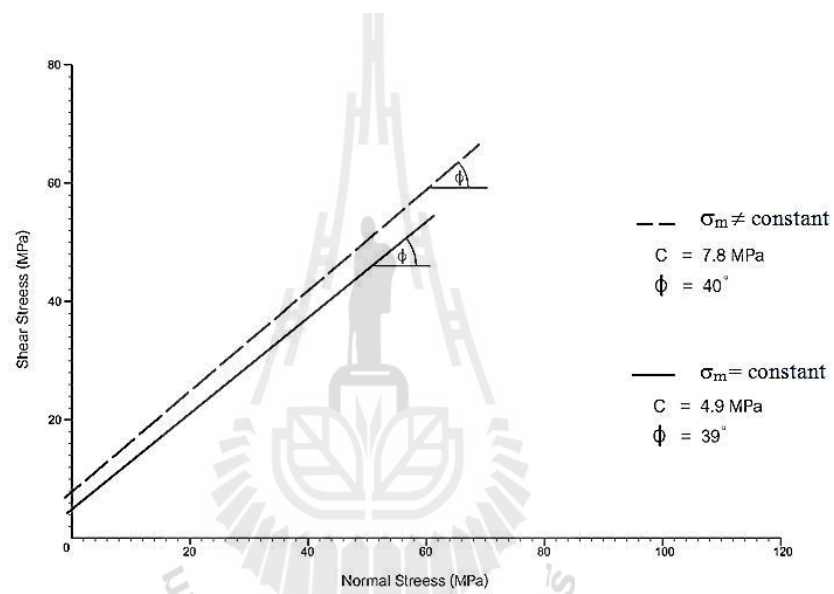


Figure 6.14 Compared results of triaxial compressive strength tests between stress path (1) ($\sigma_m \neq \text{constant}$) and the stress path (2) ($\sigma_m = \text{constant}$) on travertine in terms of Mohr's circles and Coulomb criterion.

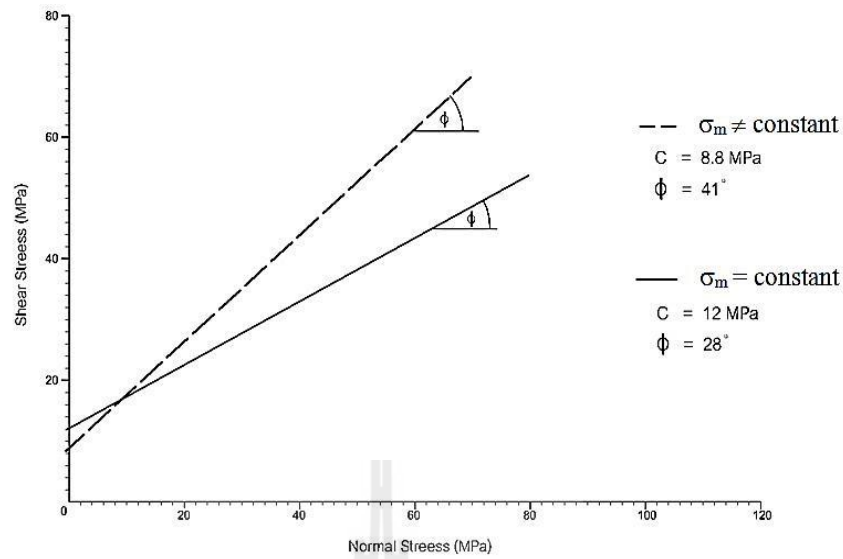


Figure 6.15 Compared results of triaxial compressive strength tests between stress path (1) ($\sigma_m \neq \text{constant}$) and the stress path (2) ($\sigma_m = \text{constant}$) on Phu Kradung sandstone in terms of Mohr's circles and Coulomb criterion.

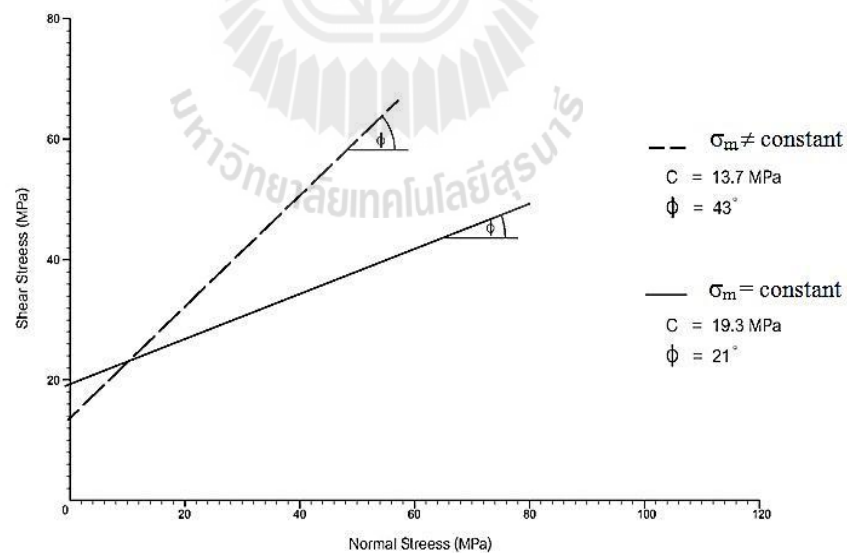


Figure 6.16 Compared results of triaxial compressive strength tests between the stress path (1) ($\sigma_m \neq \text{constant}$) and the stress path (2) ($\sigma_m = \text{constant}$) on Phu Phan sandstone in terms of Mohr's circles and Coulomb criterion.

Table 6.17 Summary of the strength results on travertine (TT) specimens from true triaxial compression test.

Specimen Number	Failure Stresses		
	σ_3 (MPa)	σ_2 (MPa)	σ_1 (MPa)
TT-PX-01	0	0.00	30.20
TT-PX-02		10.00	37.91
TT-PX-03		20.00	43.48
TT-PX-04		43.24	43.24
TT-PX-06	1	1.00	38.53
TT-PX-07		20.00	50.89
TT-PX-08		35.00	56.76
TT-PX-09		51.35	51.35
TT-PX-11	3	3.00	50.44
TT-PX-12		20.00	64.86
TT-PX-13		35.00	70.27
TT-PX-14		50.00	70.27
TT-PX-15		59.46	59.46
TT-PX-16	7	7.00	67.57
TT-PX-17		20.00	78.38
TT-PX-18		35.00	83.78
TT-PX-19		50.00	89.19
TT-PX-20		65.00	83.78
TT-PX-21		72.97	72.97
TT-PX-22	12	12.00	91.89
TT-PX-23		20.00	94.59
TT-PX-24		35.00	100.00
TT-PX-25		50.00	105.41
TT-PX-26		65.00	108.11
TT-PX-27		80.00	102.70
TT-PX-28		94.59	94.59

Table 6.18 Summary of the strength results on PP sandstone specimens from true triaxial compression test.

Specimen Number	Failure Stresses		
	σ_3 (MPa)	σ_2 (MPa)	σ_1 (MPa)
PP-PX-01	0	0.00	55.00
PP-PX-02		10.00	72.00
PP-PX-03		30.00	83.00
PP-PX-04		50.00	77.67
PP-PX-05		66.96	66.96
PP-PX-06	1	10.00	82.00
PP-PX-07		30.00	96.00
PP-PX-08		50.00	88.00
PP-PX-09		74.00	74.00
PP-PX-11	3	3.00	80.50
PP-PX-12		7.50	94.40
PP-PX-13		30.00	114.00
PP-PX-14		50.00	111.00
PP-PX-15		70.00	105.00
PP-PX-16		87.00	87.00
PP-PX-17	5	10.00	113.00
PP-PX-18		30.00	136.00
PP-PX-19		50.00	126.00
PP-PX-20		70.00	120.00
PP-PX-21		100.00	100.00
PP-PX-22	7	7.00	113.80
PP-PX-23		15.00	116.60
PP-PX-24		40.00	138.80
PP-PX-25		60.00	133.30
PP-PX-26		102.70	102.70

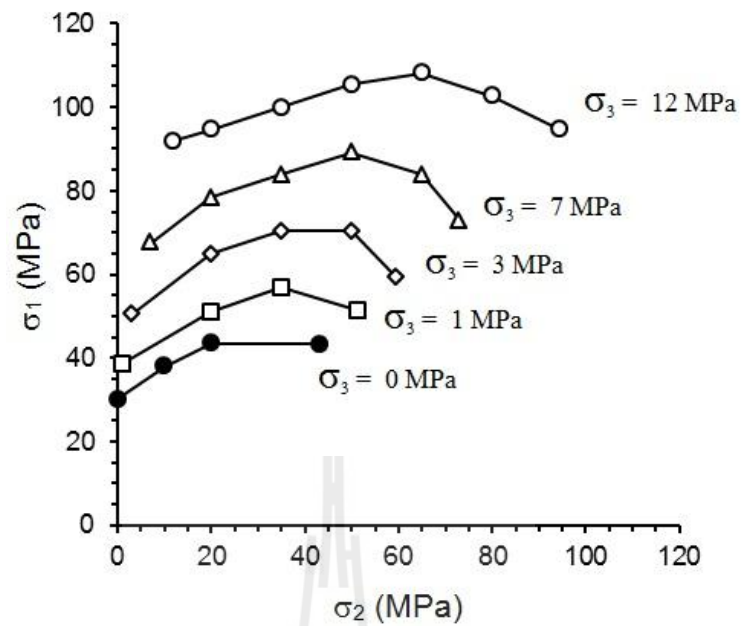


Figure 6.17 Major principal stress (σ_1) at failure as a function of σ_2 for various σ_3 values.

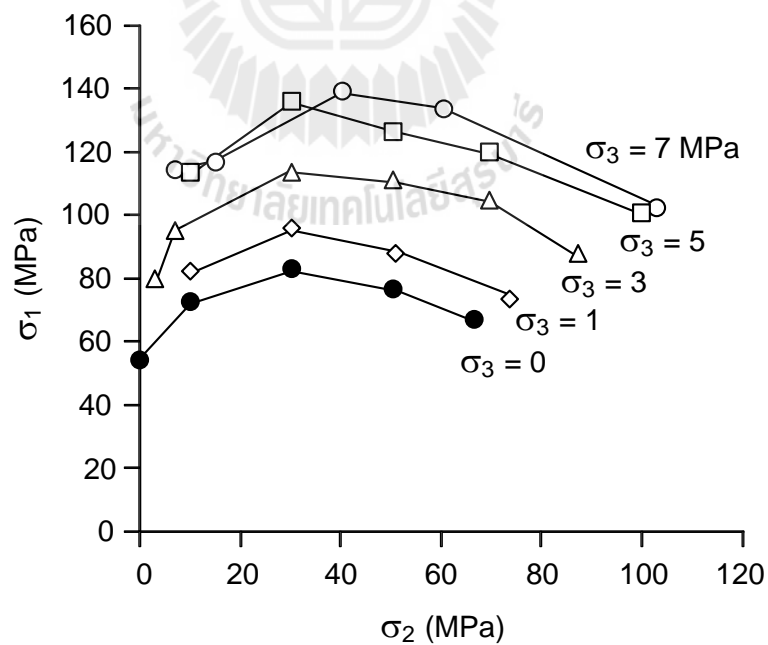


Figure 6.18 Major principal stress (σ_1) at failure as a function of σ_2 for various σ_3 values.

under stress path (2). Figures 6.14 through 6.16 clarify this issue by showing graphs to compare the strength results between the stress path (1) and (2).

For triaxial extension tests, stress path (3) ($\sigma_m \neq \text{constant}$) yields higher strengths of specimens, compared to the stress path (4) ($\sigma_m \text{ constant}$). Referred to the Table 6.9 ($\sigma_3 \approx 12 \text{ MPa}$), PK sandstone has failure stress at 103.0 MPa under stress path (3) and 87.5 MPa under stress path (4). Furthermore, if compared between the tests on triaxial extension and triaxial compression, the former gives higher strengths under similar condition. For example, under the condition $\sigma_m \neq \text{constant}$, triaxial extension stress path (3) yield higher strengths of specimens than triaxial compression stress path (1). Travertine has failure stress at 59.5 MPa under stress path (3) and 50.4 MPa under stress path (1), as shown in the Table 6.6 ($\sigma_3 = 3 \text{ MPa}$). The test results of PP, PK and TT are in the same manner as just described.

The intermediate principal stress (σ_2) may have strong influence on the different strengths of specimens under each stress path as described above. And that is why the rock strengths from triaxial extension tests are always higher than the ones from triaxial compression when under similar condition. Besides, the effect of σ_2 tends to be pronounced under greater minimum principal stress (σ_3) (Figures 6.17 and 6.18) and therefore the triaxial tests with $\sigma_m \text{ constant}$ usually yield lower strength, compared to the ones with $\sigma_m \text{ not constant}$. However, the strength results of this study as explained above agree with the outcomes of the researches elsewhere (Hardin et al., 1967; Murrell, 1963; Wiebol and Cook, 1968; Haimson and Chang, 2000; Colmenares and Zoback, 2002; Haimson, 2006).

6.4.2 Elastic parameters

The elastic parameters are calculated for the three-dimensional principal stress-strain relations. The calculations of elastic parameters are made at 30-40% of the maximum principal stresses. An attempt is made to calculate the elastic moduli along the three loading directions. It is assumed here that the Poisson's ratio (ν) of each rock type is the same for all principal planes. They are defined as 0.34, 0.26 and 0.22 for travertine, PK sandstone and PP sandstone respectively (Tables 6.19 through 6.21). The elastic moduli along the major, intermediate and minor principal directions can be calculated by (Jaeger et al., 2007)

$$\varepsilon_1 = \sigma_1 / E_1 - \nu (\sigma_2 / E_2 + \sigma_3 / E_3) \quad (6.2)$$

$$\varepsilon_2 = \sigma_2 / E_2 - \nu (\sigma_1 / E_1 + \sigma_3 / E_3) \quad (6.3)$$

$$\varepsilon_3 = \sigma_3 / E_3 - \nu (\sigma_1 / E_1 + \sigma_2 / E_2) \quad (6.4)$$

where ε_1 , ε_2 and ε_3 are the major, intermediate and minor principal strains, and E_1 , E_2 and E_3 are the elastic moduli along the major, intermediate and minor directions. The calculation results are shown in Figures 6.19 through 6.21 which suggest that the elastic moduli along the principal directions are similar. And this implies that all three types of rock specimens are isotropic. The discrepancies shown in Figures 6.19 through 6.21 are probably due to the intrinsic variability of each rock specimens.

Based on the Tables 6.19 through 6.21 and the Table 6.16, PP sandstone has higher elastic modulus and cohesion (with slightly different friction angles), compared to the other two rock types.

Table 6.19 Summary result of elastic parameters on Travertine.

σ_3 (MPa)	σ_2 (MPa)	σ_1 (MPa)	Elastic Modulus (GPa)				Poisson's ratio
			E_1	E_2	E_3	Avg.	
0	0	30.20	9.31	–	–	9.31	0.32
	43.24	43.24	9.53	16.25	–	12.89	0.33
1.00	1.00	38.58	14.68	15.02	14.36	14.69	0.33
	51.35	51.35	9.37	14.62	5.05	9.68	0.34
3.00	3.00	50.44	8.15	8.74	7.63	8.17	0.34
	59.46	59.46	7.36	12.20	5.31	8.29	0.34
5.00	52.00	52.00	7.13	10.31	8.03	8.49	0.33
7.00	7.00	67.57	7.07	8.31	7.16	7.51	0.32
	75.00	75.00	7.06	12.27	5.79	8.37	0.33
8.11	8.11	56.25	5.12	5.20	5.04	5.12	0.35
10.81	10.81	69.64	5.59	5.63	5.54	5.59	0.34
	75.00	75.00	7.39	13.14	6.56	9.03	0.34
12.00	12.00	90.00	7.05	7.34	6.78	7.06	0.33
	95.00	95.00	9.71	10.53	8.84	9.69	0.31
16.22	16.22	86.00	5.37	5.42	5.32	5.37	0.35
	93.00	93.00	5.22	8.80	4.81	6.28	0.35
27.03	27.03	109.08	5.35	5.39	5.31	5.35	0.35
	115.18	115.18	5.27	8.83	4.88	6.33	0.35
Mean \pm Standard Deviation						8.18 \pm 2.57	0.34 \pm 0.01

Table 6.20 Summary result of elastic parameters on PK Sandstone.

σ_3 (MPa)	σ_2 (MPa)	σ_1 (MPa)	Elastic Modulus (GPa)				Poisson's ratio
			E_1	E_2	E_3	Avg.	
0	0	38.88	6.48	–	–	6.48	0.24
	43.00	43.00	7.92	7.56	–	7.74	0.22
2.50	2.50	47.44	7.53	7.38	7.69	7.54	0.28
3.00	3.00	58.00	6.19	5.32	7.38	6.30	0.27
	65.00	65.00	6.92	7.71	7.08	7.24	0.22
4.50	58.00	58.00	7.53	7.61	7.61	7.53	0.29
7.00	7.00	77.75	7.17	9.33	5.75	7.42	0.27
	80.00	80.00	8.90	11.25	8.99	9.71	0.21
8.01	72.06	72.06	7.22	6.89	7.18	7.09	0.28
10.91	10.91	70.90	6.64	6.73	6.56	6.64	0.29
12.00	12.00	97.19	6.29	5.95	6.67	6.30	0.27
	103.00	103.00	9.14	9.58	9.32	9.35	0.26
12.50	87.47	87.47	6.90	7.00	6.95	6.95	0.28
16.01	16.01	85.41	8.68	8.06	9.36	8.70	0.29
18.00	108.00	108.00	7.45	7.55	7.50	7.50	0.28
24.77	24.77	24.77	6.58	6.57	9.82	7.65	0.29
Mean \pm Standard Deviation						7.51 \pm 1.00	0.26 \pm 0.03

Table 6.21 Summary result of elastic parameters on PP Sandstone.

σ_3 (MPa)	σ_2 (MPa)	σ_1 (MPa)	Elastic Modulus (GPa)				Poisson's ratio
			E_1	E_2	E_3	Avg.	
0	0.00	55.00	12.50	–	–	12.50	0.21
	0.00	50.00	13.10	12.11	12.55	12.59	0.19
	66.90	66.90	12.89	12.32	–	12.57	0.22
	55.00	55.00	14.52	13.91	13.72	14.05	0.25
1.00	1.00	68.00	16.11	12.55	13.14	13.93	0.23
	74.00	74.00	12.39	12.32	12.35	12.35	0.21
3.00	3.00	80.50	11.11	12.11	12.95	12.06	0.20
	3.00	62.00	12.32	13.32	11.92	12.52	0.25
	88.00	88.00	15.12	14.12	15.01	14.75	0.26
5.00	5.00	92.20	13.92	13.11	13.61	13.55	0.22
	98.00	98.00	12.11	11.92	10.98	11.67	0.23
	73.00	73.00	12.32	12.18	13.01	12.50	0.20
6.00	6.00	70.00	13.12	13.52	13.75	13.46	0.20
7.00	7.00	100.00	11.96	12.55	12.10	12.20	0.21
	110.00	110.00	16.13	14.92	15.11	15.39	0.22
10.50	85.00	85.00	11.23	11.43	13.12	11.93	0.21
13.50	13.50	85.00	12.55	11.45	13.36	12.45	0.23
18.00	107.00	107.00	13.34	11.44	10.07	11.62	0.23
27.00	27.00	112.00	14.91	15.11	17.09	15.70	0.24
	125.00	125.00	11.11	10.11	12.06	11.09	0.22
Mean ± Standard Deviation						12.94 ± 1.26	0.22 ± 0.02

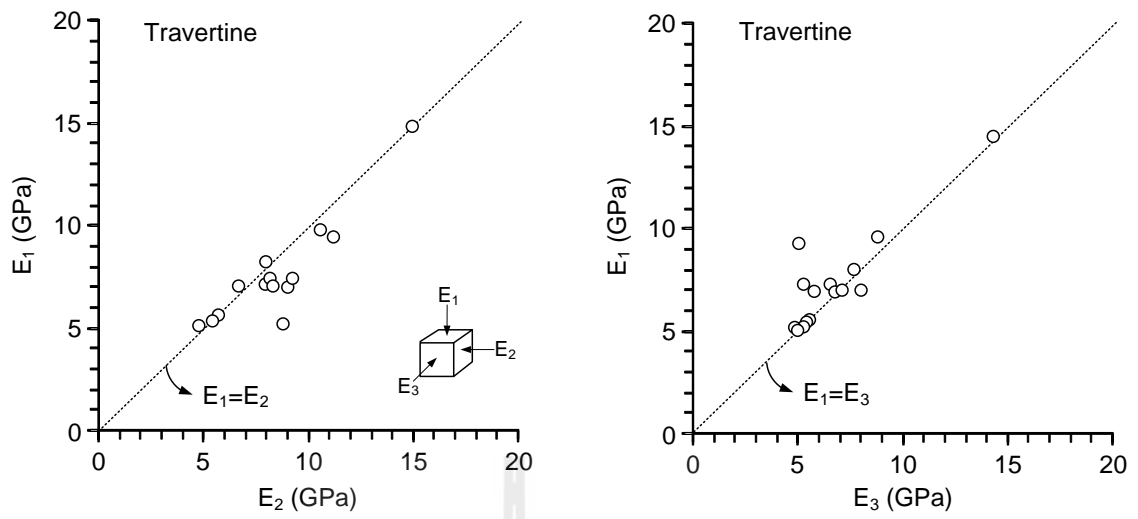


Figure 6.19 Elastic modulus calculated along the major principal axis as a function of intermediate and minor principal axes of travertine.

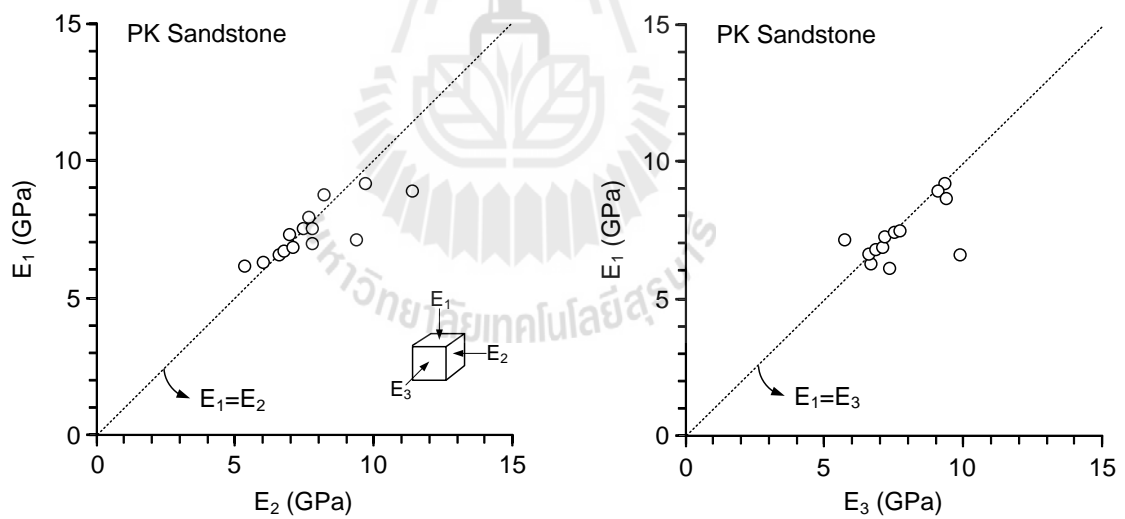


Figure 6.20 Elastic modulus calculated along the major principal axis as a function of intermediate and minor principal axes of PK sandstone.

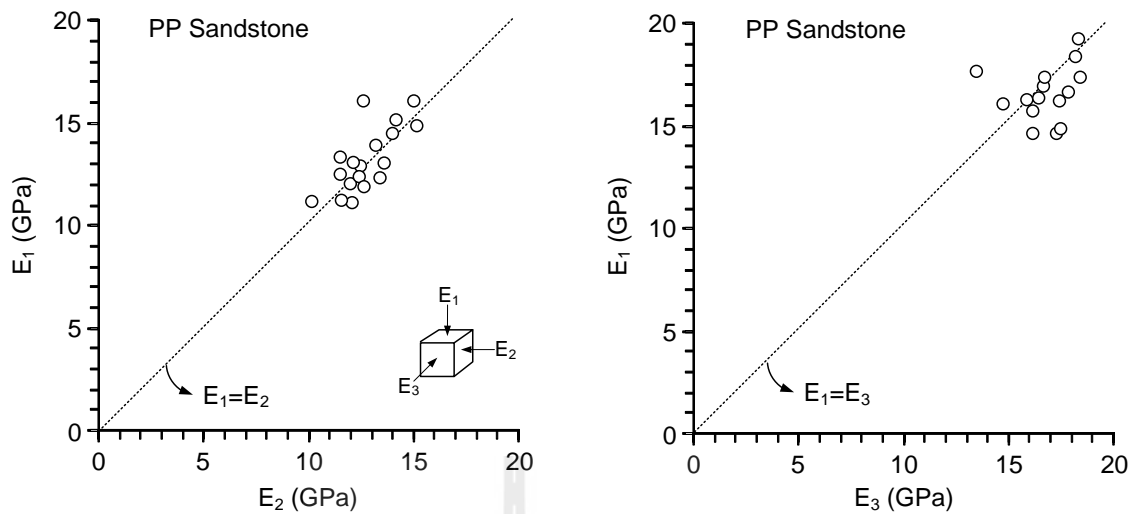


Figure 6.21 Elastic modulus calculated along the major principal axis as a function of intermediate and minor principal axes of PP sandstone.

Therefore, it has the highest compressive strength. The unconfined compressive strengths for travertine, PK and PP sandstone are 30.20, 38.88 and 55.00 MPa (Tables 6.1 through 6.3). Tables 6.19 through 6.21 also show that travertine has the highest Poisson's ratio of 0.34 ± 0.01 among the three types of rock specimens and therefore it tends to be more plastic as shown in Figure 6.17. Generally, experiments show that Poisson's ratio usually varies from 0.25 to 0.33 for rocks or metals, but may be 0.5 for rubber-like materials.

Referred to the Tables 6.22 through 6.33, the elastic parameters of the specimens of each rock type under different stress paths are described further. Generally, the stress path with σ_m not constant (stress path (1) and (3)) usually yield higher value of elastic modulus for different rock specimen than the one with σ_m constant (stress path (2) and (4)), under similar condition.

Table 6.22 Elastic modulus of travertine from the tests under stress path (1) ($\sigma_m \neq$ constant).

Stress path (1) ($\sigma_m \neq$ constant)		Elastic modulus (GPa)				Poisson's ratio
$\sigma_2 = \sigma_3$ (MPa)	σ_1 (MPa)	E_1	E_2	E_3	Avg.	
0	30.2	9.31	-	-	9.31	0.32
1	38.5	14.68	15.02	14.36	14.69	0.33
3	50.4	8.15	8.74	7.63	8.17	0.34
7	67.6	7.07	8.31	7.16	7.51	0.32
12	91.8	7.05	7.34	6.78	7.06	0.33
Mean \pm Standard Deviation					9.35 \pm 3.13	0.33 \pm 0.01

Table 6.23 Elastic modulus of travertine from the tests under stress path (2) ($\sigma_m =$ constant).

Stress path (2) ($\sigma_m =$ constant)		Elastic modulus (GPa)				Poisson's ratio
$\sigma_2 = \sigma_3$ (MPa)	σ_1 (MPa)	E_1	E_2	E_3	Avg.	
8.1	56.2	5.12	5.20	5.04	5.12	0.35
10.8	69.6	5.59	5.63	5.54	5.59	0.34
16.2	86.0	5.37	5.42	5.32	5.37	0.35
27.0	109.1	5.35	5.39	5.31	5.35	0.35
Mean \pm Standard Deviation					5.36 \pm 0.19	0.35 \pm 0.00

Table 6.24 Elastic modulus of travertine from the tests under stress path (3) ($\sigma_m \neq$ constant).

Stress path (3): triaxial extension		Elastic modulus (GPa)				Poisson's ratio
σ_3 (MPa)	$\sigma_1 = \sigma_2$ (MPa)	E_1	E_2	E_3	Avg.	
0	43.2	9.53	16.25	-	12.89	0.33
1	51.3	9.37	14.62	5.05	9.68	0.34
3	59.5	7.36	12.20	5.31	8.29	0.34
7	75.0	7.06	12.27	5.79	8.37	0.33
12	95.0	9.71	10.53	8.84	9.69	0.31
Mean \pm Standard Deviation					9.78 \pm 1.86	0.33 \pm 0.01

Table 6.25 Elastic modulus of travertine from the tests under stress path (4) ($\sigma_m =$ constant).

Stress path (4): triaxial extension		Elastic modulus (GPa)				Poisson's ratio
σ_3 (MPa)	$\sigma_1 = \sigma_2$ (MPa)	E_1	E_2	E_3	Avg.	
5	52.0	7.13	10.31	8.03	8.49	0.33
10.8	75.0	7.39	13.14	6.56	9.03	0.34
16.2	93.0	5.22	8.80	4.81	6.28	0.35
27	115.2	5.27	8.83	4.88	6.33	0.35
Mean \pm Standard Deviation					7.53 \pm 1.43	0.34 \pm 0.01

Table 6.26 Elastic modulus of PK sandstone from the tests under stress path (1) ($\sigma_m \neq$ constant).

Stress path (1) ($\sigma_m \neq$ constant)		Elastic modulus (GPa)				Poisson's ratio
$\sigma_2 = \sigma_3$ (MPa)	σ_1 (MPa)	E_1	E_2	E_3	Avg.	
0	38.9	6.48	-	-	6.48	0.24
3	58.0	6.19	5.32	7.38	6.30	0.27
7	77.7	7.17	9.33	5.75	7.42	0.27
12	97.2	6.29	5.35	6.67	6.30	0.27
Mean \pm Standard Deviation					6.62 \pm 0.54	0.26 \pm 0.01

Table 6.27 Elastic modulus of PK sandstone from the tests under stress path (2) ($\sigma_m =$ constant).

Stress path (2) ($\sigma_m =$ constant)		Elastic modulus (GPa)				Poisson's ratio
$\sigma_2 = \sigma_3$ (MPa)	σ_1 (MPa)	E_1	E_2	E_3	Avg.	
2.5	47.4	7.53	7.38	7.69	7.54	0.28
10.9	70.9	6.64	6.73	6.56	6.64	0.29
16.0	85.4	8.68	8.06	9.36	8.70	0.29
24.8	107.3	6.58	6.57	9.82	7.65	0.29
Mean \pm Standard Deviation					7.63 \pm 0.84	0.29 \pm 0.00

Table 6.28 Elastic modulus of PK sandstone from the tests under stress path (3) ($\sigma_m \neq \text{constant}$).

Stress path (3): triaxial extension		Elastic modulus (GPa)				Poisson's ratio
σ_3 (MPa)	$\sigma_1 = \sigma_2$ (MPa)	E_1	E_2	E_3	Avg.	
0	43.0	7.92	7.56	-	7.74	0.22
3	65.0	6.92	7.71	7.08	7.24	0.22
7	80.0	8.30	11.25	8.99	9.71	0.21
12	103.0	9.14	9.58	9.32	9.35	0.26
Mean \pm Standard Deviation					8.51 \pm 1.20	0.23 \pm 0.02

Table 6.29 Elastic modulus of PK sandstone from the tests under stress path (4) ($\sigma_m = \text{constant}$).

Stress path (4): triaxial extension		Elastic modulus (GPa)				Poisson's ratio
σ_3 (MPa)	$\sigma_1 = \sigma_2$ (MPa)	E_1	E_2	E_3	Avg.	
4.5	58.0	7.53	7.61	7.61	7.58	0.29
8.0	72.1	7.22	6.89	7.18	7.09	0.28
12.5	87.5	6.90	7.00	6.95	6.95	0.28
18.0	108.0	7.45	7.55	7.50	7.50	0.28
Mean \pm Standard Deviation					7.28 \pm 0.31	0.28 \pm 0.00

Table 6.30 Elastic modulus of PP sandstone from the tests under stress path (1) ($\sigma_m \neq \text{constant}$).

Stress path (1) ($\sigma_m \neq \text{constant}$)		Elastic modulus (GPa)				Poisson's ratio
$\sigma_2 = \sigma_3$ (MPa)	σ_1 (MPa)	E_1	E_2	E_3	Avg.	
0	55.0	12.50	-	-	12.50	0.21
1	68.0	16.11	12.55	13.14	13.93	0.23
3	80.5	11.11	12.11	12.95	12.06	0.20
5	92.2	13.92	13.11	13.61	13.55	0.22
7	100.0	11.96	12.55	12.10	12.20	0.21
Mean \pm Standard Deviation					12.85 \pm 0.84	0.21 \pm 0.01

Table 6.31 Elastic modulus of PP sandstone from the tests under stress path (2) ($\sigma_m = \text{constant}$).

Stress path (2) ($\sigma_m = \text{constant}$)		Elastic modulus (GPa)				Poisson's ratio
$\sigma_2 = \sigma_3$ (MPa)	σ_1 (MPa)	E_1	E_2	E_3	Avg.	
0	50.0	13.10	12.11	12.55	12.59	0.19
3	62.0	12.32	13.32	11.92	12.52	0.25
6	70.0	13.12	13.52	13.75	13.46	0.20
13.5	85.0	12.55	11.45	13.36	12.45	0.23
27	112.0	14.91	15.11	17.09	15.70	0.24
Mean \pm Standard Deviation					13.34 \pm 1.38	0.22 \pm 0.02

Table 6.32 Elastic modulus of PP sandstone from the tests under stress path (3) ($\sigma_m \neq \text{constant}$).

Stress path (3): triaxial extension		Elastic modulus (GPa)				Poisson's ratio
σ_3 (MPa)	$\sigma_1 = \sigma_2$ (MPa)	E_1	E_2	E_3	Avg.	
0	66.9	12.89	12.32	-	12.57	0.22
1	74.0	12.39	12.32	12.35	12.35	0.21
3	88.0	15.12	14.12	15.01	14.75	0.26
5	98.0	12.11	11.92	10.98	11.67	0.23
7	110.0	16.13	14.92	15.11	15.39	0.22
Mean \pm Standard Deviation					13.35 \pm 1.62	0.23 \pm 0.02

Table 6.33 Elastic modulus of PP sandstone from the tests under stress path (4) (σ_m = constant).

Stress path (4): triaxial extension		Elastic modulus (GPa)				Poisson's ratio
σ_3 (MPa)	$\sigma_1 = \sigma_2$ (MPa)	E_1	E_2	E_3	Avg.	
0	55.0	14.52	13.91	13.72	14.05	0.25
5.5	73.0	12.32	12.18	13.01	12.50	0.20
10.5	85.0	11.23	11.43	13.12	11.93	0.21
18.0	107.0	13.34	11.44	10.07	11.62	0.23
27	125.0	11.11	10.11	12.06	11.09	0.22
Mean \pm Standard Deviation					12.24 \pm 1.13	0.22 \pm 0.02

For example, for the condition of triaxial compression tests, the stress path (1) provides the elastic modulus 9.35 GPa for travertine, compared to the value 5.36 GPa under the stress path (2) (Table 6.22 and 6.23). For triaxial extension tests, the elastic modulus of PK sandstone is 8.51 GPa under the stress path (3) and 7.28 GPa under the stress path (4) (Tables 6.28 and 6.29). The test results just explained are in accordance with the strength results shown in the Tables 6.4 and 6.5, 6.8 and 6.9 and, 6.12 and 6.13.

The summarized Tables 6.34 through 6.36 further clarify the above conclusions. Furthermore, these Tables also suggest that triaxial extension normally yield higher value of the elastic modulus for each rock specimen, compared to the triaxial compression under similar condition. Under the condition σ_m not constant, PP sandstone has elastic modulus 13.35 GPa from triaxial extension tests and 12.85 GPa from triaxial compression tests (Table 6.36). However, these results as described agree with the detailed explanation of strength results on the section 6.4. The major factor that affects the different value of elastic modulus and compressive strength of different rock specimen under each stress path should be the intermediate principal

stress (σ_2). Another factor that provides the influence is the minimum principal stress (σ_3). As shown in Figure 6.17 and 6.18, the higher the σ_3 the more pronounced the σ_2 affects the failure stress. Therefore, the comparison of elastic modulus of each rock specimen under different stress path should be considered within the same range of σ_3 .

Table 6.34 Summarized elastic modulus and Poisson's ratio of travertine.

Different stress path (S.P.)	Mean elastic modulus and standard deviation	Poisson's ratio	Range of σ_3 (MPa)
S.P.(1) Triaxial compression ($\sigma_m \neq \text{constant}$)	9.35 ± 3.13	0.33 ± 0.01	0 – 12.0
S.P.(2) Triaxial compression ($\sigma_m = \text{constant}$)	5.36 ± 0.19	0.35 ± 0.00	8.1 – 27.0
S.P.(3) Triaxial extension ($\sigma_m \neq \text{constant}$)	9.78 ± 1.86	0.33 ± 0.01	0 – 12.0
S.P.(4) Triaxial extension ($\sigma_m = \text{constant}$)	7.53 ± 1.43	0.34 ± 0.01	5.0 – 27.0

Table 6.35 Summarized elastic modulus and Poisson's ratio of PK sandstone.

Different stress path (S.P.)	Mean elastic modulus and standard deviation	Poisson's ratio	Range of σ_3 (MPa)
S.P.(1) Triaxial compression ($\sigma_m \neq \text{constant}$)	6.62 ± 0.54	0.26 ± 0.01	0 – 12.0
S.P.(2) Triaxial compression ($\sigma_m = \text{constant}$)	7.63 ± 0.84	0.29 ± 0.00	2.5 – 24.8
S.P.(3) Triaxial extension ($\sigma_m \neq \text{constant}$)	8.51 ± 1.20	0.23 ± 0.02	0 – 12.0
S.P.(4) Triaxial extension ($\sigma_m = \text{constant}$)	7.28 ± 0.31	0.28 ± 0.00	4.5 – 18.0

Table 6.36 Summarized elastic modulus and Poisson's ratio of PP sandstone.

Different stress path (S.P.)	Mean elastic modulus and standard deviation	Poisson's ratio	Range of σ_3 (MPa)
S.P.(1) Triaxial compression ($\sigma_m \neq \text{constant}$)	12.85 ± 0.84	0.21 ± 0.01	0 – 7.0
S.P.(2) Triaxial compression ($\sigma_m = \text{constant}$)	13.34 ± 1.38	0.22 ± 0.02	0 – 27.0
S.P.(3) Triaxial extension ($\sigma_m \neq \text{constant}$)	13.35 ± 1.62	0.23 ± 0.02	0 – 7.0
S.P.(4) Triaxial extension ($\sigma_m = \text{constant}$)	12.24 ± 1.13	0.22 ± 0.02	0 – 27.0



CHAPTER VII

STRENGTH CRITERIA

7.1 Introduction

This chapter describes the strength analysis and criteria under biaxial and triaxial compression. The test results are compared with the modified Wiebols and Cook, Mogi, and Coulomb failure criteria. They are selected because the Coulomb criterion has been widely used in actual field applications while the modified Wiebols and Cook criterion has been claimed by many researchers to be one of the best representations of rock strengths under confinement. The Mogi provides further comparison.

7.2 Modified Wiebols and Cook criteria

The modified Wiebols and Cook criterion is proposed by Zhou (1994). The criterion is originally developed by Wiebols and Cook (1968) based on the additional energy stored around Griffith cracks due to the sliding of crack surfaces over each other. The modified version by Colmenares and Zoback (2002) defines $J_2^{1/2}$ at failure in terms of J_1 as:

$$J_2^{1/2} = A + BJ_1 + C J_1^2 \quad (7.1)$$

$$J_1 = (1/3) \times (\sigma_1 + \sigma_2 + \sigma_3) \quad (7.2)$$

$$J_2^{1/2} = [1/6 ((\sigma_1 - \sigma_2)^2 + (\sigma_1 - \sigma_3)^2 + (\sigma_2 - \sigma_3)^2)]^{1/2} = (3/2)^{1/2} \tau_{\text{oct}} \quad (7.3)$$

$$\tau_{\text{oct}} = 1/3 [(\sigma_1 - \sigma_2)^2 + (\sigma_2 - \sigma_3)^2 + (\sigma_3 - \sigma_1)^2]^{1/2} \quad (7.4)$$

The constants A, B and C depend on rock materials and the minimum principal stresses (σ_3). They can be determined under the conditions where $\sigma_2 = \sigma_3$, as follows (Colmenares and Zoback, 2002):

$$A = C_0/3^{1/2} - BC_0/3 - CC_0^2/9 \quad (7.5)$$

$$B = 3^{1/2} (q-1)/(q+2) - C/3(2C_0 + (q+2)\sigma_3) \quad (7.6)$$

$$C = [27^{1/2} / (2C_1 + (q-1)\sigma_3 - C_0)] \times \\ [[(C_1 + (q-1)\sigma_3 - C_0)/(2C_1 + (2q+1)\sigma_3 - C_0)] - [(q-1)/(q+2)]] \quad (7.7)$$

where $C_1 = (1 + 0.6\mu) C_0$;

C_0 = uniaxial; compressive strength of the rock;

$\mu = \tan \phi$;

$q = [(\mu^2 + 1)^{1/2} + \mu]^2 = \tan^2 (\pi/4 + \phi/2)$;

μ = coefficient of internal friction of the material;

ϕ = angle of internal friction

For the biaxial compression test of sandstones (PPSS, PKSS and PWSS) under three different stress paths (details in chapter V), the strength calculations in terms of $J_2^{1/2}$ and σ_m (or J_1) are in Table 7.1 through 7.3. The numerical values A, B and C are given in Table 7.4. The relationship between second order stress invariant as a function of mean stress is shown in Figure 7.1.

Table 7.1 Strength calculation in terms of σ_m and $J_2^{1/2}$ for PP sandstone specimens.

Specimen Number	Failure Stresses			σ_m (MPa)	τ_{oct} (MPa)	$J_2^{1/2}$ (MPa)
	σ_3 (MPa)	σ_2 (MPa)	σ_1 (MPa)			
PP-Bai-01	0.00	0.00	29.46	9.82	13.89	17.01
PP-Bai-02	0.00	10.00	72.00	27.33	31.85	39.00
PP-Bai-03	0.00	30.00	83.03	37.68	34.33	42.04
PP-Bai-04	0.00	50.00	77.67	42.56	32.14	39.37
PP-Bai-05	0.00	66.96	66.96	44.64	31.57	38.66
PP-path-06	0.00	0.00	49.98	16.66	23.56	28.86
PP-path-07	0.00	5.50	55.53	20.34	24.98	30.60
PP-path-08	0.00	44.40	61.09	35.16	25.78	31.58
PP-path-09	0.00	16.66	64.64	27.10	27.40	33.56
PP-path-10	0.00	33.32	65.25	32.86	26.64	32.63

Table 7.2 Strength calculation in terms of σ_m and $J_2^{1/2}$ for PK sandstone specimens.

Specimen Number	Failure Stresses			σ_m (MPa)	τ_{oct} (MPa)	$J_2^{1/2}$ (MPa)
	σ_3 (MPa)	σ_2 (MPa)	σ_1 (MPa)			
PK-Bai-01	0.00	0.00	48.00	16.00	22.63	27.71
PK-Bai-02	0.00	20.00	69.00	29.67	28.99	35.50
PK-Bai-03	0.00	30.00	78.00	36.00	32.12	39.34
PK-Bai-04	0.00	40.00	78.00	39.33	31.85	39.00
PK-Bai-05	0.00	50.00	76.00	42.00	31.54	38.63
PK-Bai-06	0.00	68.00	68.00	45.33	32.06	39.26
PK-path-07	0.00	0.00	38.80	12.93	18.29	22.40
PK-path-08	0.00	2.27	47.20	16.49	21.74	26.62
PK-path-09	0.00	5.00	53.51	19.50	24.13	29.56
PK-path-10	0.00	13.88	63.86	25.91	27.42	33.59
PK-path-11	0.00	55.33	65.44	40.26	28.76	35.23
PK-path-12	0.00	22.21	66.64	29.62	27.71	33.93
PK-path-13	0.00	40.23	70.33	36.85	28.81	35.29

Table 7.3 Strength calculation in terms of σ_m and $J_2^{1/2}$ for PW sandstone specimens.

Specimen Number	Failure Stresses			σ_m (MPa)	τ_{oct} (MPa)	$J_2^{1/2}$ (MPa)
	σ_3 (MPa)	σ_2 (MPa)	σ_1 (MPa)			
PW-Bai-01	0.00	0.00	39.00	13.00	18.38	22.52
PW-Bai-02	0.00	10.00	49.00	19.67	21.14	25.89
PW-Bai-03	0.00	21.00	55.00	25.33	22.66	27.75
PW-Bai-04	0.00	31.00	55.00	28.67	22.51	27.57
PW-Bai-05	0.00	40.00	48.97	29.66	21.29	26.07
PW-Bai-06	0.00	42.00	42.00	28.00	19.80	24.25
PW-path-07	0.00	0.00	24.00	8.00	11.31	13.86
PW-path-08	0.00	5.50	36.00	13.83	15.83	19.39
PW-path-09	0.00	8.30	41.00	16.43	17.70	21.68
PW-path-10	0.00	13.00	46.50	19.83	19.59	23.99
PW-path-11	0.00	20.00	46.00	22.00	18.83	23.07
PW-path-12	0.00	30.00	45.00	25.00	18.71	22.91

Table 7.4 Calibrated parameters of each sandstone type by the Modified Wiebols & Cook criterion under different stress paths.

Rock Types	Calibrated Parameters							
	Constant σ_2				σ_2 reduce			
	A (MPa)	B	C (MPa ⁻¹)	ϕ (°)	A (MPa)	B	C (MPa ⁻¹)	ϕ (°)
PPSS	-1.62	2.44	-0.034	50	5.50	1.96	-0.034	35
PKSS	10.38	1.31	-0.015	46	3.92	1.78	-0.025	35
PWSS	6.74	1.64	-0.033	58	0.03	2.08	-0.046	33

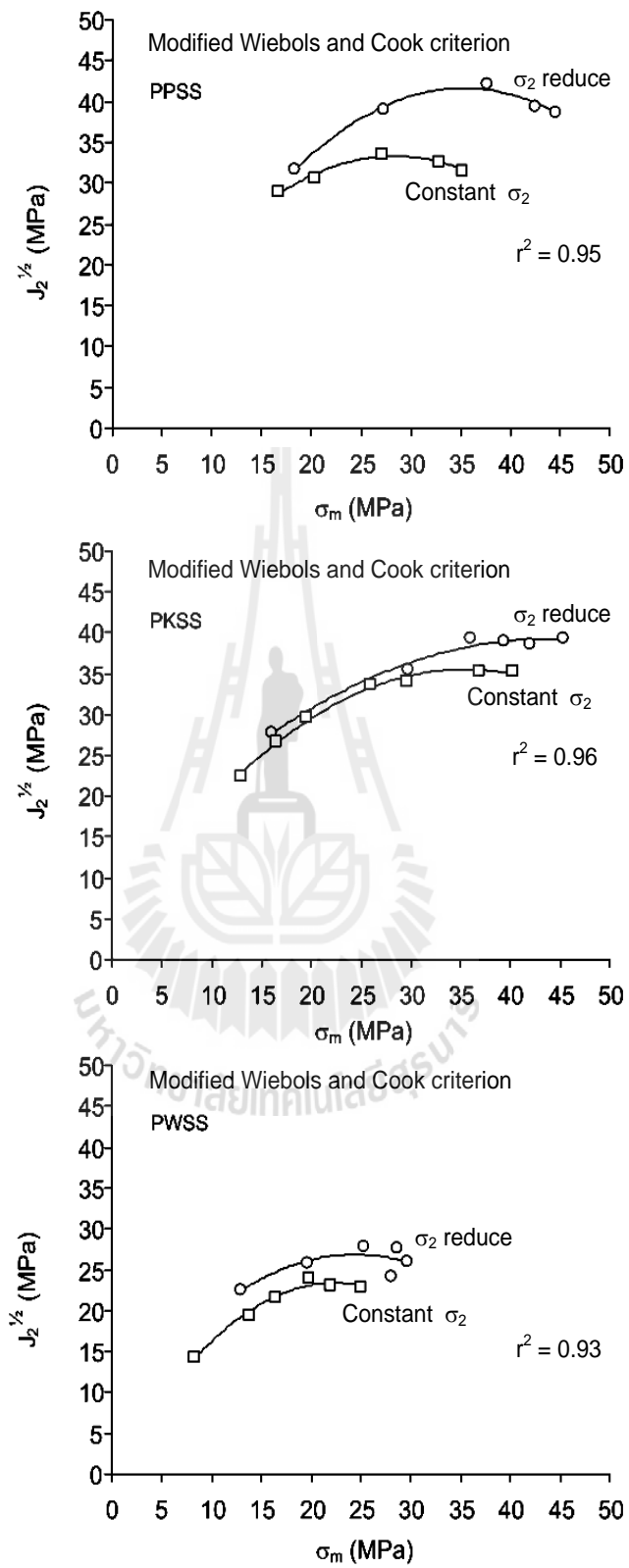


Figure 7.1 Test results fitted by the modified Wiebols & Cook criterion.

For the triaxial compression tests of travertine (TT) and sandstones (PKSS and PPSS) under four different stress paths (details in chapter VI), the strength calculations in terms of $J_2^{1/2}$ and σ_m (or J_1) are in Tables 7.5 through 7.7. The numerical values A, B and C are given in Table 7.8. The relationship between second order stress invariant as a function of mean stress is shown in Figure 7.2.

Table 7.5 Strength calculation in terms of σ_m and $J_2^{1/2}$ for Travertine specimens.

σ_3 (MPa)	σ_2 (MPa)	σ_1 (MPa)	σ_m (MPa)	τ_{oct} (MPa)	$J_2^{1/2}$ (MPa)
0	0	30.20	10.07	14.24	17.44
	43.24	43.24	28.83	20.38	27.04
1.00	1.00	38.58	13.53	17.72	20.82
	51.35	51.35	34.57	23.74	29.67
3.00	3.00	50.44	18.81	22.36	25.94
	59.46	59.46	40.64	26.62	35.17
5.00	52.00	52.00	36.33	22.16	38.13
7.00	7.00	67.57	27.19	28.55	34.48
	75.00	75.00	52.33	32.06	46.05
8.11	8.11	56.25	24.16	22.69	32.40
10.81	10.81	69.64	30.42	27.73	38.89
	75.00	75.00	53.60	30.26	53.37
12.00	12.00	90.00	38.00	36.77	45.56
	95.00	95.00	67.33	39.13	59.59
16.22	16.22	86.00	39.48	32.89	48.90
	93.00	93.00	67.41	36.19	66.77
27.03	27.03	109.08	54.38	38.68	66.28
	115.18	115.18	85.80	41.55	88.86

Table 7.6 Strength calculation in terms of σ_m and $J_2^{1/2}$ for PK sandstone specimens.

σ_3 (MPa)	σ_2 (MPa)	σ_1 (MPa)	σ_m (MPa)	τ_{oct} (MPa)	$J_2^{1/2}$ (MPa)
0	0	38.88	12.96	18.33	22.45
	43.00	43.00	28.67	14.33	34.57
2.50	2.50	47.44	17.48	21.19	27.61
3.00	3.00	58.00	21.33	25.93	31.69
	65.00	65.00	44.33	20.67	45.92
4.50	58.00	58.00	40.17	17.83	47.03
7.00	7.00	77.75	30.58	33.35	42.26
	80.00	80.00	55.67	24.33	58.26
8.01	72.06	72.06	50.71	21.35	57.85
10.91	10.91	70.90	30.91	28.28	44.25
12.00	12.00	97.19	40.40	40.16	54.10
	103.00	103.00	72.67	30.33	74.78
12.50	87.47	87.47	62.48	24.99	70.92
16.01	16.01	85.41	39.14	32.71	54.76
18.00	108.00	108.00	78.00	30.00	87.67
24.77	24.77	107.32	52.29	38.92	71.94

Table 7.7 Strength calculation in terms of σ_m and $J_2^{1/2}$ for PP sandstone specimens.

σ_3 (MPa)	σ_2 (MPa)	σ_1 (MPa)	σ_m (MPa)	τ_{oct} (MPa)	$J_2^{1/2}$ (MPa)
0	0.00	55.00	18.33	25.93	31.76
	0.00	50.00	16.67	23.57	29.88
	66.90	66.90	44.60	22.30	50.35
	55.00	55.00	36.67	18.33	46.91
1.00	1.00	68.00	23.33	31.58	37.10
	74.00	74.00	49.67	24.33	53.92
3.00	3.00	80.50	28.83	36.53	43.03
	3.00	62.00	22.67	27.81	36.72
	88.00	88.00	59.67	28.33	61.04
5.00	5.00	92.20	34.07	41.11	48.74
	98.00	98.00	67.00	31.00	67.61
	73.00	73.00	50.50	22.50	61.60
6.00	6.00	70.00	27.33	30.17	42.32
7.00	7.00	100.00	38.00	43.84	53.31
	110.00	110.00	75.67	34.33	74.54
10.50	85.00	85.00	60.17	24.83	73.52
13.50	13.50	85.00	37.33	33.71	55.03
18.00	107.00	107.00	77.33	29.67	93.35
27.00	27.00	112.00	55.33	40.07	78.65
	125.00	125.00	92.33	32.67	113.21

Table 7.8 Calibrated parameters for the Modified Wiebols and Cook criteria.

Rock Types	σ_3	Calibrated Parameters		
		A	B	C
PKSS	0	4.573	1.654	-0.021
	3	3.881	1.633	-0.015
	4	3.654	1.626	-0.014
	7	3.370	1.619	-0.011
	8	3.280	1.611	-0.008
	10	3.069	1.613	-0.009
	12	3.004	1.612	-0.009
	16.5	2.814	1.608	-0.007
	18	2.740	1.607	-0.007
	24	2.552	1.604	-0.005
PPSS	0	6.554	1.649	-0.015
	1	6.269	1.642	-0.014
	3	5.814	1.632	-0.012
	5	5.465	1.625	-0.010
	6	5.319	1.622	-0.010
	7	5.188	1.619	-0.009
	10.5	4.819	1.613	-0.008
	13.5	4.580	1.609	-0.007
	18	4.308	1.605	-0.006
	27	3.945	1.600	-0.005
Travertine	0	4.703	1.528	-0.026
	1	4.507	1.513	-0.023
	3	4.241	1.492	-0.018
	5	4.070	1.477	-0.015
	7	3.951	1.467	-0.013
	8.1	3.900	1.462	-0.012
	10.8	3.805	1.453	-0.010
	12	3.772	1.450	-0.009
	16.2	3.685	1.442	-0.008
	27	3.568	1.429	-0.005

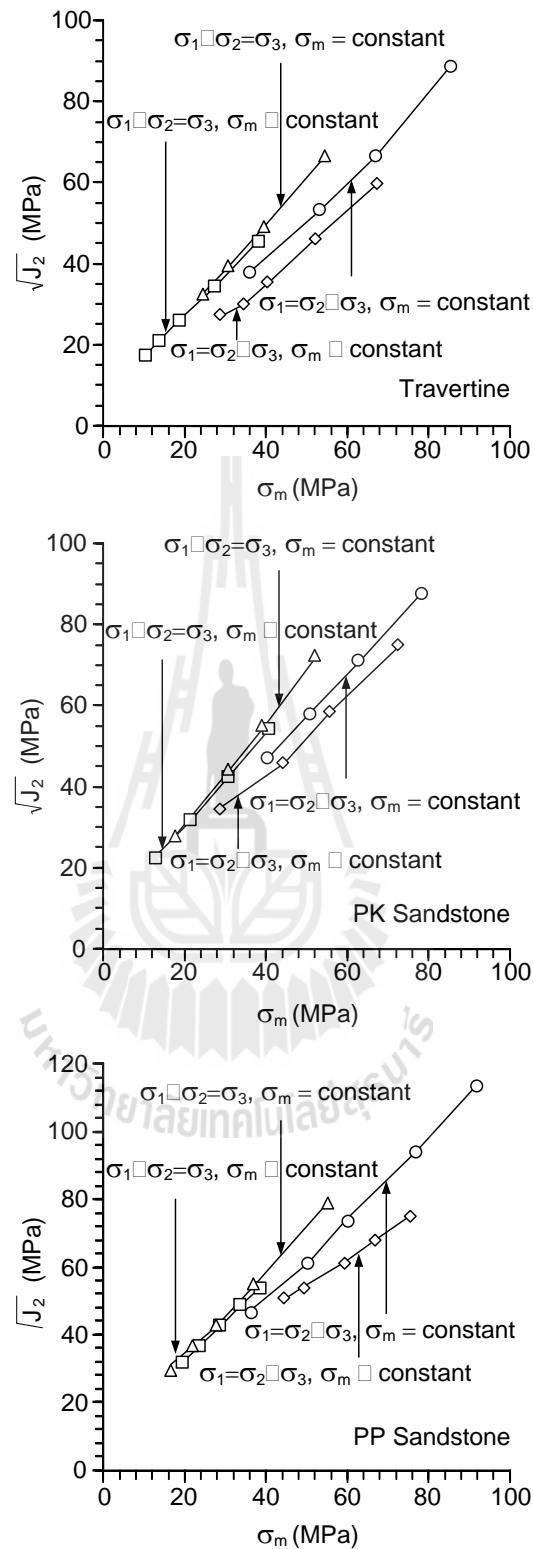


Figure 7.2 Strength results in terms of second order stress invariant as a function of mean stress (Modified Wiebols and Cook criterion).

7.3 Mogi criterion

The mogi 1971 is a generalization from the von Mises's theory. It is formulated by:

$$\tau_{\text{oct}} = f_1(\sigma_{\text{m},2}) \quad (7.8)$$

where f_1 is a monotonically increasing function. τ_{oct} and $\sigma_{\text{m},2}$ are, respectively, the octahedral shear stress and the effective mean stress. The empirical Mogi criteria on uses a power law to describe the failure stresses, defines τ_{oct} at failure in terms of $\sigma_{\text{m},2}$ as:

$$\tau_{\text{oct}} = A'(\sigma_{\text{m},2})^{B'} \quad (7.9)$$

$$\tau_{\text{oct}} = 1/3 [(\sigma_1 - \sigma_2)^2 + (\sigma_2 - \sigma_3)^2 + (\sigma_3 - \sigma_1)^2]^{1/2} \quad (7.10)$$

$$\sigma_{\text{m},2} = (\sigma_1 + \sigma_2)/2 \quad (7.11)$$

where A' and B' are constants that depend on the rock materials. For the biaxial compression test of sandstones (PP, PK and PW) under three different stress paths (details in chapter V), the strength calculations in terms of τ_{oct} and σ_{m} (or J_1) are in Table 7.1 through 7.3. The empirical constants A' and B' are given in Table 7.9. The relationship between octahedral shear stresses as a function of mean stress is shown in Figure 7.3.

Table 7.9 Calibrated parameters of each sandstone type by the Mogi (1971) empirical criterion under different stress paths.

Specimens	Calibrated Parameters	
	Constant σ_2	σ_2 reduce
PPSS	$A' = 1.27 \text{ MPa}$, $B' = 0.89$	$A' = 4.63 \text{ MPa}$, $B' = 0.50$
PKSS	$A' = 0.44 \text{ MPa}$, $B' = 1.27$	$A' = 1.83 \text{ MPa}$, $B' = 0.77$
PWSS	$A' = 3.49 \text{ MPa}$, $B' = 0.56$	$A' = 1.53 \text{ MPa}$, $B' = 0.80$



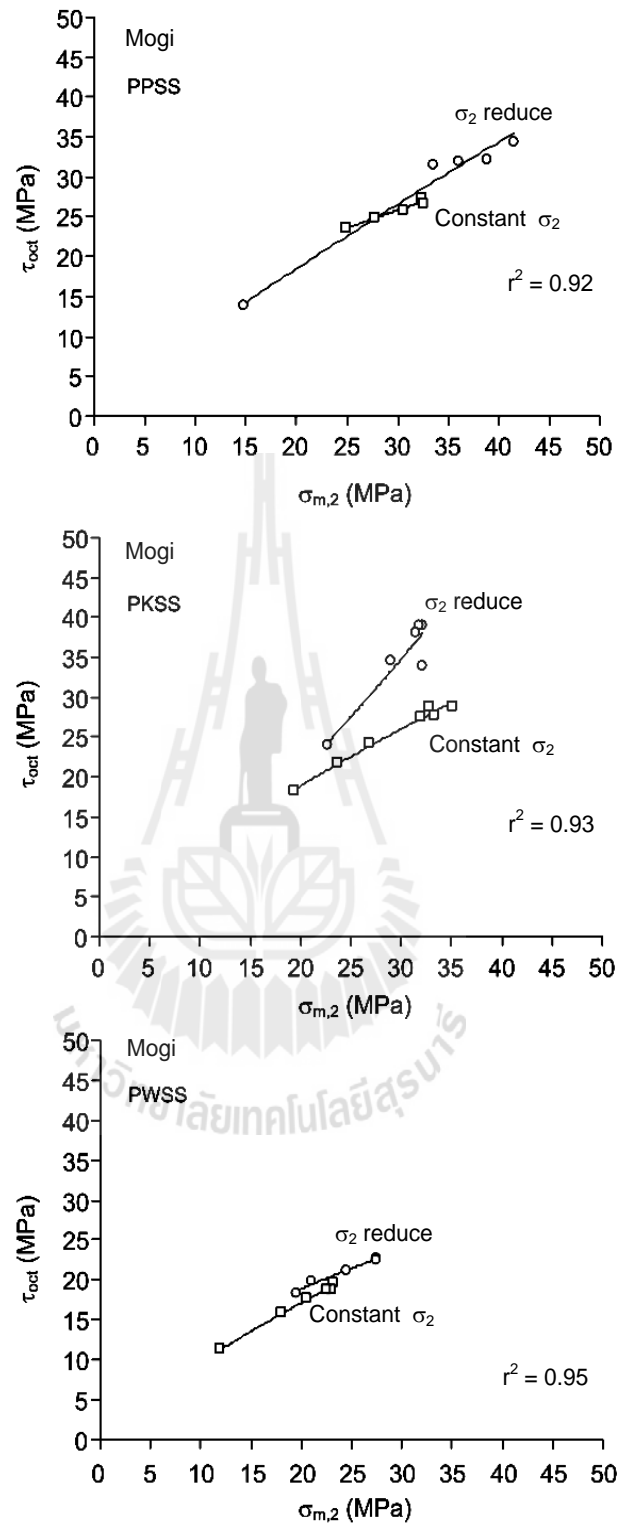


Figure 7.3 Test results fitted by the Mogi criterion.

For the triaxial compression test of TT, PKSS and PPSS under four different stress paths (details in chapter VI), the strength calculations in terms of τ_{oct} and σ_m (or J_1) are in Tables 7.5 through 7.7. The empirical constants A' and B' are given in Table 7.10. The relationship between octahedral shear stresses as a function of mean stress is shown in Figure 7.4.

Table 7.10 Calibrated parameters for the Mogi criterion.

Rock Types	Calibrated Parameters		R^2
	A'	B'	
PKSS	2.429	0.686	0.95
PPSS	3.507	0.612	0.83
Travertine	2.422	0.675	0.96

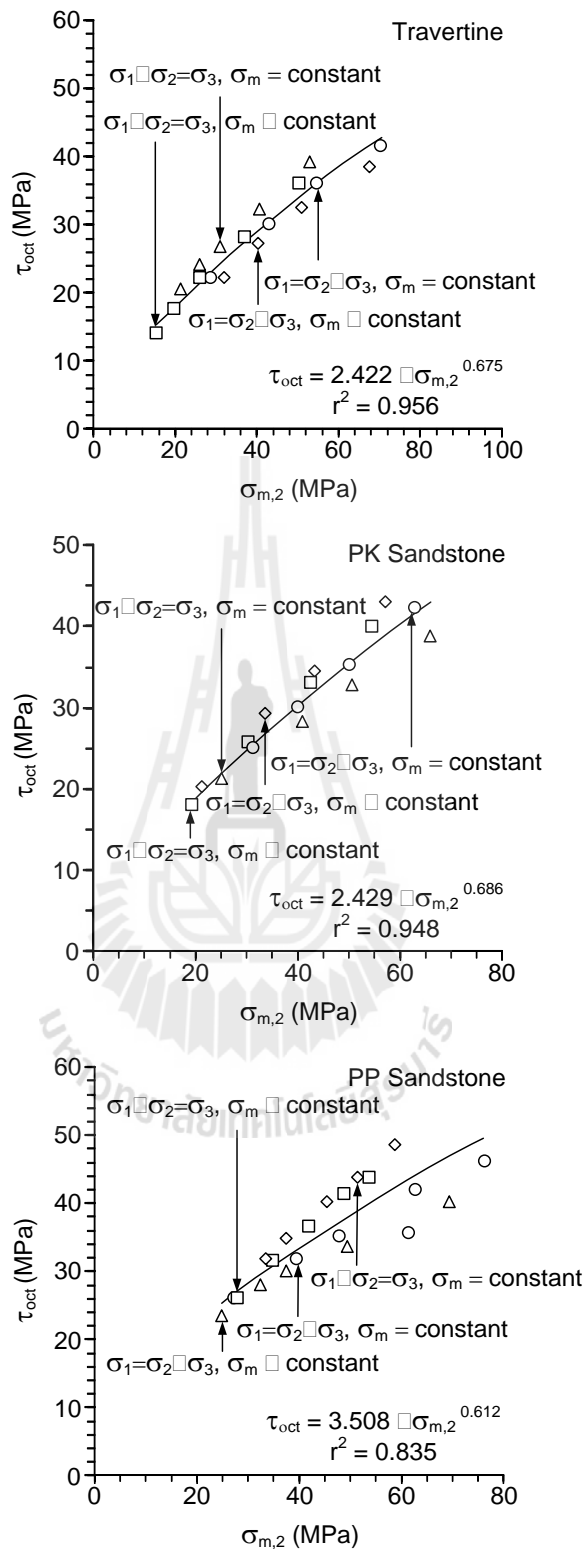


Figure 7.4 Strength results in terms of octahedral shear stresses as a function of mean stress (Mogi criterion).

7.4 Coulomb criterion

The second order stress invariant ($J_2^{1/2}$) and the first order stress invariant or the mean stress (J_1) is calculated from the test results by the following relations (Jaeger and Cook, 1979):

$$J_2^{1/2} = \sqrt{(1/6)\{(\sigma_1 - \sigma_2)^2 + (\sigma_1 - \sigma_3)^2 + (\sigma_2 - \sigma_3)^2\}} \quad (7.12)$$

$$J_1 = (\sigma_1 + \sigma_2 + \sigma_3)/3 \quad (7.13)$$

The Coulomb criterion in from of J_2 and J_1 can be expressed as (Jaeger and Cook, 1979):

$$J_2^{1/2} = \frac{2}{\sqrt{3}} [J_1 \sin\phi + S_0 \cos\phi] \quad (7.14)$$

The Coulomb criterion can also be expressed in terms of the major and minor effective principal stresses, σ_1 and σ_3 written as (Jaeger et al., 2007):

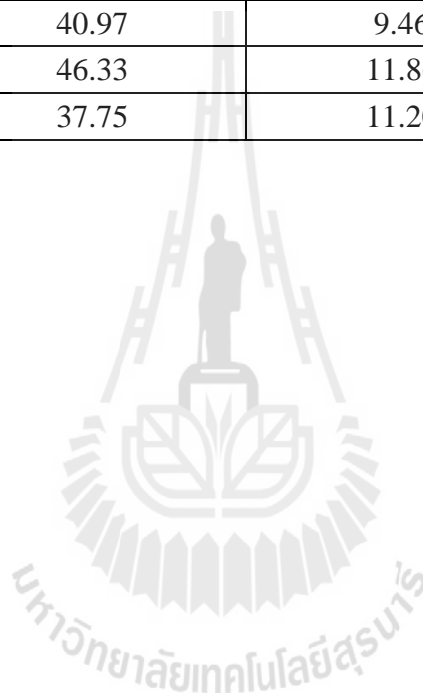
$$\sigma_1 = \sigma_c + \tan^2 (\pi/4 + \phi/2) \sigma_3 \quad (7.15)$$

where ϕ is friction angle, S_0 is cohesion, J_1 is mean stress and $J_2^{1/2}$ is the second order of stress invariant, σ_1 is the major principal effective stress at failure, σ_3 is the minimum principal effective stress at failure, σ_c is the uniaxial compressive strength.

The calibrated parameters for the Coulomb criterion are in listed Table 7.11. The relationship between second order stress invariant as a function of mean stress is shown in Figure 7.5.

Table 7.11 Calibrated parameters for the Coulomb criterion.

Rock Types	Calibrated Parameters		R^2
	ϕ (°)	c (MPa)	
PKSS	40.97	9.46	0.99
PPSS	46.33	11.86	0.99
Travertine	37.75	11.20	0.99



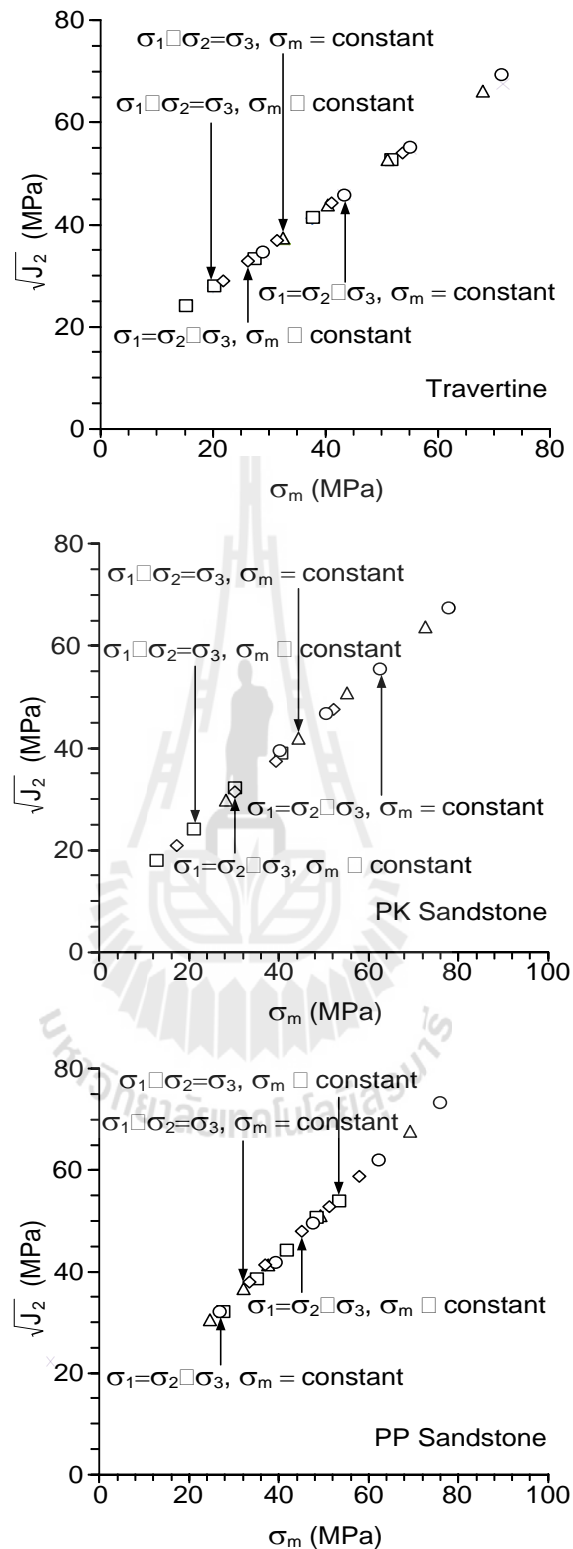


Figure 7.5 Strength results in terms of second order stress invariant as a function of mean stress (Coulomb criterion).

7.5 Discussions of the test results

For the biaxial compressive strength tests of sandstones (PP, PK and PW), the modified Wiebols and Cook and the empirical (power law) Mogi criterion can predict the biaxial compressive strengths reasonably well (Figure 7.1 and 7.3). The intermediate principal stress notably decreases the rock strengths. Tables 7.1 through 7.3 suggest that the intermediate principal stress (σ_2) affects the biaxial strength or the maximum principal stress (σ_1) of the sandstone from three different formations. The σ_1 reaches its maximum at an increased value of σ_2 , and then become lower with higher σ_2 .

Under triaxial compressive strength tests of travertine (TT) and sandstones (PK and PP), the modified Wiebols and Cook criterion and the empirical (power law) Mogi criterion can well describe the compressive strengths of them. The test results suggest that the intermediate principal stress can affect the maximum stress at failure. For the Coulomb criterion, the internal friction angles determined from the triaxial loading condition ($\sigma_2 = \sigma_3$) for PK, PP and TT are 40.97° , 46.33° and 37.75° , and the cohesions are 9.46, 11.86 and 11.20 MPa. The effect of σ_2 on the strengths of these three types of rocks can be best described by the modified Wiebols and Cook criterion. However Coulomb criterion can not describe the strengths of rocks beyond the condition where $\sigma_2 = \sigma_3$, as it can not incorporate the effects of σ_2 . This observation agrees well with the results obtained by Haimson and chang (2000), and Colmenares and Zoback (2002).

CHAPTER VIII

DISCUSSIONS AND CONCLUSIONS

The research objectives are to invent a biaxial rock testing device, to determine the compressive strength of the rocks having soft to medium strengths subjected to biaxial stress states, to investigate the influence of the intermediate stress on rock failure, and to develop three dimensional failure criterion of the rocks that can be readily applied in the design and the stability analysis of geologic structures. The efforts involve laboratory determination of the maximum principal stresses at failure of rock specimens under various intermediate principal stresses and the development of mathematical relationship between the three stresses at failure. The failure stresses are measured, and mode of failure is examined. The three dimensional strength criterions have been derived from the test results. The discussions and conclusions below are related to these aims and efforts.

8.1 Discussions

According to the scope and limitations of the research, the specimens tested in the laboratory experiments are rocks having soft to medium strengths. And the selected rock types are sandstones and travertine. The tested sandstones are from Phu Phan (PP), Phra Wihan (PW) and Phu Kradung (PK) formation (Boonsener and Sonpirom, 1997). Generally, the degree of uniformity of the rock matrix and the grain size helps reduce the intrinsic variability of the mechanical test results. The relatively large crystal sizes of the rock forming minerals may promote the orientation

of their cleavage planes to become selective weakness planes within the specimens. The selected homogeneous sandstones are fine grained and have highly uniform texture, and therefore their testing results should indirectly reflect the performance of the testing device. The average standard deviation of the sandstone elastic modulus is 5.85% for biaxial compression tests and 10.31% for triaxial compression tests. This fairly small standard deviation suggests that the fabricated rock testing device performs reasonably well.

The assumption of using the Poisson's ratios of 0.26, 0.22 and 0.34 for PK sandstone, PP sandstone and travertine to determine the elastic moduli for all principal planes should be considered as a reasonable assumption. These assumed ratios are the average values which are calculated from the results of the tests by reasonable good testing device as discussed above. In general, the Poisson's ratios from any experiment usually can vary from 0.25 to 0.33 for rocks or metals, but may be 0.5 for rubber-like materials (Rahn, 1996). Travertine seems to be more plastic, as shown in Figure 6.17. Furthermore, for PK and PP sandstones, it should be noted that all existing methods for determining the elastic modulus of rocks have assumed a value of Poisson's ratio and used the ratio 0.25 as a normal practice. These methods include the ASTM standard practices, such as dilatometer testing, flat jack testing and plate bearing testing for both on surface and in the galleries. Therefore, the use of the Poisson's ratio 0.26 and 0.22 for PK and PP sandstones to determine the elastic moduli in all principal planes should be reasonable.

The discrepancies of the test results may be partly derived from some characteristics of the selected rock types used as specimens. PK, PP and PW

sandstones are sedimentary rocks and have bedding planes. Therefore, they may show some transversely isotropic properties instead of isotropic in some specimens. Normally, the elastic modulus in the direction parallel to the bedding planes is greater than that normal to the bedding. The Poisson's ratio on the plane parallel to the bedding is lower than the ratio on the plane normal to it.

In general, under similar condition, the stress paths with σ_m not constant (stress path (1) and (3)) usually yield higher value of elastic modulus for different rock specimens than the one with σ_m constant {stress path (2) and (4)}, which results from the influence of σ_2 and σ_3 . Under the condition of triaxial extension of PK, the stress path (3) provides the mean elastic modulus at 8.51 GPa, compared to the value of 7.28 GPa under the stress path (4) (Tables 6.28 and 6.29) and this is in agreement for the isotropic rock. However, under the condition of triaxial compression tests of PK, the stress path (1) provides the mean elastic modulus of 6.62 GPa, compared to the value of 7.63 GPa under the stress path (2) (Tables 6.26 and 6.27). And, this is not in agreement, which may come from transversely isotropic properties of this sandstone. Based on the discussion above, the higher standard deviation of the sandstone elastic modulus between biaxial compression tests and triaxial compression tests (5.85% and 10.31%) may partly result from this phenomenon.

Travertine is chemical sedimentary rock with powderly grain size and compact to earthy texture. However, it is generally banded and has a few holes in its structure. Therefore, both the bands and the holes combined may be a cause of the higher standard deviation of its mean elastic modulus value. Based on the results of triaxial

compression tests of travertine (Table 6.19), the standard deviation is 31.42 %, while PK and PP sandstones yield 11.53% (Tables 6.20 and 6.21).

The sizes of the applied loading areas partly affect the outcome of the test results. Smaller areas usually cause higher degree of intrinsic variability of rock specimens, providing more standard deviation of the elastic modulus values. Therefore, the selection of the appropriate nominal sizes of specimens may enhance more consistences of the experimental results.

8.2 Conclusions

The true triaxial loading device is developed to test rock specimens under biaxial and polyaxial stress states. This device comprises three main components: two steel cross load frames, four hydraulic load cells and two hand pumps. Each load frame has two thick supporting steel plates, connected by four steel rods. They support the structures of the two load cells. The factors of safety are 46.21 for each supporting steel plate and 3.36 of each steel rod. The testing performance of this developed device is reasonably well, based on the consistent and reasonable values of the test results on strengths and elastic parameters for different specimens. Further description on this device efficiency is in the above discussion.

The biaxial compression tests are performed to investigate the effects of stress path on the compressive strengths of sandstones and their deformation. The specimens prepared from PP, PK and PW sandstones have the nominal sizes of $5.5 \times 5.5 \times 5.5 \text{ cm}^3$. These selected specimens are based on the scope and limitation of this study and have homogeneous quality with fine grain size. Three different stress paths have been implemented: (1) σ_1 increases while σ_2 is maintained constant; (2) σ_1

and σ_2 simultaneously increase; and (3) σ_1 increases while σ_2 decreases. The failure stresses are recorded and modes of failure are examined. For the first one, the intermediate stress (σ_2) is varied from 0 to 70 MPa. For the other two stress paths, the mean stress (σ_m) used in the tests ranges from 10 to 45 MPa. The stress-strain curves obtained from biaxial strength tests are shown in Figures 5.3 through 5.9. Assessment of the loading path effect on the rock elastic modulus is also attempted. The calculations of the Poisson's ratios and tangent elastic moduli are made at 50% of the maximum principal stress. The results of the calculations are shown in Tables 5.1 through 5.3. The intermediate principal stress (σ_2) notably affects the strengths of rock specimens. Based on the test results, the stress path (1) with σ_2 constant provides higher strengths than the stress path (3) with reduced σ_2 for all types of rock specimens (Figure 7.1). For the elastic parameters, the results indicate that the elastic modulus and Poisson's ratio of the sandstones are averaged as 9.2 ± 0.6 GPa and 0.22 ± 0.02 for PP, 8.2 ± 0.4 GPa and 0.22 ± 0.01 for PK, and 8.3 ± 0.5 GPa and 0.22 ± 0.02 for PW sandstones.

The modes of failure are also examined from the post-test specimens. Multiple extension fractures from induced stressed σ_1 and σ_2 are observed on sandstone specimens (Figure 5.2). The minimum principal stress (σ_3) is zero, therefore the intermediate principal stress (σ_2) and the maximum principal stress (σ_1) confine the sandstone specimens in such a way that fractures can only be developed in the direction parallel to σ_1 and σ_2 . This observed mode of failure agrees with what Cai (2008) studied about the influence of the intermediate principal stress on rock fracturing and strength near excavation boundary, using a

FEM/DEM combined numerical tool. At the boundary in an underground setting, the intermediate principal stress is often parallel to the tunnel axis, the minimum stress is zero, and the maximum principal stress is the tangential stress. A loading condition of $\sigma_3 = 0$, $\sigma_1 \neq 0$, and $\sigma_2 \neq 0$ thus exists at the boundary. It is seen from the simulation that the generation of tunnel surface parallel fractures (onion skins, spalling and slabbing) is attribute to the existence of moderate intermediate principal stress and low to zero minimum confinement.

The polyaxial compression tests are performed to investigate the effects of stress paths on the compressive strengths and the deformations of PP and PK sandstones, and travertine (TT). The specimens of the three rock types have the nominal sizes of $5.5 \times 5.5 \times 5.5 \text{ cm}^3$. Five different stress paths have been implemented: (1) σ_1 increases while σ_2 equals σ_3 ; (2) σ_1 increases while σ_2 and σ_3 decrease (σ_m constant); (3) σ_1 and σ_2 equally increase while σ_3 is constant; (4) σ_1 and σ_2 equally increase while σ_3 decreases (σ_m constant); (5) σ_1 increases with varied σ_2 and σ_3 ($\sigma_1 \neq \sigma_2 \neq \sigma_3$). The first two stress paths are triaxial compression and another two are triaxial extension while the last one is true triaxial stress condition. For all tests, neoprene sheets are used to minimize the friction at all interfaces between the loading platens and the specimen surfaces. The measured deformations are used to determine the strains along the principal axes during loading. The failure stresses are recorded and modes of failure are examined. The stress-strain curves from the start of loading to failure for all specimens are in Appendix A.

Post-failure observations of failure modes suggest that compressive shear failures are predominant in the specimens tested under low σ_2 while splitting tensile

fractures parallel to σ_1 and σ_2 directions dominate under higher σ_2 . The stress path (2) with reduced σ_3 which make the effect of σ_2 less pronounced should cause the shear failure of the specimens. The stress path (1) with σ_3 constant that enhance greater effect of σ_2 should be the cause of splitting tensile fractures. The stress path (3) and (4) which are both triaxial extension apply higher σ_2 that influence more on the degree of fractures of tensile splitting (Figures 6.4 (d) and (e)). Furthermore, the stress path (3) with σ_m not constant shows more severe splitting fractures of specimens than the stress path (4) with σ_m constant, thus suggesting more pronounced effect of σ_2 under greater σ_3 . The observed splitting tensile fractures under relatively high σ_2 also suggest that the fracture initiation has no influence from the friction at the loading interface in the σ_2 direction. As a result the increase of σ_1 with σ_2 should not be due to the interface friction. This does not agree with a conclusion drawn by Cai (2008) that friction at the interface in the σ_2 direction contributes to the increase of σ_1 at failure. The effects of the five stress paths on rock strengths have been investigated. For triaxial compression tests, stress path (1) ($\sigma_m \neq$ constant) provides higher rock strengths than stress path (2) (σ_m constant), under the same range of σ_3 (Tables 6.4, 6.8 and 6.12). This issue is clarified by the compared graphs (Figures 6.14 through 6.16). For triaxial extension tests, stress path (3) ($\sigma_m \neq$ constant) yields higher strengths of specimens than the stress path (4) ($\sigma_m =$ constant), under the same range of σ_3 (Tables 6.5, 6.9 and 6.13). Furthermore, if compared between the tests on triaxial extension and triaxial compression, the former gives higher strengths under similar condition (Tables 6.6 and 6.7, 6.10 and 6.11 and, 6.14 and 6.15). The test results on the strengths of PP, PK and TT are in the same manner.

The intermediate principal stress (σ_2) may have strong influence on the different strengths of specimens under each stress path as described above. And that is why the rock strengths from triaxial extension tests are always higher than the ones from triaxial compression when under similar condition. Besides, the effect of σ_2 tends to be more pronounced under greater minimum principal stress (σ_3) (Figures 6.17 and 6.18). Consequently, the triaxial tests with σ_m constant usually yield lower strength, compared to the ones with σ_m not constant. However, the strength results of this study as explained above agree with the outcomes of the researches elsewhere (Hardin et al., 1967; Murrel, 1963; Wiebol and Cook, 1968; Haimson and Chang, 2000; Colmenares and Zoback, 2002; Haimson, 2006).

It is postulated that the effects of the intermediate principal stress σ_2 are caused by two mechanisms working simultaneously but having opposite effects on the rock strengths: 1) the mechanism that strengthens the rock matrix in the direction normal to $\sigma_1 - \sigma_3$ plane and 2) the mechanism that induces tensile strains in the directions of σ_1 and σ_3 . The intermediate principal stress can strengthen the rock matrix on the plane normal to its direction, and hence a higher differential stress is required to induce failure. This is the same affect obtained when applying a confining pressure to a cylindrical specimen in the conventional triaxial compression testing. Considering this affect alone, the higher the magnitude of σ_2 applied, the higher σ_1 is required to fail the specimen. However, in the case of the sandstone tests, the relationship between σ_2 magnitudes and the degree of strengthening is non-linear. And this relation should depend on rock types, their

textures and compositions (e.g. grain sizes, distribution of grain sizes, cementation, pore spaces, fissures and micro-cracks, types of rock forming minerals).

The elastic parameters are also investigated. They are calculated for the three-dimensional principal stress-strain relations and are estimated at 30-40% of the maximum principal stresses. It is assumed that the Poisson's ratio (ν) of each rock type is the same for all principal planes and are defined as 0.34, 0.26 and 0.22 for travertine, PK sandstone and PP sandstone (Tables 6.19 through 6.21). The calculated E_1 , E_2 and E_3 suggest that the elastic moduli along the principal directions are similar (Figures 6.19 through 6.21) and this implies that all three types of rock specimens are isotropic. The discrepancies are probably due to the intrinsic variability of each rock specimens.

The PP sandstone has higher elastic modulus and cohesion (with slightly different friction angles) than the other two rock types (Tables 6.19 through 6.21), thus yielding the highest compressive strength. The unconfined compressive strengths for travertine, PK and PP sandstones are 30.20, 38.88 and 55.00 MPa. (Tables 6.1 through 6.3). Tables 6.19 through 6.21 also show that travertine has the highest Poisson's ratio of 0.34 ± 0.01 among the three types of rock specimens and therefore it tends to be more more plastic (Figure 6.17).

In general, the stress path with σ_m not constant (stress path (1) and (3)) usually yield higher value of elastic modulus for different rock specimen than the one with σ_m constant {stress path (2) and (4)}, under similar condition (Tables 6.22 through 6.33). These test results are in accordance with the strength results (Tables 6.4 and 6.5, 6.8 and 6.9, 6.12 and 6.13). Furthermore, the triaxial extension normally yield higher

value of the elastic modulus for each rock specimen, compared to the triaxial compression under similar condition (Tables 6.34 through 6.36). Also, the compared results between triaxial extension and triaxial compression agree with the detailed explanation of strength results on the section 6.4. The major factor that affects the different values of elastic moduli and compressive strengths of different rock specimens under each stress path should be the intermediate principal stress (σ_2). Another factor that provides the influence is the minimum principal stress (σ_3). The higher the σ_3 the more pronounced the σ_2 affects the failure stress (Figure 6.17 and 6.18). Consequently, the comparison of elastic modulus of each rock specimen under different stress path should be considered within the same range of σ_3 .

Some failure criteria along with the influence of the intermediate principal stress on rock failure are studied. The criteria include the modified Wiebols and Cook, the empirical Mogi and Coulomb. For the biaxial compressive strength tests of sandstones (PP, PK and PW), the modified Wiebols and Cook and the empirical (power law) Mogi criterion can predict the biaxial compressive strengths well (Figures 7.1 and 7.3). The former criterion provides regression analysis (r^2) 0.95, 0.96 and 0.93 while the latter yields 0.92, 0.93 and 0.95 for PP, PK and PW. Tables 7.1 through 7.3 suggest that the intermediate principal stress (σ_2) affects the biaxial strength or the maximum principal stress (σ_1) of the sandstones from three different formations. The σ_1 reaches its maximum at an increased value of σ_2 , and then become lower with higher σ_2 . Figures 6.17 and 6.18 further indicate that σ_2 has more pronounced effects on failure stress under higher σ_3 .

Under triaxial compressive strength tests of travertine (TT) and sandstones (PK and PP), the modified Wiebols and Cook criterion and the empirical (power law) Mogi criterion can well describe the compressive strengths of them. The empirical Mogi yields the regression (r^2) 0.95, 0.83 and 0.96 for PP, PK and TT specimens. The test results suggest that the intermediate principal stress can affect the maximum stress at failure. For the Coulomb criterion, the internal friction angles determined from the triaxial loading condition ($\sigma_2 = \sigma_3$) for PK, PP and TT specimens are 40.97° , 46.33° and 37.75° , and the cohesions are 9.46, 11.86 and 11.20 MPa. The effect of σ_2 on the strengths of these three types of rocks can be best described by the modified Wiebols and Cook criterion. However, Coulomb criterion can not describe the strengths of rocks beyond the condition where $\sigma_2 = \sigma_3$, as it can not incorporate the effects of σ_2 . These observations agree well with the results obtained by Haimson and Chang (2000) and Colmenares and Zoback (2002).

It is obvious that the intermediate principal stress notably affects the rock strengths. Also, all the above findings are useful to extrapolate the conventional laboratory test results to some actual in-situ conditions where $\sigma_1 \neq \sigma_2 \neq \sigma_3$.

REFERENCES

- Alexeev, A.D., Revva, V.N., Alyshev, N.A., and Zhitlyonok, D.M. (2004). True triaxial loading apparatus and its application to coal outburst prediction. **International Journal of Coal Geology**. 58(4): 245-250.
- Alsayed, M.I. (2002). Utilising the hoek triaxial cell for multiaxial testing of hollow rock cylinders. **International Journal of Rock Mechanics and Mining Sciences**. 39: 355-366.
- Bobet, A., and Einstein, H.H. (1998). Fracture coalescence in rock-type materials under uniaxial and biaxial compression. **International Journal of Rock Mechanics and Mining Sciences**. 47(7): 863-888.
- Boonsener, M., and Sonpirom, K. (1997). Correlation of tertiary rocks in northeast, Thailand. **International Conference on Stratigraphy and Tectonic Evolution of Southeast Asia and the South Pacific**. Bangkok, Thailand.
- Bunopas, S. (1992). Regional Stratigraphic Correlation in Thailand. **National Conference on Geological Resources of Thailand: Potential for Future Development, Department of mineral Resources**. Bangkok, Thailand.
- Cai, M. (2008). Influence of stress path on tunnel excavation response—Numerical tool selection and modeling strategy. **Tunnelling and Underground Space Technology**. 23: 618-628.

- Chang, C., and Haimson, B. (2005). Non-dilatant deformation and failure mechanism in two Long Valley Caldera rocks under true triaxial compression. **International Journal of Rock Mechanics and Mining Sciences**. 42: 402-414.
- Colmenares, L.B., and Zoback, M.D. (2002). A statistical evaluation of intact rock failure criteria constrained by polyaxial test data for five different rocks. **International Journal of Rock Mechanics and Mining Sciences**. 39: 695-729.
- Fakhimi, A., Carvalho, F., Ishida, T., and Labuz, J.F. (2002). Simulation of failure around a circular opening in rock. **International Journal of Rock Mechanics and Mining Sciences**. 39: 507-515.
- Haimson, B. (2006). True triaxial stresses and the brittle of rock. **Pure and Applied Geophysics**. 163: 1101-1113.
- Haimson, B., and Chang, C. (2000). A new true triaxial cell for testing mechanical properties of rock, and its use to determine rock strength and deformability of Westerly granite. **International Journal of Rock Mechanics and Mining Sciences** 37: 285-296.
- Handin, J., Heard, H.C., and Magouirk, J.N. (1967). Effect of the intermediate principal stress on failure of limestone, dolomite, and glass at different temperature and strain rate. **Journal of Geophysical Research**. 72(2): 611-640.
- Hibbeler, R.C. (2008). **Mechanics of Materials**. Singapore: Prentice-Hall, Inc. 910 pp.

- Hoek, E., and Franklin, J.A. (1970). Developments in triaxial testing equipment. **Rock Mechanics**. 2: 223-228.
- Jaeger, J.C., and Cook, N.G.W. (1979). **Fundamentals of Rock Mechanics** (3rd. Edn.), Chapman & Hall, London, pp. 105-106.
- Jaeger, J.C., Cook, N.G.W., and Zimmerman, R.W. (2007). **Fundamentals of Rock Mechanics** (4th Edn.), Oxford: Blackwood.
- Kulatilake, P.H., Park, J., and Malama, B. (2006). A new rock mass failure criterion for biaxial loading conditions. **Geotechnical and Geological Engineering**. 24: 871-888.
- Kwasniewski, M., Takahashi, M., and Li, X. (2003). Volume changes in sandstone under true triaxial compression conditions. **ISRM 2003–Technology Roadmap for Rock Mechanics**. South African Institute of Mining and Metallurgy. pp. 683-688.
- Mogi, K. (1971). Fracture and flow of rocks under high triaxial compression. **Journal of Geophysical Research**. 76: 1255- 1269.
- Murrell, S.A.F. (1963). A criterion for brittle fracture of rocks and concrete under triaxial stress, and the effect of pore pressure on the criterion. In **Proceedings 5th Symposium on Rock Mechanics** (pp. 563-577). Minnesota, USA.
- Rao, K.S., and Tiwari, R.P. (2002). Physical simulation of jointed model materials under biaxial and true triaxial stress states. **Research Report, IIT Delhi, India**, pp. 30.
- Sagong, M., Park, D., Yoo, J., and Lee, J.S. (2011). Experimental and numerical analyses of an opening in a jointed rock mass under biaxial compression.

International Journal of Rock Mechanics and Mining Sciences. 48(7): 1055-1067.

Sahouryeh, E., Dyskin, A.V., and Germanovich, L.N. (2002). Crack growth under biaxial compression. **Engineering Fracture Mechanics.** 69(18): 2187-2198.

Song, I., and Haimson, B.C. (1997). Polyaxial strength criteria and their use in estimating in situ stress magnitudes from borehole breakout dimensions. **International Journal of Rock Mechanics and Mining Sciences.** 34(3-4): 116.e1-116.e16.

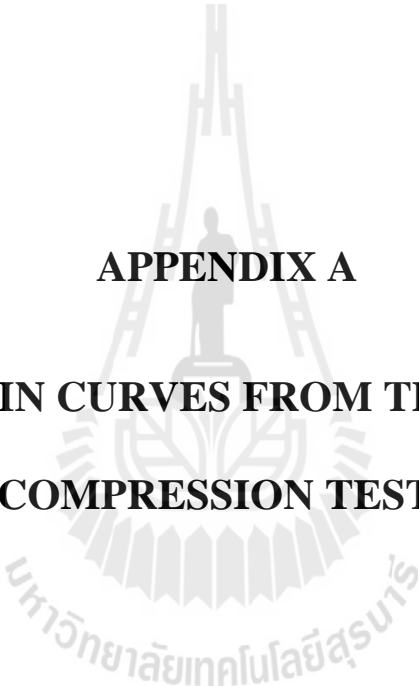
Sriapai, T., Samsri, P., and Fuenkajorn, K. (2011). Polyaxial strengths of Maha Sarakham salt. In **Proceedings of the Third Thailand Rock Mechanics Symposium** (pp. 79-87). Nakhon Ratchasima, Thailand.

Tiwari, R.P., and Rao, K.S. (2004). Physical modeling of a rock mass under a true triaxial stress state. **International Journal of Rock Mechanics and Mining Sciences.** 41(3).

Walsri, C., Poonprakon, P., Thosuwan, R., and Fuenkajorn, K. (2009). Compressive and tensile strengths of sandstones under true triaxial stresses. In **Proceedings of the Second Thailand Symposium on Rock Mechanics** (pp. 199-218). Chonburi, Thailand.

Walsri, C., Poonprakon, P., Thosuwan, R., and Fuenkajorn, K. (2009). Compressive and tensile strengths of sandstones under true triaxial stresses. In **Proceedings of the Second Thailand Rock Mechanics Symposium** (pp. 199-218). Nakhon Ratchasima, Thailand.

- Wawersik, W.R., Carlson, L.W., Holcomb D. J., and Williams, R.J. (1997). New method for true-triaxial rock testing. **International Journal of Rock Mechanics and Mining Sciences**. 34(3): 365-365.
- Wiebols, G.A., and Cook, N.G.W. (1968). An energy criterion for the strength of rock in polyaxial compression. **International Journal of Rock Mechanics and Mining Sciences**. 5: 529-549.
- You, M. (2008). True-triaxial strength criteria for rock. **International Journal of Rock Mechanics and Mining Sciences**. 46: 115-127.
- Yun, X., Mitri, H.S., Yang, X., and Wang, Y. (2010). Experimental investigation into biaxial compressive strength of granite. **International Journal of Rock Mechanics and Mining Sciences**. 47(2): 334-341.
- Zhou, S.A. (1994). Program to mode the initial shape and extent of borehole break out. **Computers and Geosciences**. 20(7-8): 1143-60.
- Zhu, W.C., Liu, J., Tang, C.A., Zhao, X.D., and Brandy, B.H. (2005). Simulation of progresses around underground excavations under biaxial compression. **Tunnelling and Underground Space Technology**. 20(3): 231-247.



APPENDIX A

**STRESS-STRAIN CURVES FROM THE POLYAXIAL
COMPRESSION TESTS**

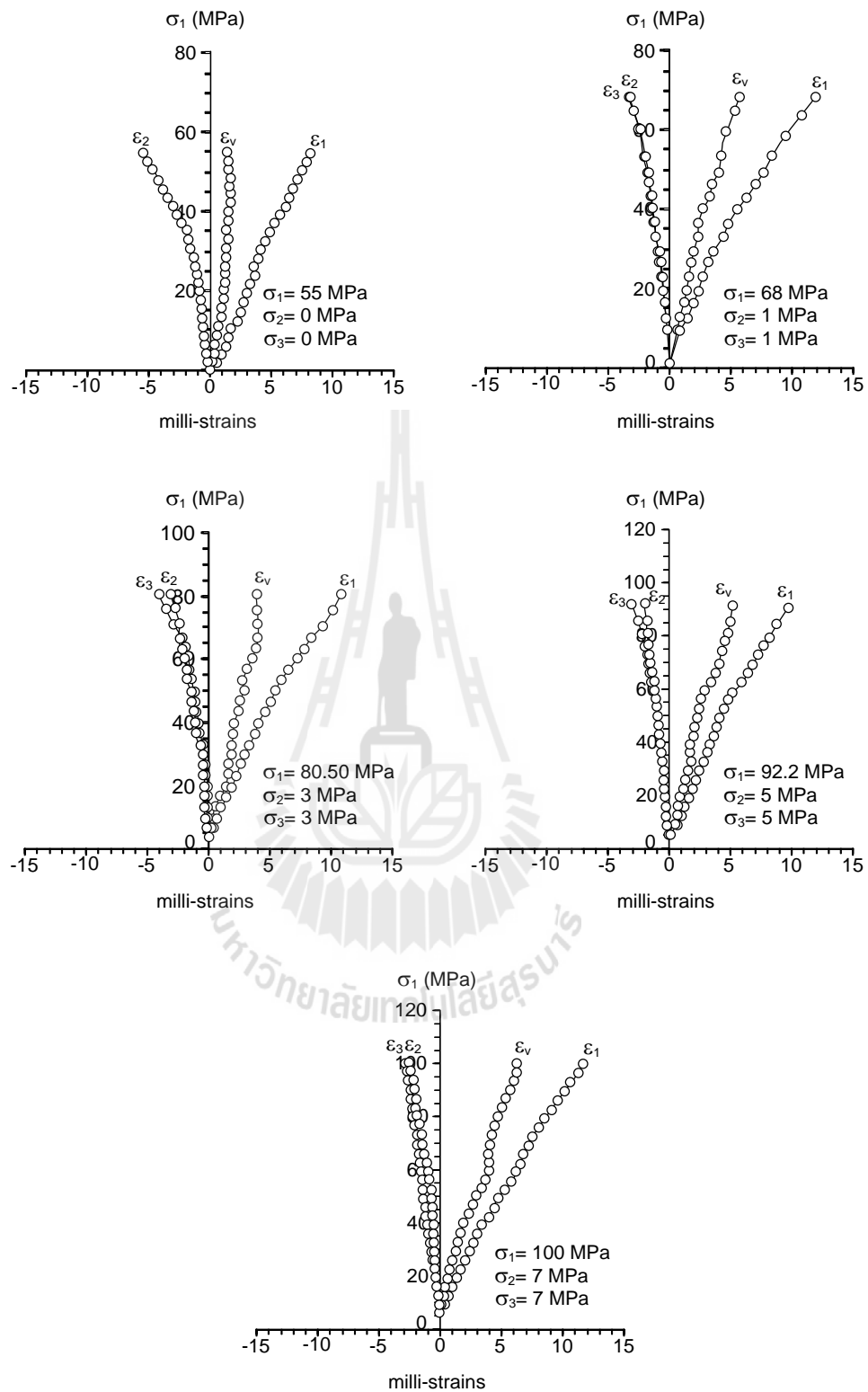


Figure A.1 Stress-strain curves from triaxial testing of PP sandstone: Stress path (1)

σ_1 increase while σ_2 and σ_3 maintained constant ($\sigma_1 \neq \sigma_2 = \sigma_3$).

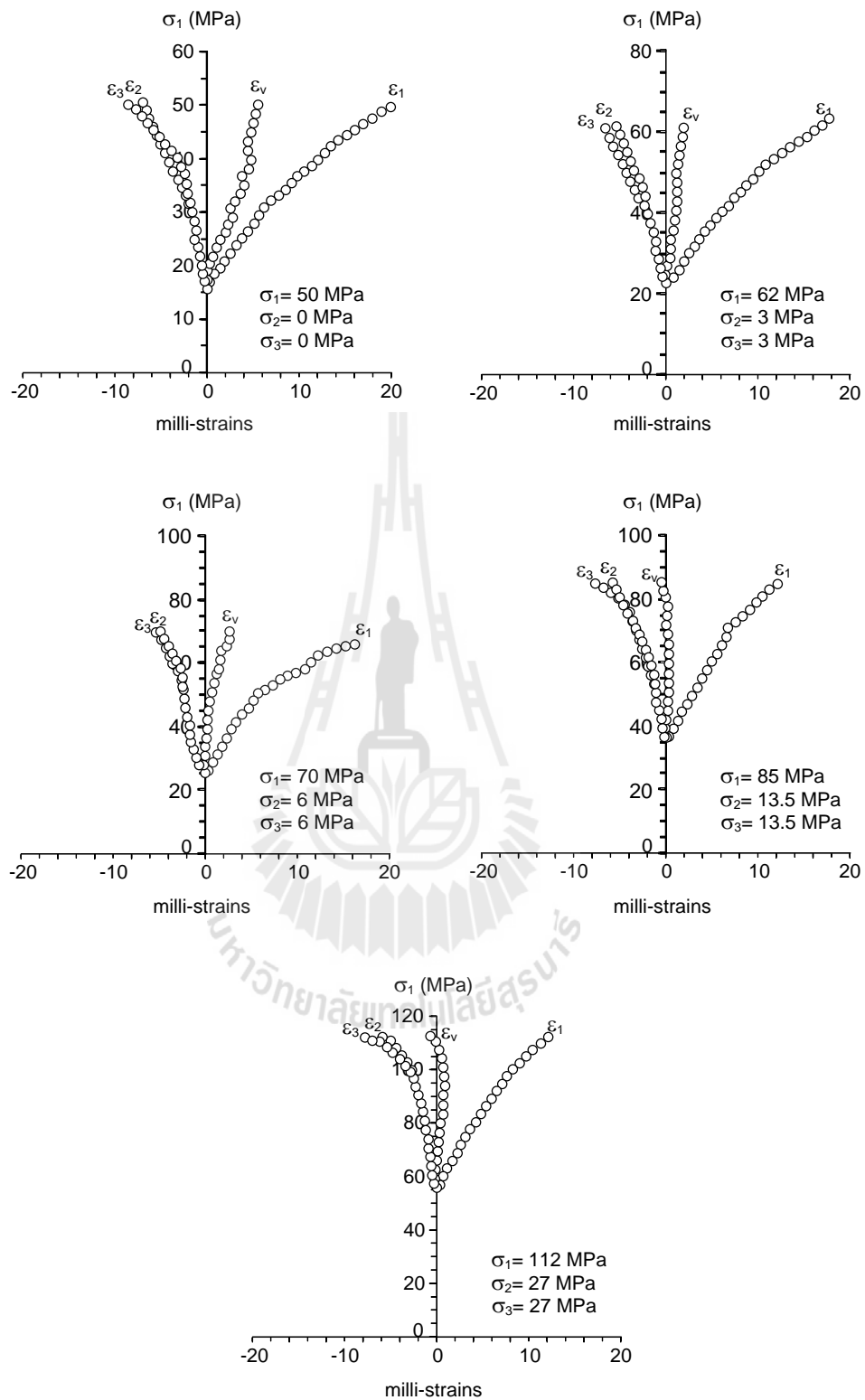


Figure A.2 Stress-strain curves from triaxial testing of PP sandstone: Stress path (2)

σ_1 increase while σ_2 and σ_3 equally decrease ($\sigma_1 \neq \sigma_2 = \sigma_3$).

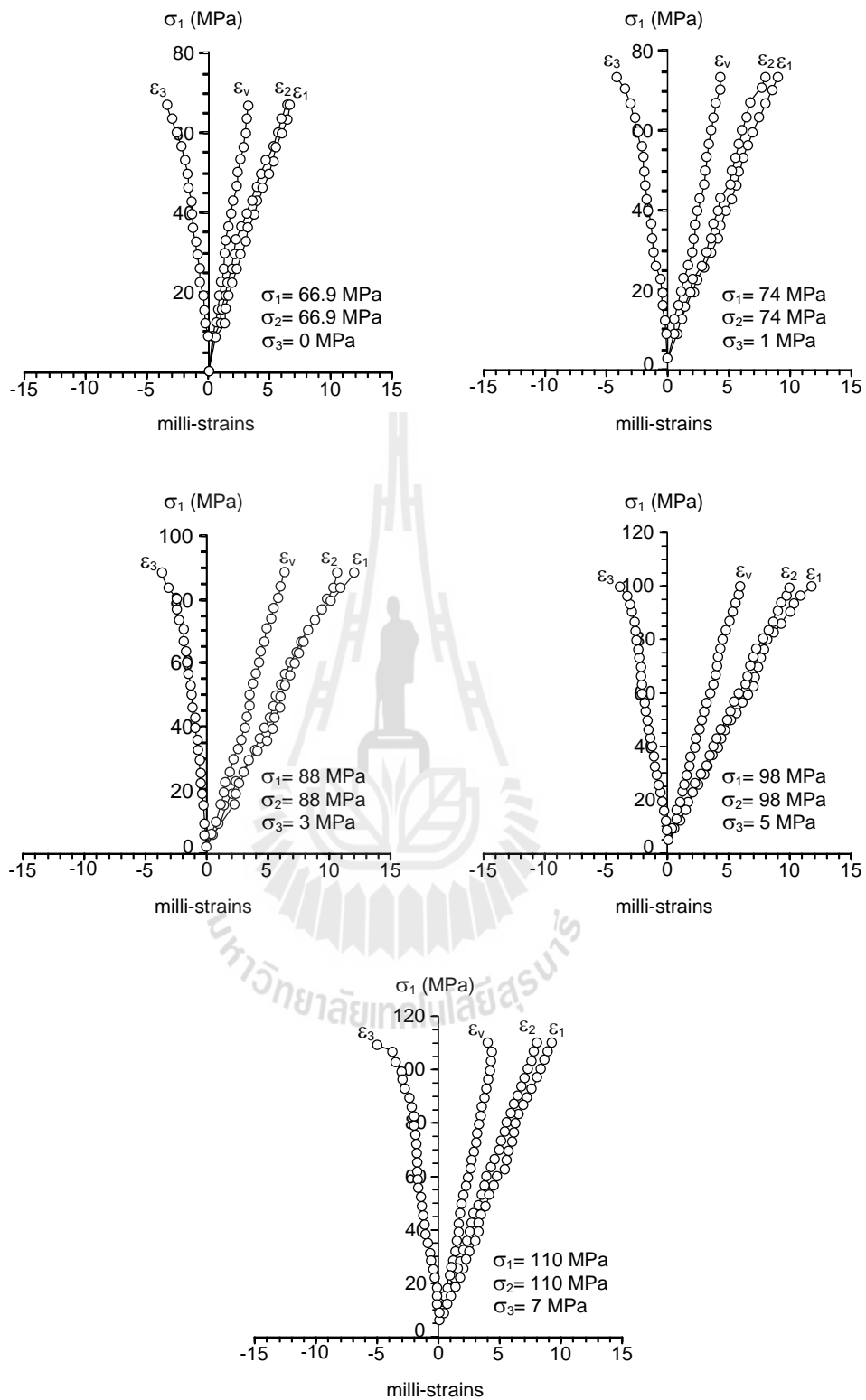


Figure A.3 Stress-strain curves from triaxial testing of PP sandstone: Stress path (3)

σ_1 and σ_2 equally increase while σ_3 maintained constant ($\sigma_1 = \sigma_2 \neq \sigma_3$).

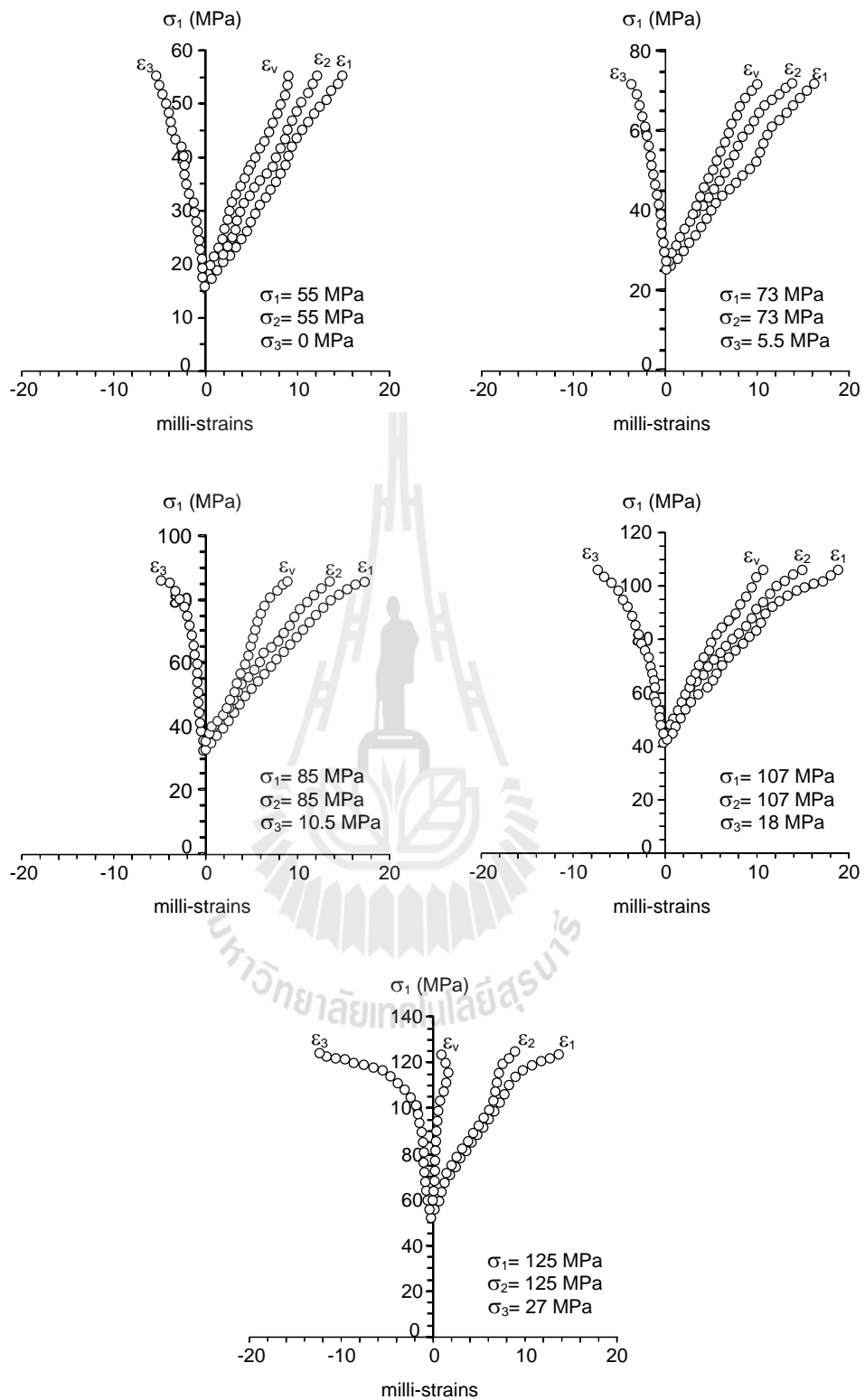


Figure A.4 Stress-strain curves from triaxial testing of PP sandstone: Stress path (4)

σ_1 and σ_2 equally increase while σ_3 decrease ($\sigma_1 = \sigma_2 \neq \sigma_3$).

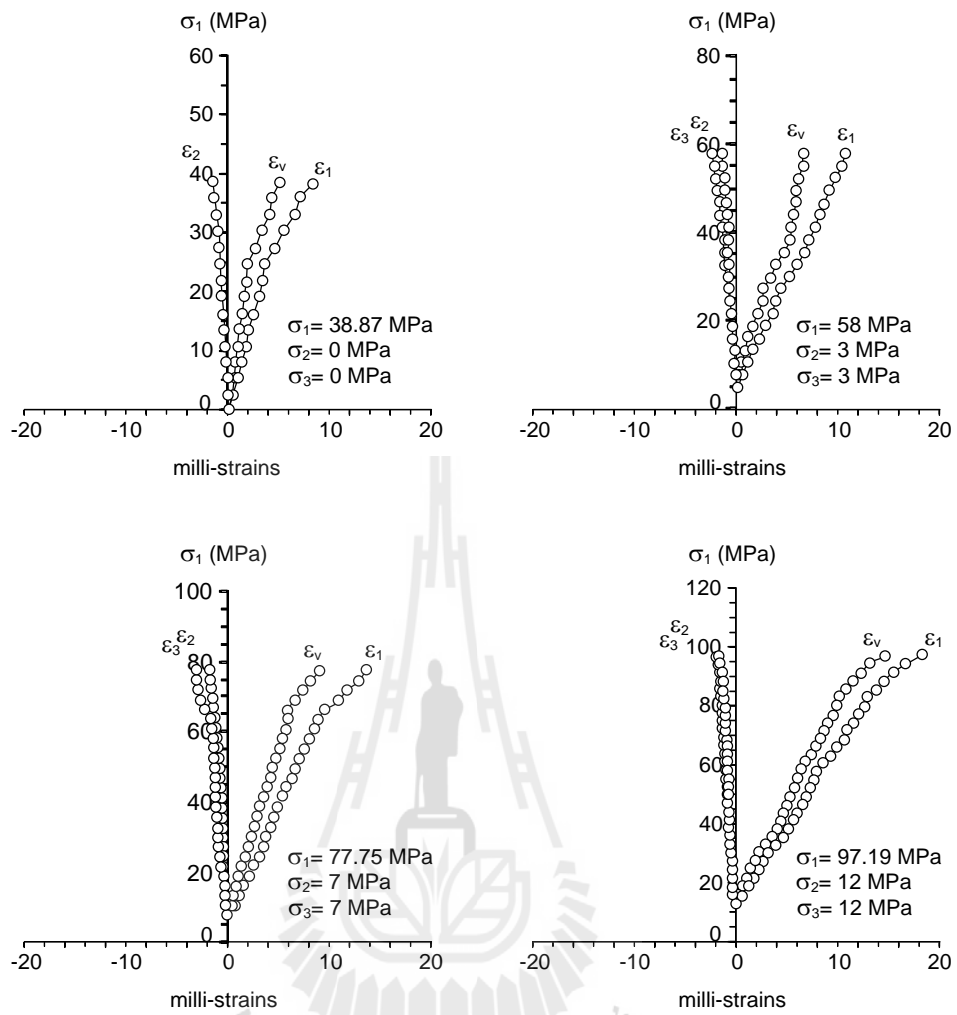


Figure A.5 Stress-strain curves from triaxial testing of PK sandstone: Stress path (1)

σ_1 increase while σ_2 and σ_3 maintained constant ($\sigma_1 \neq \sigma_2 = \sigma_3$).

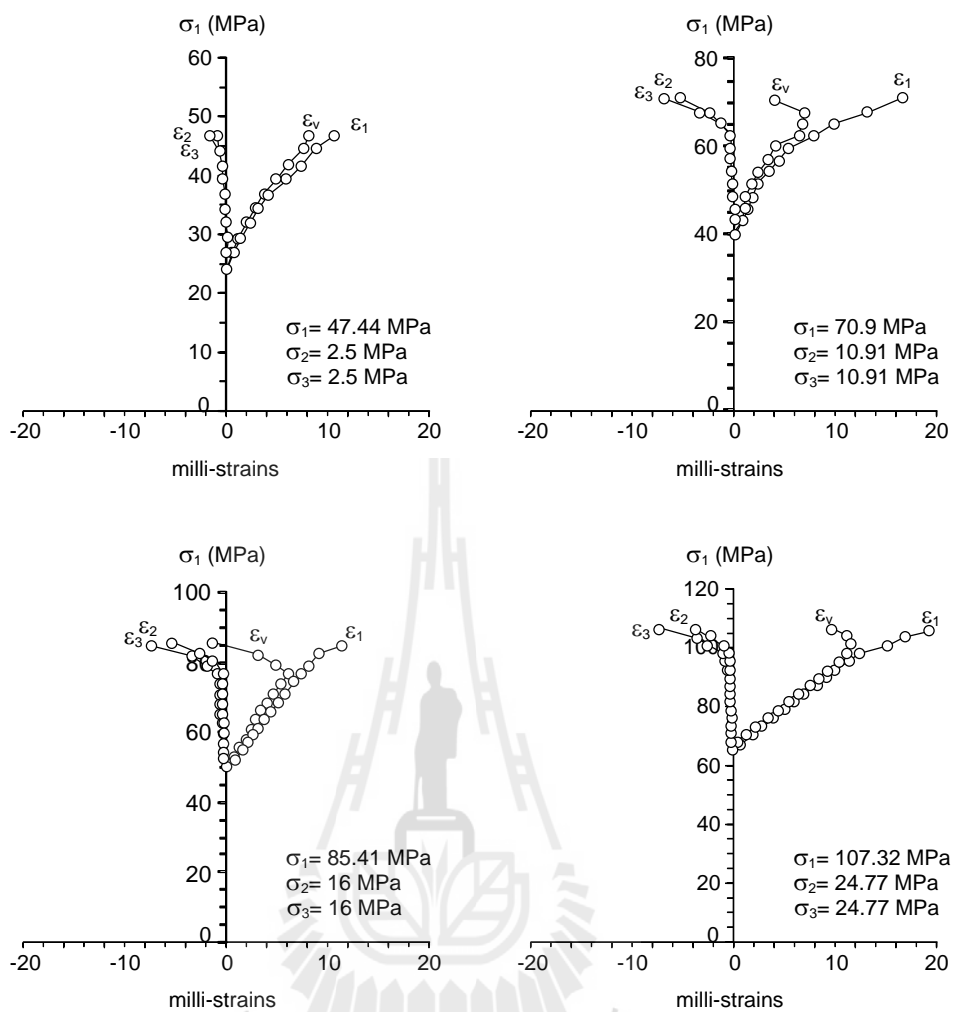


Figure A.6 Stress-strain curves from triaxial testing of PK sandstone: Stress path (2)

σ_1 increase while σ_2 and σ_3 maintained constant ($\sigma_1 \neq \sigma_2 = \sigma_3$).

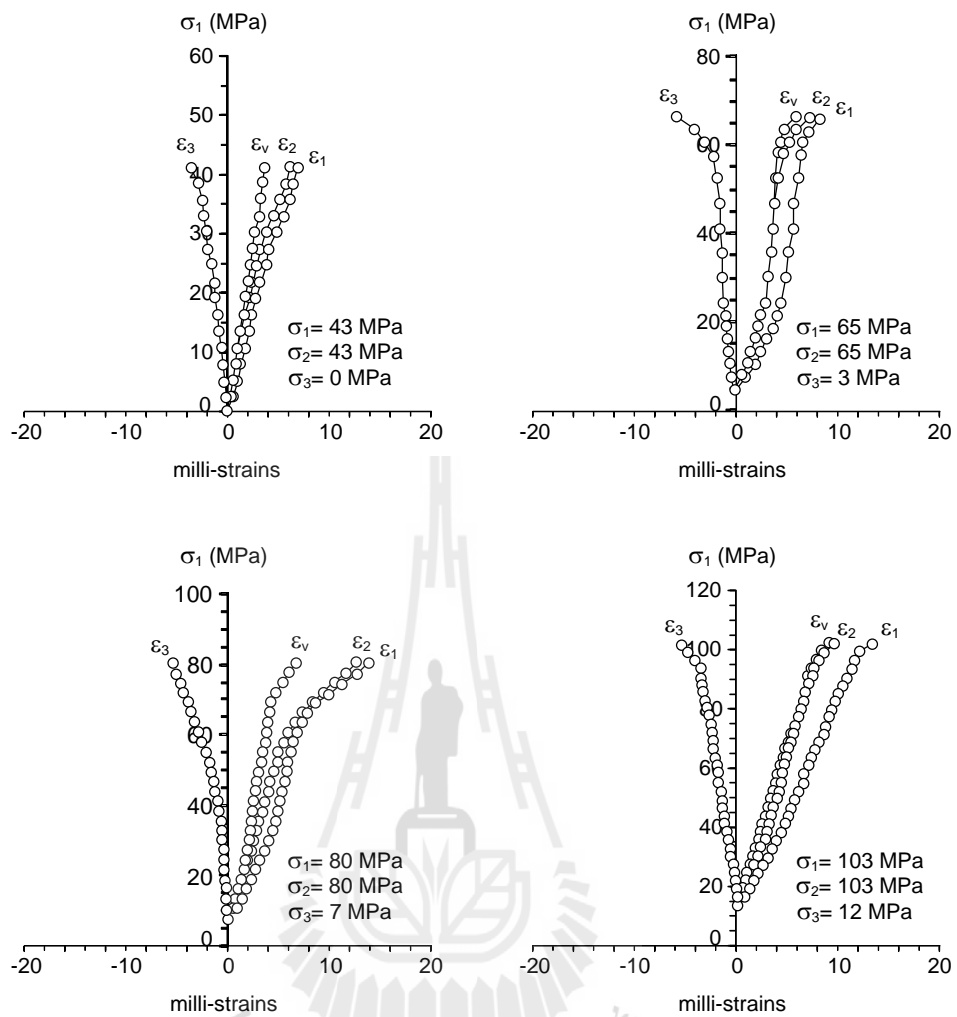


Figure A.7 Stress-strain curves from triaxial testing of PK sandstone: Stress path (3)

σ_1 and σ_2 equally increase while σ_3 maintained constant ($\sigma_1 = \sigma_2 \neq \sigma_3$).

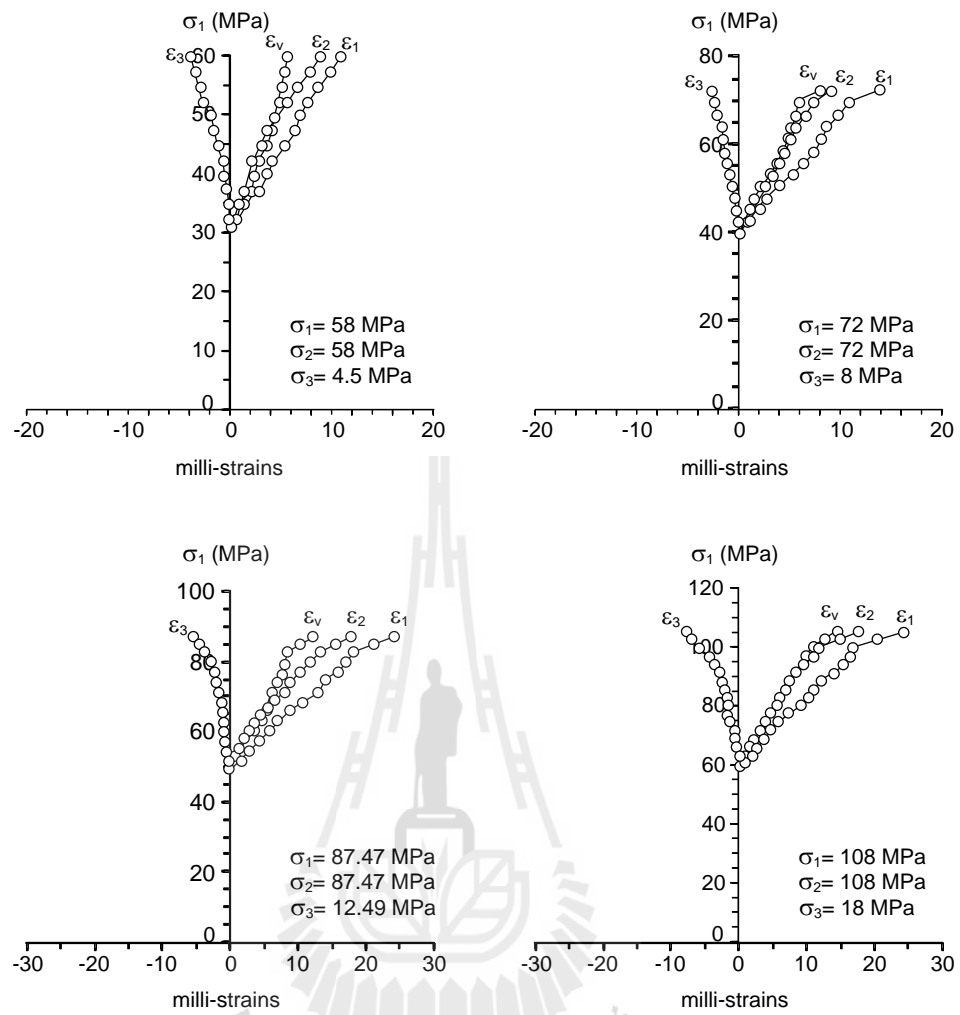


Figure A.8 Stress-strain curves from triaxial testing of PK sandstone: Stress path (4)

σ_1 and σ_2 equally increase while σ_3 decreases ($\sigma_1 = \sigma_2 \neq \sigma_3$).

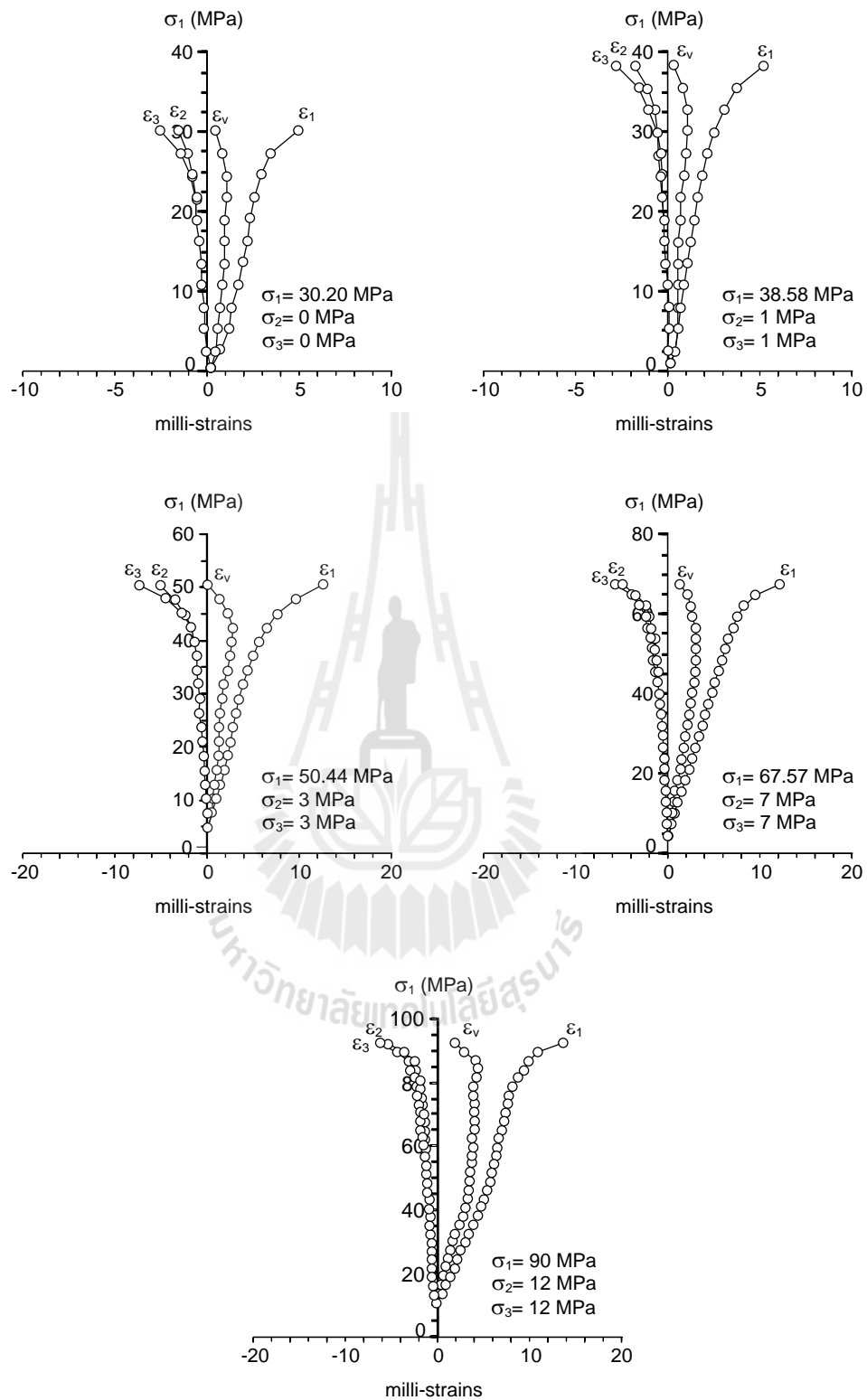


Figure A.9 Stress-strain curves from triaxial testing of travertine: Stress path (1) σ_1 increases while σ_2 equals σ_3 ($\sigma_m \neq \text{constant}$).

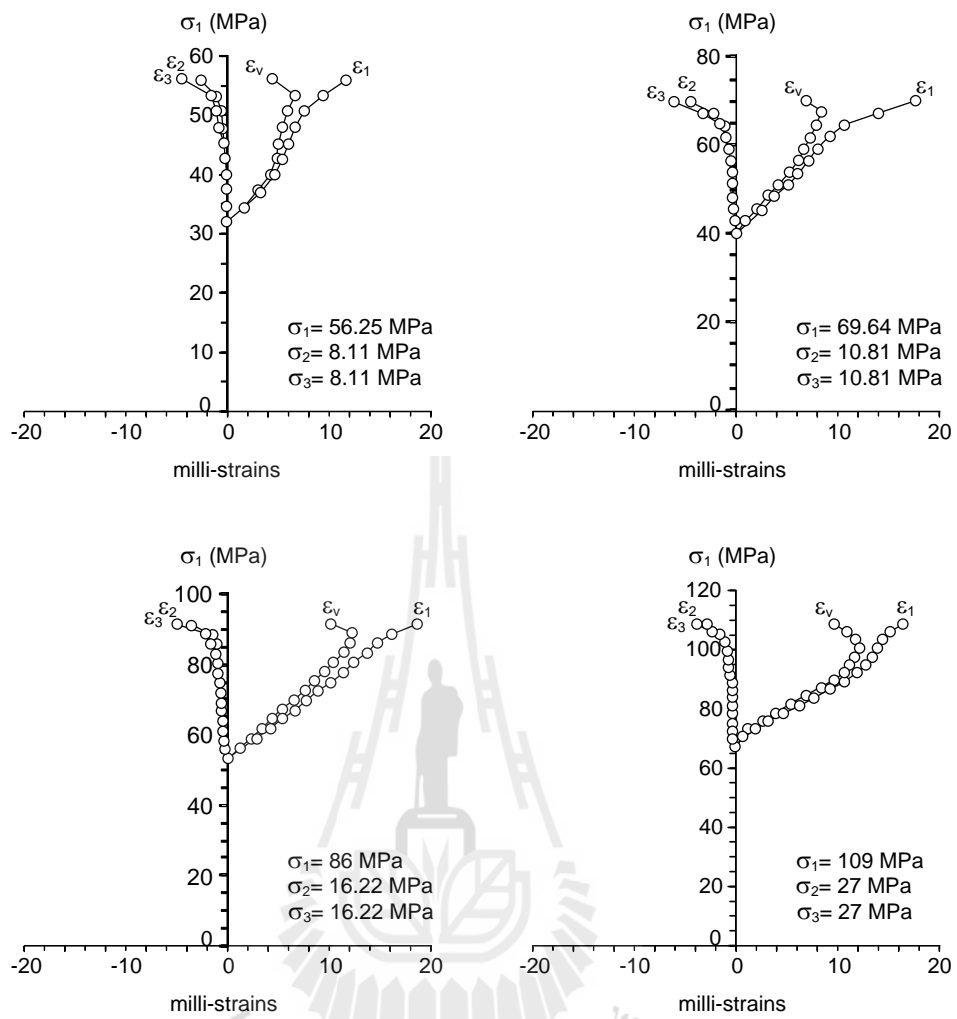


Figure A.10 Stress-strain curves from triaxial testing of travertine: Stress path (2) σ_1 increases while σ_2 equals σ_3 ($\sigma_m = \text{constant}$).

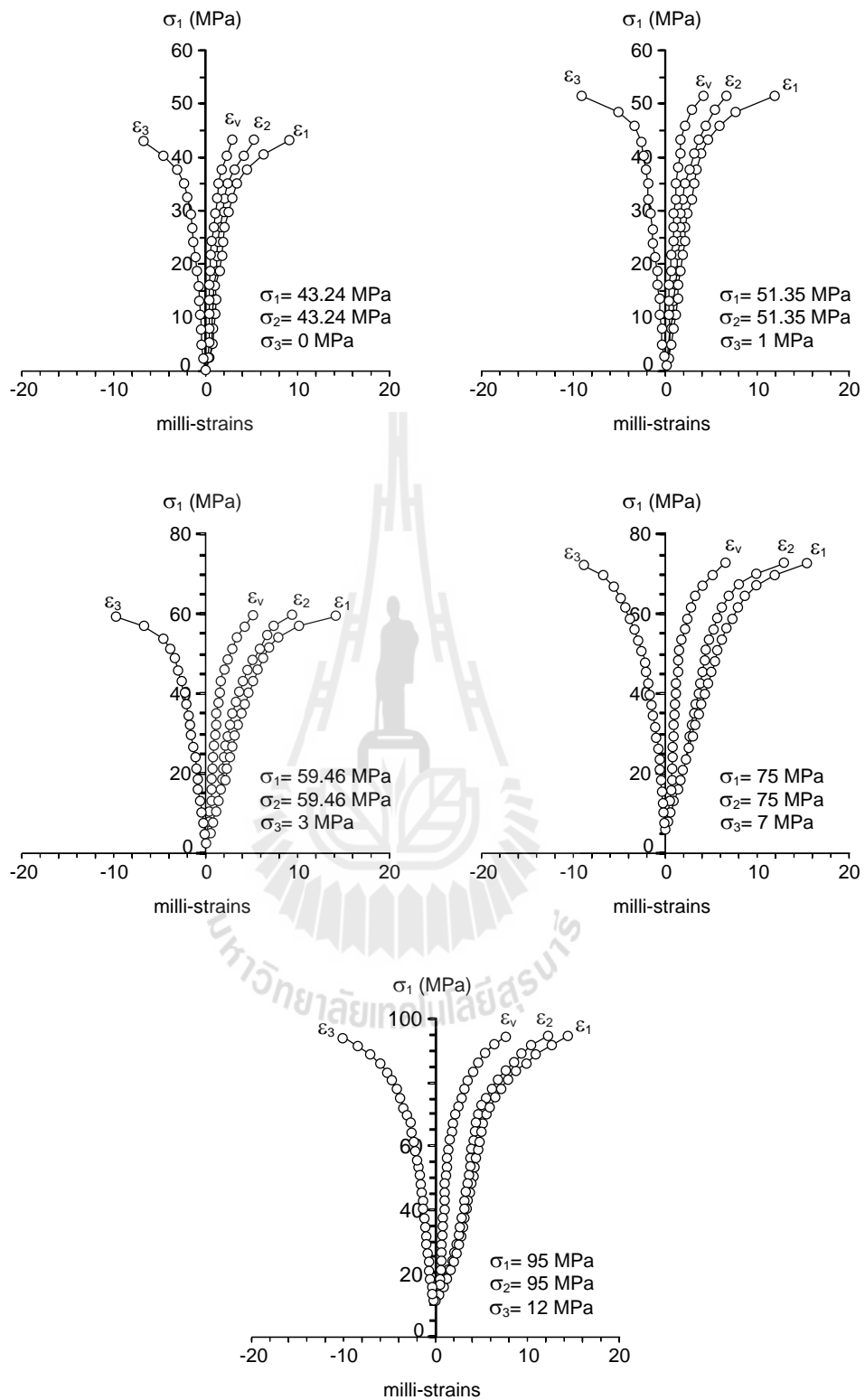


Figure A.11 Stress-strain curves from triaxial testing of travertine: Stress path (3) σ_1

and σ_2 equally increase while σ_3 maintained constant ($\sigma_m \neq \text{constant}$)

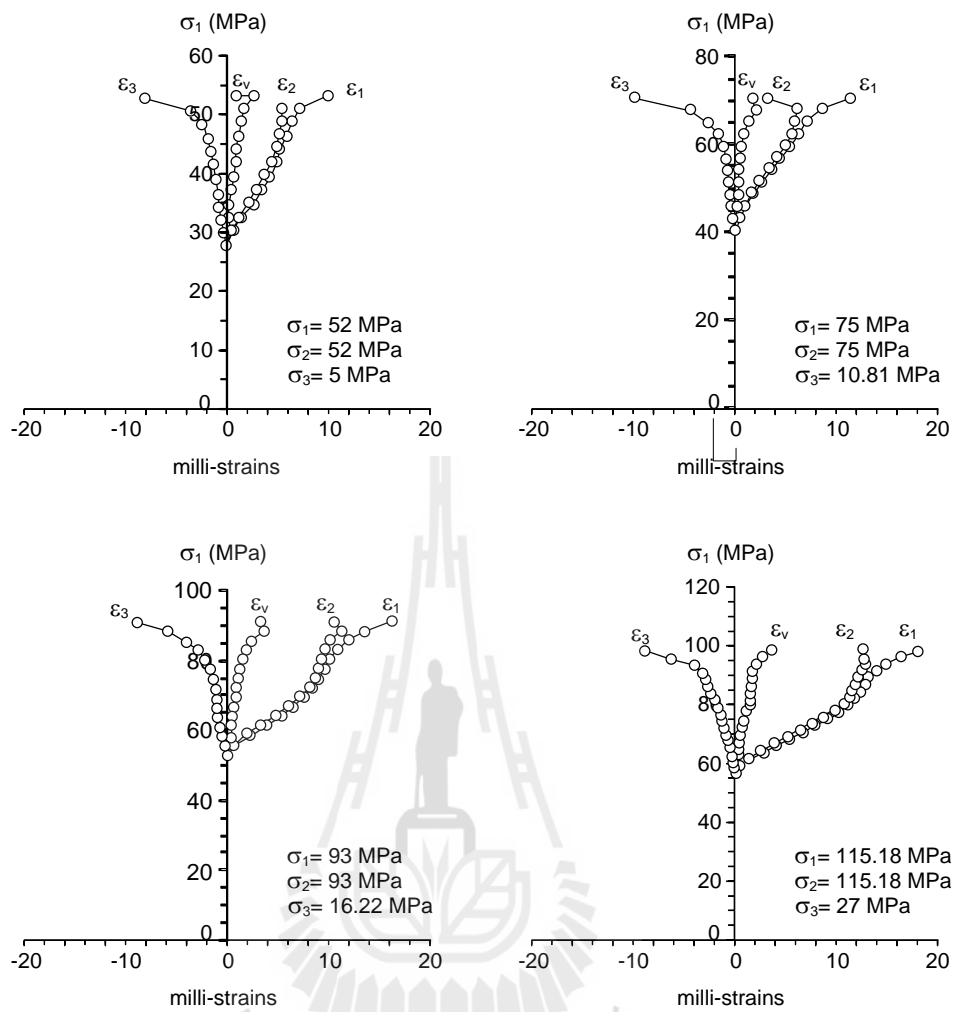
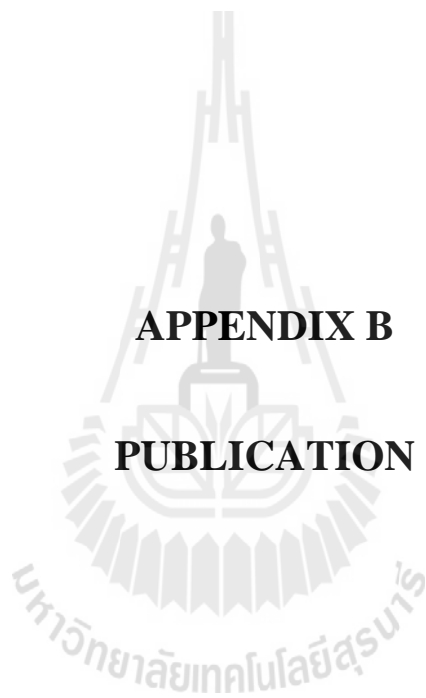


Figure A.12 Stress-strain curves from triaxial testing of travertine: Stress path (4) σ_1 and σ_2 equally increase while σ_3 decreases ($\sigma_m = \text{constant}$).

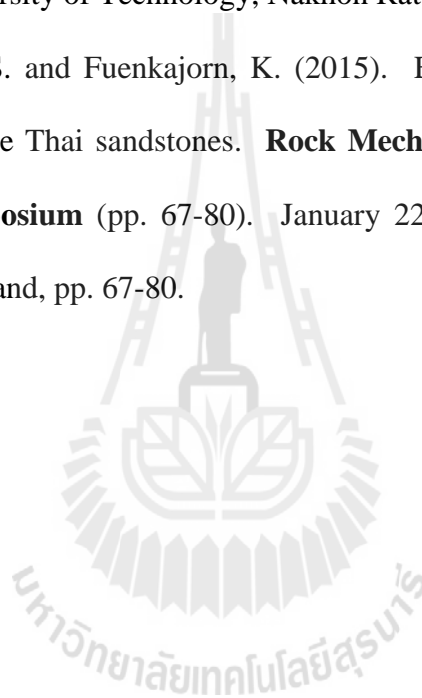
APPENDIX B

PUBLICATION



List of Publication

- Komenthammasopon, S. and Fuenkajorn, K. (2014). Effect of stress path on biaxial strengths of three Thai sandstones. **International Conference on Advances in Civil Engineering for Sustainable Development** (pp. 249-253). August 27-29, Suranaree University of Technology, Nakhon Ratchasima, Thailand, pp. 249-253.
- Komenthammasopon, S. and Fuenkajorn, K. (2015). Effects of stress path on biaxial strengths of three Thai sandstones. **Rock Mechanics Proceedings of the Fifth Thailand Symposium** (pp. 67-80). January 22-23, Romantic Resort and Spa, Khao Yai, Thailand, pp. 67-80.



Effect of Stress Path on Biaxial Strengths of Three Thai Sandstones

S. Komenthammasopon & K. Fuenkajorn

Suranaree University of Technology, Nakhon Ratchasima, Thailand

ABSTRACT: Biaxial compression testing has been performed to investigate the effects of stress path on compressive strengths of sandstones. The specimens are prepared from sandstones from Phu Phan, Phra Wihan and Phu Kradung formations. A biaxial load frame has been fabricated. The specimens have the nominal size of $5.5 \times 5.5 \times 5.5 \text{ cm}^3$. Three different stress paths have been implemented: 1) σ_1 increases while σ_2 are maintained constant; 2) σ_1 and σ_2 equally increase; and 3) σ_1 increases while σ_2 decreases. The results indicate that the elastic modulus and Poisson's ratio of the sandstones are averaged as $9.2 \pm 0.6 \text{ GPa}$ and 0.22 ± 0.02 for PP, $8.2 \pm 0.4 \text{ GPa}$ and 0.22 ± 0.01 for PK, and $8.3 \pm 0.5 \text{ GPa}$ and 0.22 ± 0.02 for PW. The modified Wiebols and Cook can predict the biaxial compressive strengths reasonably well. The intermediate principal stress notably decreases the rock strengths. These findings are useful to extrapolate the conventional laboratory test results ($\sigma_1 > \sigma_2, \sigma_3 = 0$) to some actual in-situ condition ($\sigma_1 \neq \sigma_2 \neq \sigma_3$).

1 INTRODUCTION

Stress path or sequence and duration of directional loading are one of the factors affecting the mechanical behavior of rocks. The stress path dependency is even more pronounced in soft rocks that exhibit plastic behavior when subjected to load (Chen and Zhang 1991, Shames and Cozzarelli 1997). The issue of stress path dependency is important in various disciplines, especially in geomechanic problems, e.g. dams, footings, tunnels, underground mines, open channels, retaining walls and slope embankments. The stress conditions in the rock mass may subject to different stress paths through the processes of construction and operation. For most rock mechanics analyses, stress path independence is often assumed. Rare experimental work has been performed to verify this phenomenon. Only the theoretical implication has been shown, particularly when complex behavior of rock material has to be dealt with. If the stress path dependency is significant, the laboratory test method should be re-designed to detect or measure such factors, and hence to obtain test results that are more representative to the actual in-situ conditions. Analysis and design of engineering structures in soft rock may need to recognize the effect of stress path because soft rocks exhibit their plastic behavior when they are under loading.

The mechanical behavior of rock is commonly analyzed either by the principle of elasticity or inelasticity. In most cases, the principle of elasticity is

often used or assumed for the stress-strain analysis, because it is convenient for practical applications. Under this assumption the effect of the different loading directions and sequences (stress path) is ignored (Chen and Zhang 1991). For some rocks, the assumption of inelastic behavior is more suitable than linearly elastic, especially for soft rock. The mechanical behavior of soft rock is important for the analysis and design of geological engineering structures, such as nuclear waste repository, storage caverns and underground salt mines. Chen and Zhang (1991) and Shames and Cozzarelli (1997) suggest that the analysis of materials in the plastic range is dependent of stress path. The influence of stress path or loading sequence and direction should therefore be considered to realistically analyze the engineering structures in soft formation.

This study involves performing biaxial compression test in order to investigate the effects of stress path on biaxial strength and deformability of sandstones. Three different stress paths have been implemented: (1) σ_1 increases while σ_2 and σ_3 are maintained constant; (2) σ_1 increases while σ_3 decreases and σ_2 is constant; (3) σ_1 increases while σ_2 and σ_3 decrease. Also, some strength criteria are studied to help predict the rock compressive strength.

2 ROCK SAMPLES

The rock specimens used for the biaxial strengths test is Phu Phan (PP), Phra Wihan (PW) and Phu Kradung (PK) sandstones (Boonsener and Sonpirom 1997). They are in the lower and the middle formation in the Khorat basin in northeastern Thailand. These three types of sandstone have homogeneous quality with soft to medium strength and their typical colors are yellowish, white and greenish respectively. The sandstone specimens are prepared to obtain cubical specimens with nominal dimensions of $55 \times 55 \times 55 \text{ mm}^3$.

3 BIAXIAL ROCK TESTING DEVICE

The biaxial rock testing device is developed in order to determine the biaxial compressive strengths of the rock specimens with soft to medium strengths. This device comprises two steel cross load frames, four hydraulic load cells and two hand pumps.

Each load frame has two thick steel plates ($430 \times 430 \times 38 \text{ mm}^3$), connected together with four steel rods with 36 millimeters in diameter. They support the structures of the two load cells. The four load cells, installed at the bases of the load frames, will be connected to the two hand pumps which have the capacity of applying load up to 1000 kN. Besides the three major components, other accessories to measure and monitor the testing include two 4-inch pressure gauges and three dial gauges. The two pressure gauges are installed at the two hand pumps to monitor the exerted load, while the three dial gauges measure the deformation in three principal directions for further strain calculation.

For biaxial rock testing, the rock specimens and the device need to be prepared first. The neoprene will be attached to the specimen surfaces in order to minimize the friction at the interfaces between the loading platens and the rock surfaces. The loading is exerted in a biaxial manner, providing intermediate principal stress (σ_2), maximum principal stress (σ_1) and no minimum stress ($\sigma_3 = 0$). For the preparation of the testing device, the platen and the three dial gauges for displacement measurement will be arranged and adjusted in order to make sure of the precision reading with no alignment when exerting loads. After all the preparation has been finished, the rock specimens will be put in at the center of the crossed frameworks among the four platens. At first, the appropriate slight load will be exerted by the two hand pumps in order to help hold the specimen in place before testing.

4 BIAXIAL COMPRESSION TEST

The biaxial compression tests are performed in three different stress paths as described before, in order to determine the compressive strength and deformation of the sandstone specimens under biaxial stress states. For all tests, neoprene sheets are used to minimize the friction at all interfaces between the loading platen and the specimen surfaces. The measured deformation of sandstone specimens are used to determine the strains along the principal axes during loading. The failure stresses are recorded and mode of failure is examined (Fig. 1). For the first stress path, the intermediate stress (σ_2) is varied from 0 to 70 MPa. For the other two stress paths, the mean stress (σ_m) used in the test ranges from 10 to 45 MPa. The calculations of the Poisson's ratios and tangent elastic moduli are made at 50% of the maximum principal stress. The results indicate that the elastic modulus and Poisson's ratio of the sandstone from different formations are averaged to be $9.2 \pm 0.6 \text{ GPa}$ and 0.22 ± 0.02 for PP sandstone, $8.2 \pm 0.4 \text{ GPa}$ and 0.22 ± 0.01 for PK sandstone and $8.3 \pm 0.5 \text{ GPa}$ and 0.22 ± 0.02 for PW sandstone, as shown in Tables 1 through 3. The tables also provide the octahedral shear strength (τ_{oct}), mean stress (σ_m), and the second order of the stress deviation ($J_2^{1/2}$) at failure. These parameters can be calculated from the principal stresses at failure.

5 STRENGTH CRITERIA

5.1 Modified wiebols and cook criterion

The modified Wiebols and Cook criterion is proposed by Zhou (Zhou 1994). The criterion is originally developed by Wiebols and Cook (Wiebols and Cook 1968) based on the additional energy stored around Griffith cracks due to the sliding of crack surfaces over each other. The modified version defined $J_2^{1/2}$ at failure in terms of J_1 as:

$$J_2^{1/2} = A + BJ_1 + CJ_1^2 \quad (1)$$

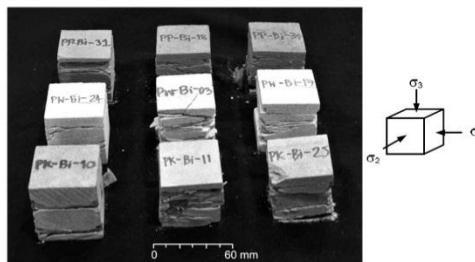


Figure 1. Sandstone specimens with multiple extension fractures from induced stresses of σ_1 and σ_2 .

Table 1. Compressive strengths and elastic parameters of PP sandstone specimens.

Specimen Number	Failure Stresses			σ_m (MPa)	τ_{oct} (MPa)	$J_2^{1/2}$ (MPa)	Elastic Modulus (GPa)	Poisson's Ratio (ν)
	σ_3 (MPa)	σ_2 (MPa)	σ_1 (MPa)					
PP-Bai-01	0.00	0.00	29.46	9.82	13.89	17.01	8.5	0.21
PP-Bai-02	0.00	10.00	72.00	27.33	31.85	39.00	9.1	0.22
PP-Bai-03	0.00	30.00	83.03	37.68	34.33	42.04	9.33	0.25
PP-Bai-04	0.00	50.00	77.67	42.56	32.14	39.37	9.6	0.18
PP-Bai-05	0.00	66.96	66.96	44.64	31.57	38.66	9.8	0.19
PP-path-06	0.00	0.00	49.98	16.66	23.56	28.86	8.7	0.25
PP-path-07	0.00	5.50	55.53	20.34	24.98	30.60	9.7	0.21
PP-path-08	0.00	44.40	61.09	35.16	25.78	31.58	8.3	0.22
PP-path-09	0.00	16.66	64.64	27.10	27.40	33.56	10.2	0.23
PP-path-10	0.00	33.32	65.25	32.86	26.64	32.63	9.20	0.20
Mean \pm Standard Deviation							9.2 \pm 0.6	0.22 \pm 0.02

Table 2. Compressive strengths and elastic parameters of PK sandstone specimens.

Specimen Number	Failure Stresses			σ_m (MPa)	τ_{oct} (MPa)	$J_2^{1/2}$ (MPa)	Elastic Modulus (GPa)	Poisson's Ratio (ν)
	σ_3 (MPa)	σ_2 (MPa)	σ_1 (MPa)					
PK-Bai-01	0.00	0.00	48.00	16.00	22.63	27.71	7.82	0.21
PK-Bai-02	0.00	20.00	69.00	29.67	28.99	35.50	8.12	0.22
PK-Bai-03	0.00	30.00	78.00	36.00	32.12	39.34	7.98	0.20
PK-Bai-04	0.00	40.00	78.00	39.33	31.85	39.00	8.54	0.23
PK-Bai-05	0.00	50.00	76.00	42.00	31.54	38.63	8.11	0.22
PK-Bai-06	0.00	68.00	68.00	45.33	32.06	39.26	8.23	0.21
PK-path-07	0.00	0.00	38.80	12.93	18.29	22.40	8.18	0.23
PK-path-08	0.00	2.27	47.20	16.49	21.74	26.62	8.32	0.24
PK-path-09	0.00	5.00	53.51	19.50	24.13	29.56	7.22	0.22
PK-path-10	0.00	13.88	63.86	25.91	27.42	33.59	7.44	0.21
PK-path-11	0.00	55.33	65.44	40.26	28.76	35.23	7.86	0.23
PK-path-12	0.00	22.21	66.64	29.62	27.71	33.93	8.23	0.22
PK-path-13	0.00	40.23	70.33	36.85	28.81	35.29	7.55	0.21
Mean \pm Standard Deviation							8.0 \pm 0.4	0.22 \pm 0.01

Table 3. Compressive strengths and elastic parameters of PW sandstone specimens.

Specimen Number	Failure Stresses			σ_m (MPa)	τ_{oct} (MPa)	$J_2^{1/2}$ (MPa)	Elastic Modulus (GPa)	Poisson's Ratio
	σ_3 (MPa)	σ_2 (MPa)	σ_1 (MPa)					
PW-Bai-01	0.00	0.00	39.00	13.00	18.38	22.52	8.30	0.23
PW-Bai-02	0.00	10.00	49.00	19.67	21.14	25.89	7.90	0.22
PW-Bai-03	0.00	21.00	55.00	25.33	22.66	27.75	8.43	0.20
PW-Bai-04	0.00	31.00	55.00	28.67	22.51	27.57	7.32	0.21
PW-Bai-05	0.00	40.00	48.97	29.66	21.29	26.07	9.43	0.25
PW-Bai-06	0.00	42.00	42.00	28.00	19.80	24.25	8.77	0.19
PW-path-07	0.00	0.00	24.00	8.00	11.31	13.86	8.45	0.21
PW-path-08	0.00	5.50	36.00	13.83	15.83	19.39	8.67	0.23
PW-path-09	0.00	8.30	41.00	16.43	17.70	21.68	8.37	0.22
PW-path-10	0.00	13.00	46.50	19.83	19.59	23.99	7.98	0.23
PW-path-11	0.00	20.00	46.00	22.00	18.83	23.07	7.93	0.22
PW-path-12	0.00	30.00	45.00	25.00	18.71	22.91	8.11	0.24
Mean \pm Standard Deviation							8.3 \pm 0.5	0.22 \pm 0.02

Table 4. Calibrated parameters of each sandstone type by the Modified Wiebols and Cook criterion under different stress paths.

Rock Types	Calibrated Parameters							
	Biaxial stress				Stress path			
	A (MPa)	B	C (MPa ⁻¹)	ϕ (°)	A (MPa)	B	C (MPa ⁻¹)	ϕ (°)
PP sandstone	-1.62	2.44	-0.034	50	5.50	1.96	-0.034	35
PK sandstone	10.38	1.31	-0.015	46	3.92	1.78	-0.025	35
PW sandstone	6.74	1.64	-0.033	58	0.03	2.08	-0.046	33

The constant J_1 is in terms of σ_1 , σ_2 and σ_3 as defined by:

$$J_1 = (1/3) \times (\sigma_1 + \sigma_2 + \sigma_3) \quad (2)$$

The constant A , B and C depend on rock material and the minimum principal stresses (σ_3) (Table 4). They can be determined under the conditions where $\sigma_3 = 0$, as follows (Colmenares and Zoback 2002):

$$C = [27^{1/2} / (2C_1 + (q-1)\sigma_3 - C_0) \times \{[(C_1 + (q-1)\sigma_3 - C_0)/(2C_1 + (2q+1)\sigma_3 - C_0)] - [(q-1)/(q+2)]\}] \quad (3)$$

where $C_1 = (1 + 0.6\mu) C_0$, $C_0 =$ uniaxial compressive strength of the rock, $\mu_i = \tan\phi$, $q = [(\mu^2 + 1)^{1/2} + \mu]^2 = \tan^2(\pi/4 + \phi/2)$, $\mu =$ coefficient of internal friction of the material, $\phi =$ angle of internal friction. The friction angles for different sandstone specimens on each condition, biaxial stress: $\phi = 50^\circ$ for PP, $\phi = 46^\circ$ for PK, $\phi = 58^\circ$ for PW; stress path: $\phi = 35^\circ$ for PP, $\phi = 35^\circ$ for PK, $\phi = 33^\circ$ for PW, and

$$A = C_0/3^{1/2} - BC_0/3 - CC_0^2/9 \quad (4)$$

$$B = 3^{1/2} (q-1)/(q+2) - C/3(2C_0 + (q+2)\sigma_3) \quad (5)$$

By substitute Equation 2 in Equation 1, we obtain:

$$J_2^{3/2} = [1/6((\sigma_1 - \sigma_2)^2 + (\sigma_1 - \sigma_3)^2 + (\sigma_2 - \sigma_3)^2)]^{1/2} = (3/2)^{1/2} \tau_{oct} \quad (6)$$

And octahedral shear and mean stresses (τ_{oct} and σ_m) at failure for all specimens can be calculated using the following relations (Jaeger et al. 2007):

$$\tau_{oct} = 1/3 [(\sigma_1 - \sigma_2)^2 + (\sigma_2 - \sigma_3)^2 + (\sigma_3 - \sigma_1)^2]^{1/2} \quad (7)$$

$$\sigma_m = (\sigma_1 + \sigma_2 + \sigma_3)/3 \quad (8)$$

The relationship between second order stress invariant as a function of octahedral shear stresses shown in Figure 2.

5.1 Mogi (1971) empirical criterion

The empirical Mogi criterion used here defines $\tau_{oct,f}$ in terms of the effective mean stress ($\sigma_{m,2}$) using a power equation relation (You 2008).

$$\tau_{oct} = A' (\sigma_{m,2})^{B'} \quad (9)$$

$$\sigma_{m,2} = (\sigma_1 + \sigma_2)/2 \quad (10)$$

where A' and B' are empirical constants (Table 5).

6 DISCUSSIONS AND CONCLUSIONS

The results indicate that the elastic modulus and Poisson's ratio of the sandstones are averaged as 9.2

± 0.6 GPa and 0.22 ± 0.02 for PP, 8.2 ± 0.4 GPa and 0.22 ± 0.01 for PK, and 8.3 ± 0.5 GPa and 0.22 ± 0.02 for PW. The modified Wiebols and Cook can predict the biaxial compressive strengths reasonably well (Fig. 2). The intermediate principal stress notably decreases the rock strengths. These findings are useful to extrapolate the conventional laboratory test results ($\sigma_1 > \sigma_2 = \sigma_3$) to some actual in-situ condition ($\sigma_1 \neq \sigma_2 \neq \sigma_3$).

Tables 1 through 3 suggest that the intermediate principal stress (σ_2) affects the biaxial strength or the maximum principal stress (σ_1) of the sandstone from three different formations. The σ_1 reaches its maximum at an increased value of σ_2 , and then become lower with higher σ_2 . Figure 6 clearly suggests that the intermediate principal stress notably affect the rock strengths. Such affect is not linear. The stress path effect acts on the mechanical behavior of soft rocks that exhibits its plastic behavior when subjecting to load.

It is postulated that the effects of the intermediate principal stress σ_2 are caused by two mechanisms working simultaneously but having opposite effects on the rock strengths: 1) the mechanism that strengthens the rock matrix in the direction normal to $\sigma_1 - \sigma_3$ plane and 2) the mechanism that induces tensile strains in the directions of σ_1 and σ_3 . The intermediate principal stress can strengthen the rock matrix on the plane normal to its direction, and hence a higher differential stress is required to induce failure. This is the same affect obtained when applying a confining pressure to a cylindrical specimen in the conventional triaxial compression testing. Considering this affect alone, the higher the magnitude of σ_2 applied, the higher σ_1 is required to fail the specimen. However, in the case of this test of sandstone, the relationship between σ_2 magnitudes and the degree of strengthening is non-linear. And this relation should depend on rock types, their textures and compositions (e.g. grain sizes, distribution of grain sizes, cementation, pore spaces, fissures and micro-cracks, types of rock forming minerals).

ACKNOWLEDGEMENTS

This study is funded by Suranaree University of Technology and by the Higher Education Promotion and National Research University of Thailand. Permission to publish this paper is gratefully acknowledged.

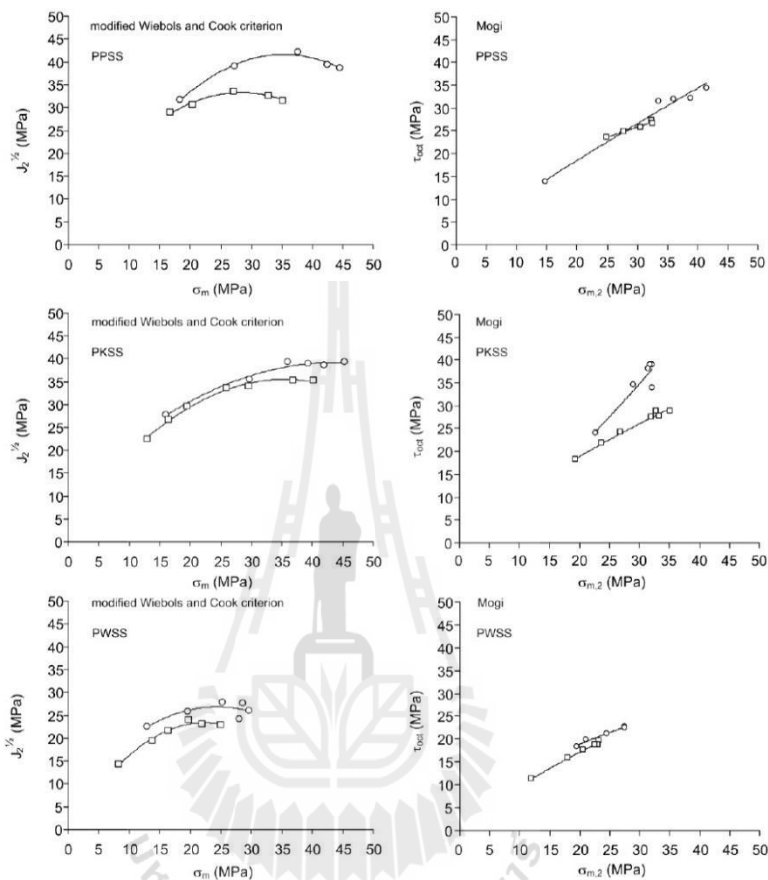


Figure 2. The test results fitted by the modified Wiebols and Cook criterion (left), and Mogi criterion (right).

Table 5. Calibrated parameters of each sandstone type by the Mogi (1971) empirical criterion under different stress paths.

Specimens	Calibrated Parameters	
	Biaxial stress	Stress path
PP	$A' = 1.27 \text{ MPa}, B' = 0.89$	$A' = 4.63 \text{ MPa}, B' = 0.50$
PK	$A' = 0.44 \text{ MPa}, B' = 1.27$	$A' = 1.83 \text{ MPa}, B' = 0.77$
PW	$A' = 3.49 \text{ MPa}, B' = 0.56$	$A' = 1.53 \text{ MPa}, B' = 0.80$

REFERENCES

Boonsener, M. and Sonpirom, K. 1997. Correlation of tertiary rocks in northeast, Thailand. International Conference on Stratigraphy and Tectonic Evolution of Southeast Asia and the South Pacific, Bangkok, Thailand, 19-24 August 1997.

Chen, W.F. and Zhang, H. 1991. Structural plasticity, theory, problems and CAE software. New York-Berlin: Springer.

Jaeger, J.C., Cook, N.G.W. and Zimmerman, R.W. 2007. Fundamentals of rock mechanics. 4th ed. Oxford: Blackweel.

Mogi, K. 1971. Fracture and flow of rocks under high triaxial compression. Journal of Geophysical Research 76: 1255-1269.

Shames, I.H. and Cozzarelli, F.A. 1997. Elastic and inelastic stress analysis. (Revised printing). Philadelphia: Taylor and Francis.

Wiebols, G.A. and Cook, N.G.W. 1968. An energy criterion for the strength of rock in polyaxial compression. International Journal of Rock Mechanics and Mining Sciences 5: 529-549.

You, M. 2008. True-triaxial strength criteria for rock. International Journal of Rock Mechanics and Mining Sciences 46: 115-127.

Zhou, S.A. 1994. Program to mode the initial shape and extent of borehole break out. Computers and Geosciences 20(7-8):1143-60.

Effects of stress path on biaxial strengths of three Thai sandstones

S. Komenthammasopon & K. Fuenkajorn
*School of Geotechnology, Institute of Engineering, Suranaree University of Technology,
 Thailand*

Keywords: Polyaxial, stress path, strength, elasticity

ABSTRACT: The effects of stress paths on compressive strengths of sandstones have been studied through the biaxial compression tests. The prepared specimens are sandstones from three different formations: Phu Phan (PP), Phra Wihan (PW) and Phu Kradung (PK) formation. A true triaxial loading device is developed to test rock specimens under biaxial and polyaxial stress states. The specimens have the nominal sizes of $5.5 \times 5.5 \times 5.5 \text{ cm}^3$. Three different stress paths have been implemented: 1) σ_1 increases while σ_2 are maintained constant; 2) σ_1 and σ_2 equally increase; and 3) σ_1 increases while σ_2 decreases. For the first stress path, the intermediate principal stress (σ_2) is varied from 0 to 70 MPa and for the other two, the mean stress (σ_m) ranges from 10-45 MPa. The results indicate that the elastic modulus and Poisson's ratio of the sandstones are averaged as $9.2 \pm 0.6 \text{ GPa}$ and 0.22 ± 0.02 for PP, $8.2 \pm 0.4 \text{ GPa}$ and 0.22 ± 0.01 for PK, and $8.3 \pm 0.5 \text{ GPa}$ and 0.22 ± 0.02 for PW. The modified Wiebols and Cook can predict the biaxial compressive strengths well and the regression analysis results are 0.95, 0.93 and 0.96 for PP, PW and PK. The intermediate principal stress notably decreases the rock strengths. These findings are useful to extrapolate the conventional laboratory test results ($\sigma_1 > \sigma_2, \sigma_3 = 0$) to some actual in-situ condition ($\sigma_1 \neq \sigma_2 \neq \sigma_3$).

1 INTRODUCTION

Engineering structures (eg. underground excavation, dam foundation, rock slope, nuclear waste disposition) are usually located in complex stress states, which are affected by several factors such as different loading paths, lithologic characters, anisotropy, environment, etc. Since Jaeger pointed out "the possibility of rock failure dependent to the loading path is worth of an argumentative problem" in 1967 (Jaeger JC, 1967) the effect of loading paths on mechanical behavior of rocks has been investigated in past several decades to understand and explore the fracture mechanism of various rock engineering under different loading paths (Cai M, 2008).

Stress path or sequence and duration of directional loading are one of the factors affecting the mechanical rock behavior. The stress path dependency is even more pronounced in soft rocks that exhibit plastic behavior when subjecting to load (Chen & Zhang, 1991; Shames & Cozzarelli, 1997). The issue of stress path dependency is important in various disciplines, especially in geomechanic problems, e.g. dams, footings, tunnels, underground mines, open channels, retaining walls and slope embankments. The stress conditions in the rock mass may subject to different stress paths through the processes of construction and operation. For most

Effects of stress path on biaxial strengths of three Thai sandstones

rock mechanics analyses, stress path independence is often assumed. Rare experimental work has been performed to verify this phenomenon. Only the theoretical implication has been shown, particularly when complex behavior of rock material has to be dealt with. If the stress path dependency is significant, the laboratory test method should be re-designed to detect or measure such factors, and hence to obtain test results that are more representative to the actual in-situ conditions. Analysis and design of engineering structures in soft rock may need to recognize the effect of stress path because soft rocks exhibit their plastic behavior when they are under loading.

The mechanical behavior of rock is commonly analyzed either by the principle of elasticity or inelasticity. In most cases, the principle of elasticity is often used or assumed for the stress-strain analysis, because it is convenient for practical applications. Under this assumption the effect of the different loading directions and sequences (stress path) is ignored (Chen & Zhang, 1991). For some rocks, the assumption of inelastic behavior is more suitable than linearly elastic, especially for soft rock. The mechanical behavior of soft rock is important for the analysis and design of geological engineering structures, such as nuclear waste repository, storage caverns and underground salt mines. Chen & Zhang (1991) and Shames & Cozzarelli (1997) suggest that the analysis of materials in the plastic range is dependent of stress path. The influence of stress path or loading sequence and direction should therefore be considered to realistically analyze the engineering structures in soft formation.

This study involves performing biaxial compression test in order to investigate the effects of stress path on biaxial strength and deformability of sandstones. Three different stress paths have been implemented: (1) σ_1 increases while σ_2 and σ_3 are maintained constant; (2) σ_1 increases while σ_3 decreases and σ_2 is constant; (3) σ_1 increases while σ_2 and σ_3 decrease. Also, some strength criteria are studied to help predict the rock compressive strength.

2 ROCK SAMPLES

The rock specimens used for the biaxial strengths test is Phu Phan (PP), Phra Wihan (PW) and Phu Kradung (PK) sandstones (Boonsener & Sonpirom, 1997). They are in the lower and the middle formation in the Khorat basin in northeastern Thailand. These three types of sandstone have homogeneous quality with soft to medium strength and their typical colors are yellowish, white and greenish respectively. The sandstone specimens are prepared to obtain cubical specimens with nominal dimensions of $55 \times 55 \times 55 \text{ mm}^3$ (Figure 1).

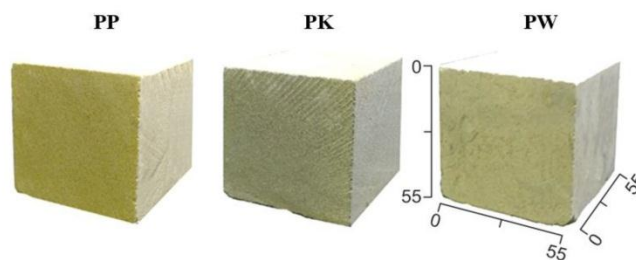


Figure 1. Sandstones specimens with nominal size of $55 \times 55 \times 55 \text{ mm}^3$.

3 BIAXIAL ROCK TESTING DEVICE

The biaxial rock testing device is developed in order to determine the biaxial compressive strengths of the rock specimens with soft to medium strengths. This device comprises two steel cross load frames, four hydraulic load cells and two hand pumps (Figures 2 through 4).

Each load frame has two thick steel plates ($430 \times 430 \times 38 \text{ mm}^3$), connected together with four steel rods with 36 millimeters in diameter. They support the structures of the two load cells. The four load cells, installed at the bases of the load frames, will be connected to the two hand pumps which have the capacity of applying load up to 1000 kN. Besides the three major components, other accessories to measure and monitor the testing include two 4-inch pressure gauges and three dial gauges. The two pressure gauges are installed at the two hand pumps to monitor the exerted load, while the three dial gauges measure the deformation in three principal directions for further strain calculation (Figure 5).

For biaxial rock testing, the rock specimens and the device need to be prepared first. The neoprene will be attached to the specimen surfaces in order to minimize the friction at the interfaces between the loading platens and the rock surfaces. The loading is exerted in a biaxial manner, providing intermediate principal stress (σ_2), maximum principal stress (σ_1) and no minimum stress ($\sigma_3=0$). For the preparation of the testing device, the platen and the three dial gauges for displacement measurement will be arranged and adjusted in order to make sure of the precision reading with no alignment when exerting loads. After all the preparation has been finished, the rock specimens will be put in at the center of the crossed frameworks among the four platens. At first, the appropriate slight load will be exerted by the two hand pumps in order to help hold the specimen in place before testing.

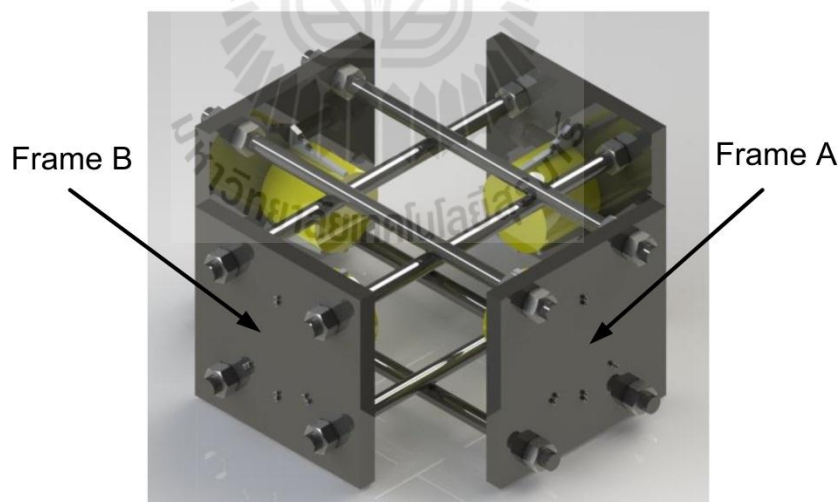


Figure 2. Two steel cross load frames (frame A and B), the main parts of the biaxial rock testing device.

Effects of stress path on biaxial strengths of three Thai sandstones

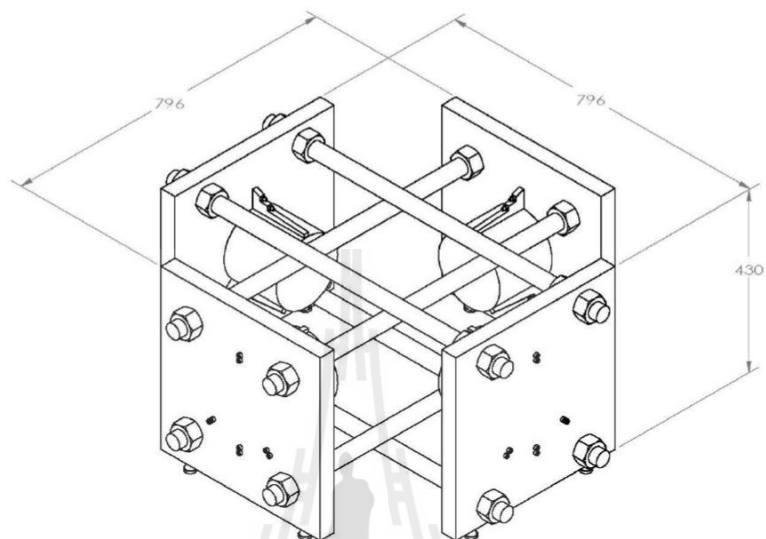


Figure 3. Two steel cross load frames (frame A and B) with dimensions.

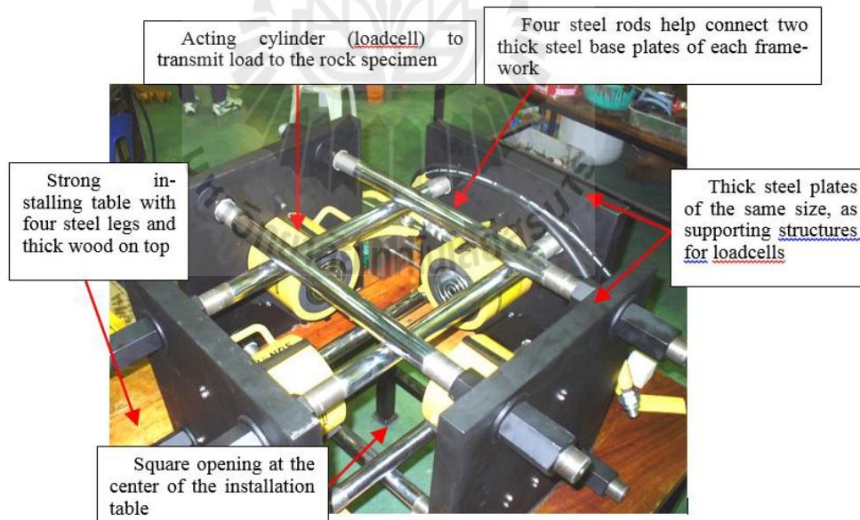


Figure 4. Biaxial rock testing device made from two crossed steel frames, main components.



Figure 5. Components of biaxial rock testing devices: main components and accessories.

4 BIAXIAL COMPRESSION TEST

The biaxial compression tests are performed in three different stress paths as described before, in order to determine the compressive strength and deformation of the sandstone specimens under biaxial stress states. For all tests, neoprene sheets are used to minimize the friction at all interfaces between the loading platen and the specimen surfaces (Figure 6). The measured deformation of sandstone specimens are used to determine the strains along the principal axes during loading. The failure stresses are recorded and mode of failure is examined (Figure 7). For the first stress path, the intermediate stress (σ_2) is varied from 0 to 70 MPa. For the other two stress paths, the mean stress (σ_m) used in the test ranges from 10 to 45 MPa. The calculations of the Poisson's ratios and tangent elastic moduli are made at 50% of the maximum principal stress. The results indicate that the elastic modulus and Poisson's ratio of the sandstone from different formations are averaged to be 9.2 ± 0.6 GPa and 0.22 ± 0.02 for PP sandstone, 8.2 ± 0.4 GPa and 0.22 ± 0.01 for PK sandstone and 8.3 ± 0.5 GPa and 0.22 ± 0.02 for PW sandstone, as shown in Tables 1 through 3. The tables also provide the octahedral shear strength (τ_{oct}), mean stress (σ_m), and the second order of the stress deviation ($J_2^{1/2}$) at failure. These parameters can be calculated from the principal stresses at failure. Based on the Tables 1 through 3, Figure 8 shows the relationship between the intermediate principal stress (σ_2) and the failure stress (σ_1).

5 STRENGTH CRITERIA

5.1 Modified wiebols and cook criterion

The modified Wiebols & Cook criterion is proposed by Zhou (Zhou, 1994). The criterion is originally developed by Wiebols and Cook (Wiebols & Cook, 1968) based on the additional energy stored around Griffith cracks due to the sliding of crack surfaces over each other. The modified version defined $J_2^{1/2}$ at failure in terms of J_1 as:

$$J_2^{1/2} = A + BJ_1 + CJ_1^2 \quad (1)$$

Effects of stress path on biaxial strengths of three Thai sandstones

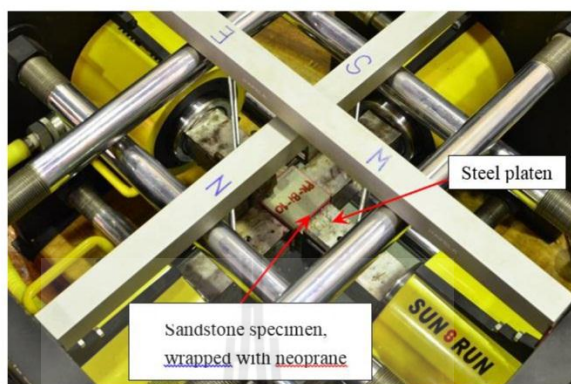


Figure 6. The operation during biaxial compression test of sandstone specimen PK.

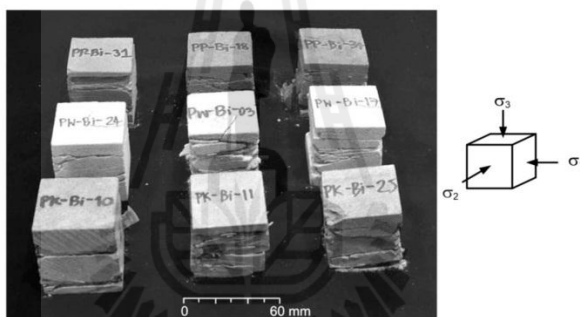


Figure 7. Sandstone specimens with multiple extension fractures from induced stresses of σ_1 and σ_2 .

Table 1. Compressive strengths and elastic parameters of PP sandstone specimens.

Specimen Number	Failure Stresses			σ_m (MPa)	τ_{oct} (MPa)	$J_2^{1/2}$ (MPa)	Elastic Modulus (GPa)	Poisson's Ratio (ν)
	σ_3 (MPa)	σ_2 (MPa)	σ_1 (MPa)					
PP-Bai-01	0.00	0.00	29.46	9.82	13.89	17.01	8.5	0.21
PP-Bai-02	0.00	10.00	72.00	27.33	31.85	39.00	9.1	0.22
PP-Bai-03	0.00	30.00	83.03	37.68	34.33	42.04	9.3	0.25
PP-Bai-04	0.00	50.00	77.67	42.56	32.14	39.37	9.6	0.18
PP-Bai-05	0.00	66.96	66.96	44.64	31.57	38.66	9.8	0.19
PP-path-06	0.00	0.00	49.98	16.66	23.56	28.86	8.7	0.25
PP-path-07	0.00	5.50	55.53	20.34	24.98	30.60	9.7	0.21
PP-path-08	0.00	44.40	61.09	35.16	25.78	31.58	8.3	0.22
PP-path-09	0.00	16.66	64.64	27.10	27.40	33.56	10.2	0.23
PP-path-10	0.00	33.32	65.25	32.86	26.64	32.63	9.2	0.20
Mean \pm Standard Deviation							9.2 \pm 0.6	0.22 \pm 0.02

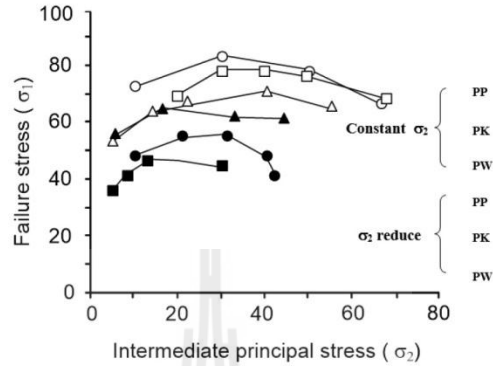
Table 2. Compressive strengths and elastic parameters of PK sandstone specimens.

Specimen Number	Failure Stresses			σ_m (MPa)	τ_{oct} (MPa)	$J_2^{1/2}$ (MPa)	Elastic Modulus (GPa)	Poisson's Ratio (ν)
	σ_3 (MPa)	σ_2 (MPa)	σ_1 (MPa)					
PK-Bai-01	0.00	0.00	48.00	16.00	22.63	27.71	7.82	0.21
PK-Bai-02	0.00	20.00	69.00	29.67	28.99	35.50	8.12	0.22
PK-Bai-03	0.00	30.00	78.00	36.00	32.12	39.34	7.98	0.20
PK-Bai-04	0.00	40.00	78.00	39.33	31.85	39.00	8.54	0.23
PK-Bai-05	0.00	50.00	76.00	42.00	31.54	38.63	8.11	0.22
PK-Bai-06	0.00	68.00	68.00	45.33	32.06	39.26	8.23	0.21
PK-path-07	0.00	0.00	38.80	12.93	18.29	22.40	8.18	0.23
PK-path-08	0.00	2.27	47.20	16.49	21.74	26.62	8.32	0.24
PK-path-09	0.00	5.00	53.51	19.50	24.13	29.56	7.22	0.22
PK-path-10	0.00	13.88	63.86	25.91	27.42	33.59	7.44	0.21
PK-path-11	0.00	55.33	65.44	40.26	28.76	35.23	7.86	0.23
PK-path-12	0.00	22.21	66.64	29.62	27.71	33.93	8.23	0.22
PK-path-13	0.00	40.23	70.33	36.85	28.81	35.29	7.55	0.21
Mean \pm Standard Deviation							8.0 \pm 0.4	0.22 \pm 0.01

Table 3. Compressive strengths and elastic parameters of PW sandstone specimens.

Specimen Number	Failure Stresses			σ_m (MPa)	τ_{oct} (MPa)	$J_2^{1/2}$ (MPa)	Elastic Modulus (GPa)	Poisson's Ratio (ν)
	σ_3 (MPa)	σ_2 (MPa)	σ_1 (MPa)					
PW-Bai-01	0.00	0.00	39.00	13.00	18.38	22.52	8.30	0.23
PW-Bai-02	0.00	10.00	49.00	19.67	21.14	25.89	7.90	0.22
PW-Bai-03	0.00	21.00	55.00	25.33	22.66	27.75	8.43	0.20
PW-Bai-04	0.00	31.00	55.00	28.67	22.51	27.57	7.32	0.21
PW-Bai-05	0.00	40.00	48.97	29.66	21.29	26.07	9.43	0.25
PW-Bai-06	0.00	42.00	42.00	28.00	19.80	24.25	8.77	0.19
PW-path-07	0.00	0.00	24.00	8.00	11.31	13.86	8.45	0.21
PW-path-08	0.00	5.50	36.00	13.83	15.83	19.39	8.67	0.23
PW-path-09	0.00	8.30	41.00	16.43	17.70	21.68	8.37	0.22
PW-path-10	0.00	13.00	46.50	19.83	19.59	23.99	7.98	0.23
PW-path-11	0.00	20.00	46.00	22.00	18.83	23.07	7.93	0.22
PW-path-12	0.00	30.00	45.00	25.00	18.71	22.91	8.11	0.24
Mean \pm Standard Deviation							8.3 \pm 0.5	0.22 \pm 0.02

Effects of stress path on biaxial strengths of three Thai sandstones

Figure 8. Failure stress (σ_1) as a function of Intermediate principal stress (σ_2) under stress path (1).

The constant J_1 is in terms of σ_1 , σ_2 and σ_3 as defined by:

$$J_1 = (1/3) \times (\sigma_1 + \sigma_2 + \sigma_3) \quad (2)$$

The constant A , B and C depend on rock material and the minimum principal stresses (σ_3) (Table 4). They can be determined under the conditions where $\sigma_3=0$, as follows (Colmenares & Zoback, 2002):

$$C = [27^{1/2} / (2C_1 + (q-1)\sigma_3 - C_0) \times [(C_1 + (q-1)\sigma_3 - C_0) / (2C_1 + (2q+1)\sigma_3 - C_0)] - [(q-1)/(q+2)]] \quad (3)$$

where $C_1=(1+0.6\mu) C_0$, C_0 = uniaxial compressive strength of the rock, $\mu_i=\tan\phi$, $q=[(\mu^2+1)^{1/2} + \mu]^2 = \tan^2(\pi/4 + \phi/2)$, μ =coefficient of internal friction of the material, ϕ = angle of internal friction. The friction angles for different sandstone specimens on each condition, biaxial stress: $\phi=50^\circ$ for PP, $\phi=46^\circ$ for PK, $\phi=58^\circ$ for PW; stress path: $\phi=35^\circ$ for PP, $\phi=35^\circ$ for PK, $\phi=33^\circ$ for PW, and

$$A = C_0/3^{1/2} - BC_0/3 - CC_0^2/9 \quad (4)$$

$$B = 3^{1/2} (q-1)/(q+2) - C/3(2C_0 + (q+2)\sigma_3) \quad (5)$$

By substitute Equation 2 in Equation 1, we obtain:

$$J_2^{1/2} = [1/6((\sigma_1 - \sigma_2)^2 + (\sigma_1 - \sigma_3)^2 + (\sigma_2 - \sigma_3)^2)]^{1/2} = (3/2)^{1/2} \tau_{oct} \quad (6)$$

And octahedral shear and mean stresses (τ_{oct} and σ_m) at failure for all specimens can be calculated using the following relations (Jaeger et al., 2007):

$$\tau_{oct} = 1/3 [(\sigma_1 - \sigma_2)^2 + (\sigma_2 - \sigma_3)^2 + (\sigma_3 - \sigma_1)^2]^{1/2} \quad (7)$$

$$\sigma_m = (\sigma_1 + \sigma_2 + \sigma_3)/3 \quad (8)$$

Table 4. Calibrated parameters of each sandstone type by the Modified Wiebols & Cook criterion under different stress paths.

Rock Types	Calibrated Parameters								R ²
	Constant σ_2				σ_2 reduce				
	A (MPa)	B	C (MPa ⁻¹)	ϕ (°)	A (MPa)	B	C (MPa ⁻¹)	ϕ (°)	
PPSS	-1.62	2.44	-0.034	50	5.50	1.96	-0.034	35	0.95
PKSS	10.38	1.31	-0.015	46	3.92	1.78	-0.025	35	0.96
PWSS	6.74	1.64	-0.033	58	0.03	2.08	-0.046	33	0.93

The relationship between second order stress invariant as a function of octahedral shear stresses shown in Figure 9.

5.2 Mogi (1971) empirical criterion

The empirical Mogi criterion used here defines $\tau_{oct,f}$ in terms of the effective mean stress ($\sigma_{m,2}$) using a power equation relation (You, 2008).

$$\tau_{oct} = A' (\sigma_{m,2})^{B'} \quad (9)$$

$$\sigma_{m,2} = (\sigma_1 + \sigma_2)/2 \quad (10)$$

where A' and B' are empirical constants (Table 5). The test results fitted by Mogi criterion are shown in Figure 10.

Table 5. Calibrated parameters of each sandstone type by the Mogi (1971) empirical criterion under different stress paths

Specimens	Calibrated Parameters		R ²
	Constant σ_2	σ_2 reduce	
PPSS	$A' = 1.27 \text{ MPa}, B' = 0.89$	$A' = 4.63 \text{ MPa}, B' = 0.50$	0.92
PKSS	$A' = 0.44 \text{ MPa}, B' = 1.27$	$A' = 1.83 \text{ MPa}, B' = 0.77$	0.93
PWSS	$A' = 3.49 \text{ MPa}, B' = 0.56$	$A' = 1.53 \text{ MPa}, B' = 0.80$	0.95

6 DISCUSSIONS AND CONCLUSIONS

The results indicate that the elastic modulus and Poisson's ratio of the sandstones are averaged as $9.2 \pm 0.6 \text{ GPa}$ and 0.22 ± 0.02 for PP, $8.2 \pm 0.4 \text{ GPa}$ and 0.22 ± 0.01 for PK, and $8.3 \pm 0.5 \text{ GPa}$ and 0.22 ± 0.02 for PW. The modified Wiebols and Cook and the empirical Mogi can predict the biaxial compressive strengths well (Figures 9 and 10). The former criterion provides regression analysis r^2 0.95, 0.96 and 0.93 while the latter yields 0.92, 0.93 and 0.95 for PP, PK and PW. The intermediate principal stress notably decreases the rock strengths. These findings are useful to extrapolate the conventional laboratory test results ($\sigma_1 > \sigma_2 = \sigma_3$) to some actual in-situ condition ($\sigma_1 \neq \sigma_2 \neq \sigma_3$).

Effects of stress path on biaxial strengths of three Thai sandstones

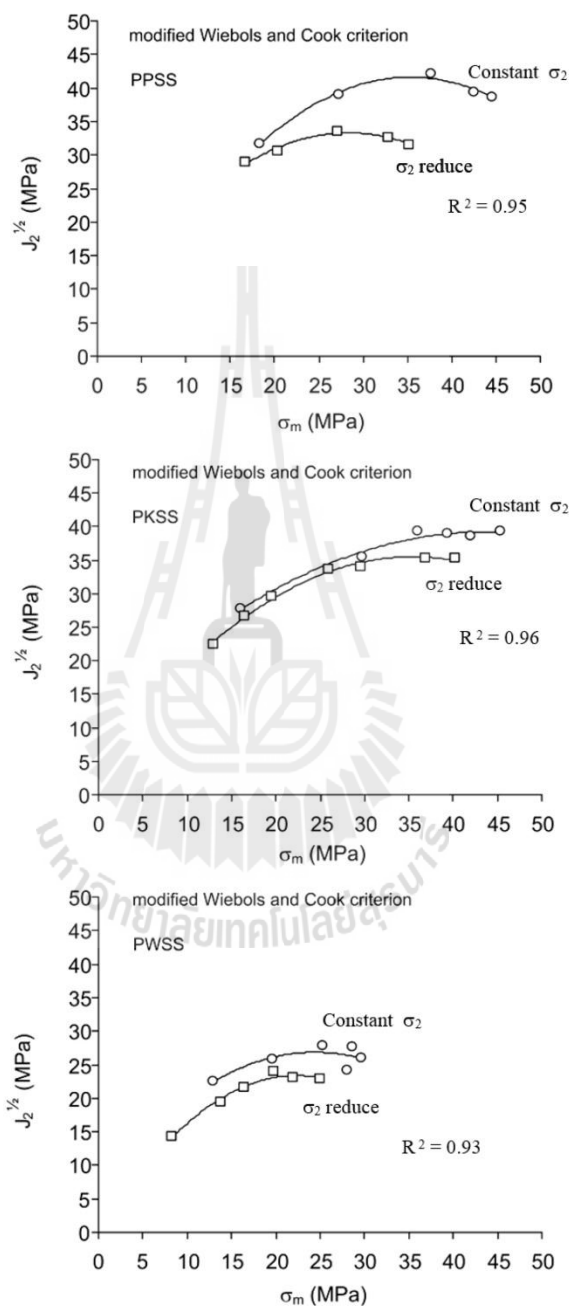


Figure 9. Test results fitted by the modified Wiebols & Cook criterion.

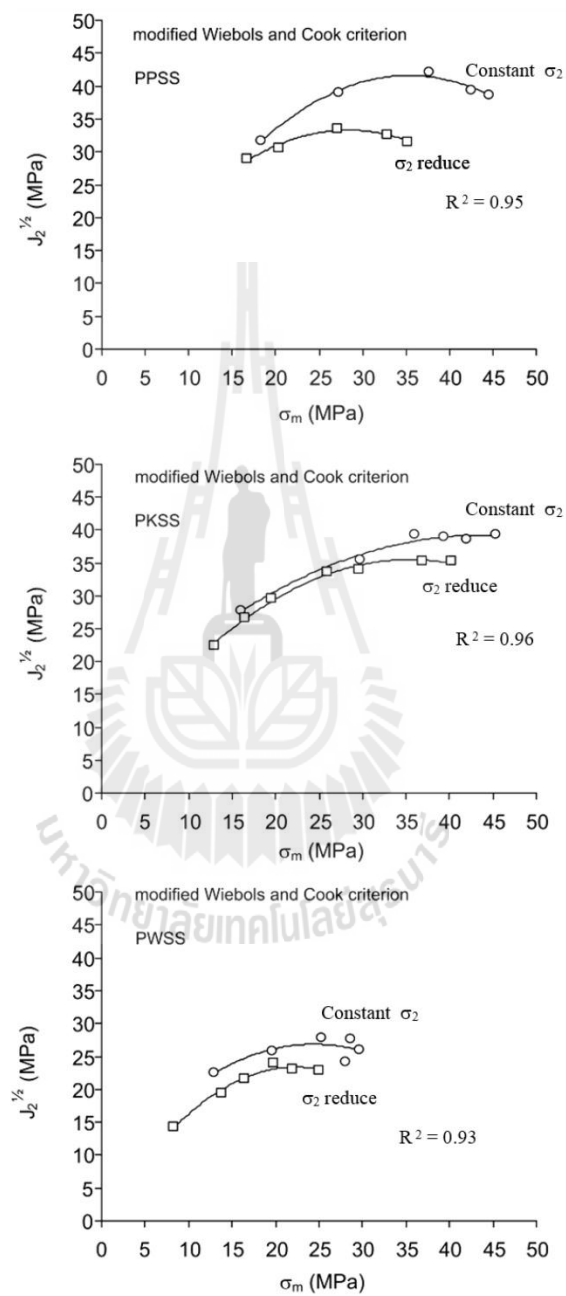


Figure 10. Test results fitted by the Mogi criterion.

Tables 1 through 3 suggest that the intermediate principal stress (σ_2) affects the biaxial strength or the maximum principal stress (σ_1) of the sandstone from three different formations. The σ_1 reaches its maximum at an increased value of σ_2 , and then become lower with higher σ_2 . Figure 8 clearly suggests that the intermediate principal stress notably affect the rock strengths. Due to the influence of σ_2 on failure stress, this Figure also shows that the compressive strengths of the specimens of each rock type under constant σ_2 is higher than the ones with reduced σ_2 . Such affect is not linear. The stress path effect acts on the mechanical behavior of soft rocks that exhibits its plastic behavior when subjecting to load.

It is postulated that the effects of the intermediate principal stress σ_2 are caused by two mechanisms working simultaneously but having opposite effects on the rock strengths: 1) the mechanism that strengthens the rock matrix in the direction normal to $\sigma_1 - \sigma_3$ plane and 2) the mechanism that induces tensile strains in the directions of σ_1 and σ_3 . The intermediate principal stress can strengthen the rock matrix on the plane normal to its direction, and hence a higher differential stress is required to induce failure. This is the same affect obtained when applying a confining pressure to a cylindrical specimen in the conventional triaxial compression testing. Considering this affect alone, the higher the magnitude of σ_2 applied, the higher σ_1 is required to fail the specimen. However, in the case of this test of sandstone, the relationship between σ_2 magnitudes and the degree of strengthening is non-linear. And this relation should depend on rock types, their textures and compositions (e.g. grain sizes, distribution of grain sizes, cementation, pore spaces, fissures and micro-cracks, types of rock forming minerals).

ACKNOWLEDGEMENTS

This study is funded by Suranaree University of Technology and by the Higher Education Promotion and National Research University of Thailand. Permission to publish this paper is gratefully acknowledged.

REFERENCES

- Boonsener, M. & Sonpirom, K. 1997. Correlation of tertiary rocks in northeast, Thailand. *International Conference on Stratigraphy and Tectonic Evolution of Southeast Asia and the South Pacific*, Bangkok, Thailand, 19-24 August 1997.
- Cai M (2008) Influence of stress path on tunnel excavation response—Numerical tool selection and modeling strategy. *Tunn Undergr Space Technol* 23:618–628.
- Chen, W.F. & Zhang, H. 1991. *Structural plasticity, theory, problems and CAE software*.
- Jaeger J.C. 1967. Brittle fracture of rocks. *Proceedings of eighth symposium on rock mechanics*. Port City, Baltimore, pp 3–57.
- Jaeger, J.C., Cook, N.G.W. & Zimmerman, R.W. 2007. *Fundamentals of rock mechanics*. 4th ed. Oxford: Blackwood.
- Mogi, K. 1971. Fracture and flow of rocks under high triaxial compression. *Journal of Geophysical Research* 76: 1255- 1269. New York-Berlin: Springer.
- Shames, I.H. & Cozzarelli, F.A. 1997. *Elastic and inelastic stress analysis*. (Revised printing). Philadelphia: Taylor & Francis.
- Shen MY, Shi ZM, Zhang L. 2003. Deformation properties of samples under different loading paths. *Chin J Rock Mech Eng* 22 (8):1234–1238.
- Wang B, Zhu JB, Wu AQ et al. 2008. Experimental study on mechanical properties of Jinping marble under loading and unloading stress paths. *Chin J Rock Mech Eng* 27(10):2138–2145.

- Wiebols, G.A. & Cook, N.G.W. 1968. An energy criterion for the strength of rock in polyaxial compression. *International Journal of Rock Mechanics & Mining Sciences* 5: 529-549.
- Xiong SH, Zhou HM. 2006. Deformation properties of rock mass of TGP permanent shiplock slopes under complex stress paths. *Chin J Rock Mech Eng* 25(Supp.2):3636-3641.
- You, M. 2008. True-triaxial strength criteria for rock. *International Journal of Rock Mechanics & Mining Sciences* 46: 115-127.
- Zhou, S.A. 1994. Program to mode the initial shape and extent of borehole break out. *Computers & Geosciences* 20(7-8):1143-60.



BIOGRAPHY

Mr. Surachai Komenthammasopon was born on January 18th, 1960 in Bangkok, Thailand. He graduated from Chulalongkorn University in 1983 and started working as a mining engineer at the Department of Mineral Resources (DMR), Ministry of Industry. After serving DMR for two years, he was awarded the scholarship to study abroad. He achieved his Master Degree in Mining Engineering at South Dakota School of Mines and Technology, USA in 1988. He had worked for DMR for five years after graduation, involving in two major projects: Tin project (Thai - German joint research project on tin mining and dressing) and DMR technical support project for private mining companies. During the years 1993 to 2006 after resigning from DMR, he joined private companies (Chai International (ICI subsidiary), Diethelm, Handling Groups, Sino-Thai Resources Development and Akara Mining), dealing with explosives sales and technical services, services of civil and mining machinery, sales of crushing equipment and turnkey plant, quarry operation and management, and gold mining operation. Meanwhile, he was occasionally an invited instructor to teach Geology for Engineers for some universities: Kasetsart (Kamphaengsaen), Niwattana, Western, Srinakharinwirot (Ongkharak), Kasem Bundit, and Rajamangala University of Technology Thanyaburi or RMUTT. He started his teaching career at RMUTT in 2006. In the late 2008, he was invited as an expertise in mining engineering from Engineering Service Center from Chiang Mai University for the project owned by Department of Primary Industries and Mines (DPIM). The project title was The Investigation of the Use of Explosives in Thai Mining Industry. He later

commenced his study towards his doctoral degree at Suranaree University of Technology (SUT) in 2010. Since joining RMUTT and during his graduate study he has published three research papers. The Investigation of Compressive Strength of Concrete in Case Study using Granite Dust from Thai Crushing Plant as Replacement for Sand ,and The Investigation of Compressive Strength of Concrete in Case Study using Graded Granite Dust from Thai Crushing Plant as Replacement for Sand both were published in Princess of Naradhiwas University Journal. Effect of Stress Path on Biaxial Strengths of Three Thai Sandstones was for International Conference on Advanced Civil Engineering for Sustainable Development. He has obtained his license as a Professional Engineer (P.E.) on tertiary level since 2002 and is now an instructor / an Assistant Professor at RMUTT.

